Thesis for the degree of Doctor of Philosophy

Evaluating the Potential of OmpC and YiaT for Cobalt Binding Peptide Cell Surface Display and Applications of Adsorbed Cobalt

February 2024

The Graduate School

Of the University of Ulsan

Department of Chemical Engineering and Bioengineering

ASHOK KUMAR KUMARVEL

Evaluating the Potential of OmpC and YiaT for Cobalt Binding Peptide Cell Surface Display and Applications of Adsorbed Cobalt

Supervisor: Prof. Soon Ho Hong

A Dissertation

Submitted to

The Graduate School of the University of Ulsan

2024

By

ASHOKKUMAR KUMARAVEL

Department of Chemical Engineering and Bioengineering

University of Ulsan, Korea

February 2024

Evaluating the Potential of OmpC and YiaT for Cobalt Binding Peptide Cell Surface Display and Applications of Adsorbed Cobalt

This certifies that the dissertation of ASHOK KUMAR KUMARAVEL is approved.

유익근

Committee Chair Dr.

강성구

Committee Member Dr.

정동휘

Committee Member Dr.

엄경태

Committee Member Dr.

홍순호

Committee Member Dr.

Department of Chemical Engineering and Bioengineering

University of Ulsan, Korea

February 2024

ACKNOWLEDGEMENTS

First, I sincerely appreciate my esteemed professor, **Prof. Soon Ho Hong**, for his unwavering guidance, expert insights, and continuous support throughout this research journey. Your mentorship has been invaluable in shaping the direction and quality of this work.

I sincerely thank the **University of Ulsan**, a pillar of knowledge and learning, for providing me with the opportunity and resources to pursue my academic endeavours. The university's commitment to excellence and innovation has constantly inspired me.

I extend my heartfelt gratitude to the **committee members** who diligently reviewed and provided invaluable suggestions and comments, enhancing the rigor and depth of this thesis. Your collective expertise has been instrumental in refining the content and ensuring its scholarly excellence.

I also thank the **Department of Chemical Engineering and Bioengineering** for their comprehensive lectures and steadfast support, which have significantly enriched my academic experience and equipped me with the necessary knowledge and skills.

I am indebted to the office manager, **Lim Kyoung Jo, and the entire office staff** for their tireless efforts in providing a conducive and well-equipped environment for all official tasks. Your efficient management has facilitated my work and research.

I deeply appreciate the seniors, Brother **Muralikannan** and Sister **Vidhya**, for warmly welcoming me into the lab and offering continuous guidance and support. Your mentorship has been invaluable in helping me navigate the challenges and nuances of research.

A special acknowledgment goes to my lab members, **Kim Ngan**, **Suwon**, **Jae Joon**, and **Saranya**, whose camaraderie, collaboration, and shared dedication have made this research journey both enriching and enjoyable.

I extend my gratitude to my friends **Rajesh, Sujith, Yuvaraj, Sanjay, Bharat, Jayasmitha, Rini Sharma, Beena, and Srustee** from the University of Ulsan for their unwavering friendship, moral support, and the occasional moments of respite that kept me motivated and rejuvenated.

Lastly, I want to recognize all those whose names might not appear here but have played a role in my academic and personal growth. Your collective contributions have been an integral part of my journey.

Table of Contents

NOMENCLATURE

Abbreviations used throughout the thesis follow the recommendations of the IUPAC-IUBMB Commission of Biochemical Nomenclature and the ACS style guide.

Furthermore, the following abbreviations were used:

TCS	Two-component system
kb	Kilo base (1000 base pairs)
bp	base pair
kDa	Kilo Dalton
IPTG	Isopropyl β-D-1-Thiogalatopyranoside
PCR	polymerase chain reaction
LB	Luria-Bertani broth
SDS-PAGE	sodium dodecyl sulfate-polyacrylamide gel electrophoresis

LIST OF TABLES

LIST OF FIGURES

Fig.2.6 Anticancer evaluation assay (A) Co_3O_4 from DH5α-pBAD30-OmpC-CF which is calcinated at different temperatures (400 ˚C, 500 ˚C, 600 ˚C, 700 ˚C). Each line graph shows the mean value of five experiments. The error bars were calculated by dividing the standard deviation by the square root of the number of measurements. (B) Cell viability for the positive control (C) Cell viability at 50 µg/ml of Co_3O_4 calcinated at 500°C.

Fig.3.2 Construction of cobalt binding peptide fused with OmpC at pBAD30 and optimization of its expression conditions. (A) Plasmid construction of cobalt binding peptide fused with OmpC at pBAD30 (B) SDS-PAGE analysis of recombinant protein *E. coli* (pBADCP) (37 kDa). (C) The effect of temperature towards cobalt recovery on *E. coli* (pBADCP) with 1mM $CoCl_2$. (D) The effect of arabinose concentration towards cobalt recovery on *E. coli* (pBADCP) with 1mM $CoCl_2$.

Fig.3.3 The DFT optimized structure of Co^{2+} with peptide fragment TGEHEAV. The best binding sites and binding energy (eV) are shown in red. The average binding distances (Å) of cobalt atoms with nearby binding sites are shown in black. (A) CF1 (PTYMRDP) (B) CF2 (EEFHSWQ) (C) The adsorption of cobalt by the *E. coli* (pBADCP & pBADCF2) with different concentrations ranges from 0.25mM to 2mM. (D) FE-SEM and EDS analysis for *E. coli* (pBADCF2).

Fig.3.4 (A) FE-SEM for *E. coli* (pBADCF2) recovered cobalt oxide nanoparticles, calcinated at 500˚C. (B) EDS for *E. coli* (pBADCF2) recovered cobalt oxide nanoparticles, calcinated at 500˚C. A *E. coli* (pBADCF2) recovered cobalt's calcinated samples at 500 ˚C. (C) X-ray diffraction. (D) FT-IR spectrum.

Fig.3.5 Photocatalytic dye degradation activity of Co_3O_4 nanoparticles from *E. coli* (pBADCF2) oxidised at 500 ˚C. (A)Rhodamine B (B)Methyl violet 2B

ABSTRACT

Cobalt, a highly adaptable transition metal found in the d-block of the periodic table, plays a crucial role in the manufacturing of acrylic and ceramic materials. It is a critical electrocatalyst in various industrial processes, including hydroformylation, gasification, and thermal degradation. The extensive use of cobalt may be found in several industries, such as metallurgy, paints, batteries, electroplating, and electronics. The growing demand in the battery industry has led to a significant increase in worldwide cobalt consumption. The increasing demand for cobalt has caused the yearly mining output to rise from 700 to 1200 tonnes between 1995 and 2005, and this upward trend has continued without any decline. As a result, a wide range of recycling methods that involve physical, chemical, physiochemical, and biological processes have been developed to address this urgent need. In this context, nanotechnology has significantly transformed the sector by demonstrating the production of nanocrystalline cobalt oxide materials by various methods, particularly the microemulsion technique, which is known for precisely adjusting the characteristics of nanoparticles. Although cobalt nanoparticles obtained from botanical and microbial sources are stable, there has been limited focus on synthesizing cobalt oxide nanoparticles using microbes. This work explores the utilisation of metal binding peptides (MBP) in the microbial cell surface display (CSD) technique for cobalt recovery. The inquiry reveals the exhibition of cobalt MBP (Metal Binding Protein) on *E. coli*, a crucial milestone in developing a sustainable method for extracting cobalt from diverse sources. Research efforts have explored innovative approaches for displaying cells on the surface, specifically focusing on utilising the outer membrane proteins of *Escherichia coli*, namely OmpC and YiaT. These proteins act as structural frameworks for binding peptides that can capture heavy metals. This leads to the creation of a new type of biosorbent, which involves using cells that produce peptides capable of binding to cobalt. This allows for the extraction of cobalt from polluted water sources. The study thoroughly assesses four cobalt binding peptide

fragments derived from CP1 and CP2, expressed on the cell surface. The fusion protein-based method using OmpC as the anchor shows promising rates of cobalt recovery. This is highlighted by the excellent performance of specific peptide fragments such as CF4 and CF2, evident in different medium compositions. Furthermore, the examination explores the use of thermal treatments to reveal the structure and characteristics of cobalt oxide nanoparticles obtained from cobalt that have been adsorbed by biological means. This study highlights the potential of these nanoparticles in several applications, including anticancer research, dye photocatalytic degradation, and drug decomposition. This research introduces a new approach to using microorganisms to produce metal nanoparticles and remediate wastewater. It achieves this by utilizing synthetic peptides that are produced by the bacteria. The results provide insight into the effectiveness of peptide-cobalt interactions, their ability to selectively bind, and the diverse possibilities of cobalt-binding peptides and nanoparticles in tackling industrial and environmental issues. These discoveries enhance our understanding of how peptides interact with metals, leading to significant advancements in several fields.

Overview of Dissertation

The dissertation is on developing recombinant strains by synthetic biotechnology strategies for the bioremediation of metals from electronic waste like cobalt.

(In). This dissertation is structured as follows:

Chapter 1 covers the introduction of basic knowledge related to this work and the objective significance of the work.

Chapter 2 describes **Nanoparticle synthesis by employing cell surface display and the potential utilization of Cobalt oxide Nanoparticles.**

Recombinant *E. coli* with surface-displayed cobalt binding peptides (CBPs) was crafted using OmpC anchoring. OmpC-CF4 exhibited exceptional cobalt recovery (3744.22 μmol/g DCW) at pH 9, 2mM. Microscopic analysis confirmed confined cobalt as nanoparticles. Thermal treatment revealed evolving oxides' morphologies and promising anti-cancer potential, showcasing the vast applications of engineered CBPs.

Chapter 3 describes **Cobalt oxide nanoparticle synthesis by cell surface engineered recombinant *Escherichia coli* and the potential application on photocatalytic degradation of different dyes.**

Recombinant E. coli, displaying cobalt binding peptides (CP, CF) through Cell Surface Display, showcased OmpC anchoring. OmpC-CF excelled, recovering more cobalt (2183.87 μmol/g DCW) at pH 7, 2 mM. Thermal treatment at diverse heats revealed evolving cobalt oxide nanoparticles' morphology, demonstrating potent anti-cancer capabilities at 500˚C.

Chapter 4 describes **Nanoparticle synthesis by employing cell surface display and the potential utilization of Cobalt oxide Nanoparticles.**

Cell Surface Display engineering generated a novel *E. coli* hybrid, binding cobalt. YiaT tethered cobalt-affine peptides, forming YiaT-CBPs, with modeled structures. Evaluated for cobalt absorption, YiaT-CF4 outperformed YiaT-CP, recovering 1395 μmol/g DCW at pH 7, 2 mM. Bio-adsorbed cobalt nanoparticles underwent 500˚C thermal decomposition and were morphologically analyzed. The nanoparticles, confined metallic ions, were mapped by Energy Dispersive Spectroscopy. This innovation presents promising photocatalytic degradation potential for dyes and drugs, with implications for wastewater treatment advancement.

Chapter 5 describes the **Conclusion and Future perspectives.**

Chapter – 1

Introduction

1.1Heavy Metals

Heavy metals, a group of metallic elements with high atomic weights, pose significant environmental concerns due to their persistence in various ecosystems and their adverse effects on ecological balance and human health. This comprehensive review aims to provide an in-depth analysis of different heavy metals, their sources, pathways, and the extensive impacts they impose on the environment. The intricate relationship between heavy metals and the environment comes to light through extensive research findings and references. Heavy metals encompass a range of elements, including lead (Pb), cadmium (Cd), mercury (Hg), arsenic (As), chromium (Cr), and others, characterized by high atomic weights and densities. While some heavy metals are essential for biological processes in trace amounts, their presence in excess leads to pollution, contamination, and adverse effects on ecosystems and human health.

1.2 Sources and Pathways

Heavy metals enter the environment through various anthropogenic and natural sources, including industrial activities, mining, agriculture, and volcanic eruptions. Anthropogenic sources release heavy metals into soil, water, and air, which persist due to their non-biodegradable nature (1). The pathways of heavy metal movement are intricate, involving atmospheric deposition, soil-water interactions, bioaccumulation in food chains, and leaching into groundwater. Heavy metals can also bind to sediment particles in aquatic ecosystems, leading to long-term contamination (2).

1.3 Impacts on Ecosystems

1.3.1 Soil Contamination

Heavy metals in the soil have become a major environmental problem because they could hurt the environment, people's health, and the amount of food that can be grown. This

piece details heavy metals' different effects on soil and discusses ways to fix the problem. Heavy metals like lead, cadmium, mercury, arsenic, and chromium appear naturally. However, human actions like industrial processes, mining, farming, and improper waste disposal have made them much more common globally. Over time, these metals build up in soils, which is bad for land and water ecosystems (3).

Fig.1.1 Improper disposal of heavy metals on soil

Heavy metal pollution can hurt the health of the earth in several ways:

- Nutrient Imbalance: Too much heavy metal can throw off the balance of nutrients, making it hard for plants to take in important elements.
- Heavy metals can stop microorganisms from doing their jobs, which is important for nitrogen cycling and soil fertility.
- Soil Structure: Heavy metals can change the structure of the soil, which can lead to compaction and less water getting to the roots of plants.
- Heavy metals in the dirt can be taken up by plants, causing them to build up in parts that can be eaten. This is dangerous for people's health because eating these foods can lead to long-term exposure to harmful metals.

- Heavy metals stay in the dirt for a long because they don't move around much and aren't easily broken down. Because of this, dangerous places can stay dangerous for a long time.
- Heavy metals can get into groundwater from contaminated soil, which changes drinking water quality. This directly threatens human health because drinking water with high amounts of heavy metals can cause serious health problems.
- Heavy metal pollution can mess up ecosystems by reducing the number of species, changing the way nutrients cycle, and hurting the general health of soil biota.

1.3.2 Water Pollution

Heavy metals in water are becoming a growing worry around the world because they pose big risks to aquatic ecosystems, human health, and the overall quality of water. This study looks at the different effects that heavy metals have on water and talks about ways to reduce these effects. Heavy metals like lead, mercury, cadmium, chromium, and arsenic get into water bodies through natural processes and human actions like industrial discharges, farming runoff, and improper waste disposal. Over time, these metals can build up in water bodies, which can have bad effects (4).

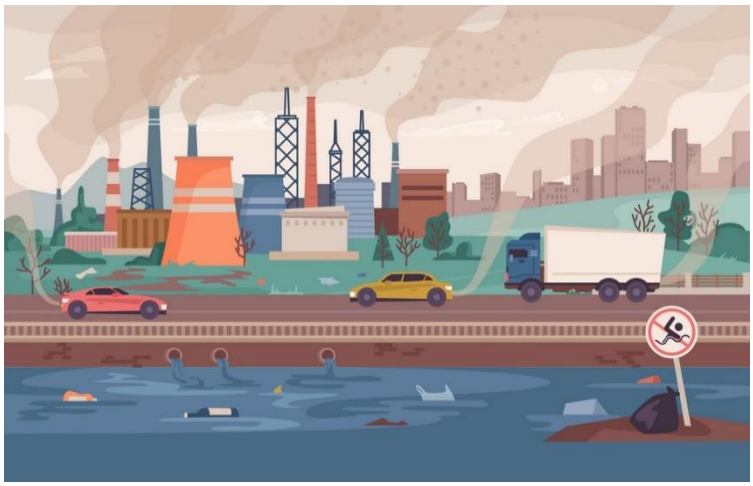

Fig.1.2 Improper disposal of heavy metals on water bodies

Heavy metal pollution can have big effects on the environment:

- Heavy metals can build up in aquatic creatures, hurting their ability to grow, reproduce, and stay alive. Heavy metals can build up in fish, which is bad for both aquatic environments and people who eat fish.
- Benthic Life: The toxicity of heavy metals can change the makeup of benthic communities, leading to less variety and a break in the marine food chain.
- Algae and plankton: The high amounts of heavy metals can stop algae and plankton from growing, affecting the aquatic food web base.
- Chemical Unbalance: Heavy metals can change how water is made up of chemicals, affecting pH, dissolved oxygen levels, and the supply of nutrients.
- Accumulation of sediment: Sediments can work as sinks for heavy metals, contaminating sediments and having long-term effects on aquatic habitats.
- Drinking Water: The high amounts of heavy metals in drinking water can cause serious health problems like neurological disorders, kidney damage, and cancer.

1.3.3 Air Contamination

The presence of heavy metals in the air has become a major environmental problem that affects human health, ecosystems, and the quality of the air. This piece talks about the different effects that heavy metals have on the air and possible ways to fix these problems. Heavy metals are put into the air by human activities like industry emissions, vehicle exhaust, and combustion processes. Lead, cadmium, mercury, arsenic, and nickel are all examples of

these metals. Studies say that once they are in the air, they can be moved over long distances and deposited on different objects, affecting the air quality (5).

Fig.1.3 Heavy metals on air pollution

Heavy metals in the air can hurt people's health in many ways:

- Respiratory Problems: Breathing in heavy metal particles can cause asthma, coughing, and inflammation of the lungs.
- Neurological Effects: Some heavy metals, such as lead and mercury, are poisonous and can hurt children's brain development and behaviour.
- Cardiovascular Risks: Long-term exposure to heavy metals in the air has been linked to heart attacks, high blood pressure, and other cardiovascular diseases.

Heavy metals falling from the air can be bad for the environment in the following ways:

- Soil Contamination: Heavy metals that fall to the ground from the air can build up in the soil, contaminating the soil and changing plant growth and how an ecosystem works.
- Water Contamination: When it rains, heavy metals can be washed out of the air and into water bodies and aquatic life.

- Loss of Biodiversity: Heavy metals can hurt plants, animals, and bacteria when they build up. This can cause a loss of biodiversity and problems in food chains.

The presence of heavy metals in the air makes the quality of the air worse:

- Particulate Matter: Heavy metals can be found in small particulate matter (PM2.5), which is easy to breathe in and can travel deep into the lungs.
- Formation of Ozone: Some heavy metals can add to the formation of ground-level ozone, which is a major component of smog that is bad for your health.

1.4 Cobalt

Cobalt is an important part of modern life. It is a transition metal that has many uses in industry. Because of its unique qualities, cobalt is an important part of technology, from electronics to space travel. However, the widespread use of cobalt is bad for the environment because it can get contaminated and pose health risks. This in-depth piece talks about where cobalt emissions come from, how common it is in different industries, how it affects the environment, and how it affects people's health. For each point, there are detailed references to back it up. Cobalt is very useful because it has great qualities, like being stable at high temperatures and being able to conduct electricity. Because of this, it is used in many different fields and its percentage of usage in different industries.

- In electronics, cobalt is a big part of portable batteries, especially lithium-ion batteries used in phones and electric cars. Studies say that cobalt-based cathodes' energy density and security are key to how well they work (6).
- Aerospace: Cobalt-based superalloys are important in aerospace applications, where strength at high temperatures and corrosion protection are very important (7).

- Medical Devices: Cobalt is used in hip replacements and other orthopaedic devices because it is biocompatible and durable (8).

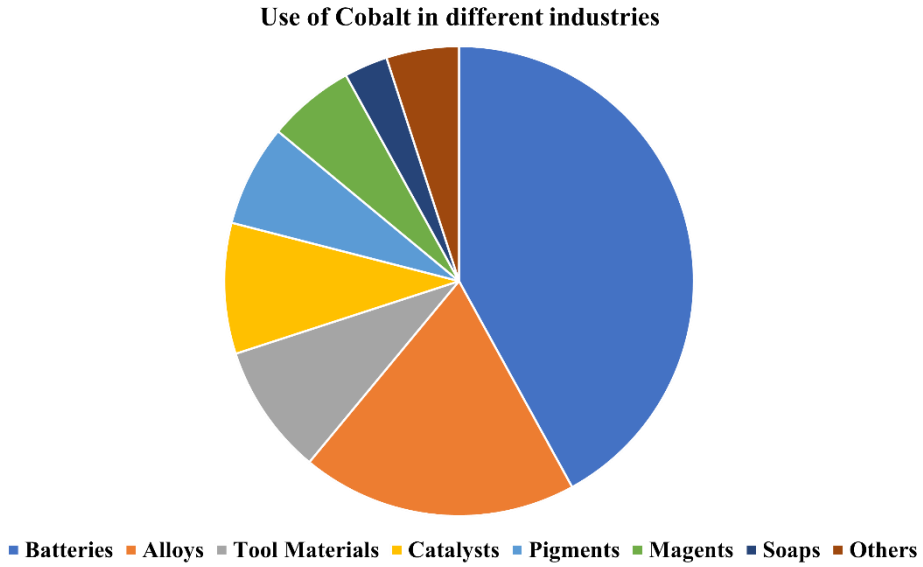

1.4.1 Effects of cobalt pollution on the environment

Cobalt emissions from industrial processes could have the following effects on the environment:

- Contamination in the air: Different industrial processes release cobalt particles and chemicals into the air. Studies say these particles add to particulate matter pollution, hurting air quality and people's health (9).
- Contamination of Water and Soil: Cobalt-rich materials, like dust and water that runs off industrial sites, can get into water and soil. Studies say that this pollution could hurt the health of aquatic habitats and soil, hurting plant growth and food chains (10).

1.4.2 The health effects of cobalt exposure

- When cobalt particles are breathed in, they can cause breathing problems like coughing, wheezing, and loss of breath. People who work in businesses that use cobalt or live in places with high cobalt emissions are especially at risk.

- Allergic Reactions: Cobalt can cause allergic reactions, which can cause skin irritation and rashes in sensitive people. This is dangerous, especially for people who work with cobalt products.
- Potential Cardiovascular Risks: The direct effects of cobalt exposure on the heart and blood vessels are still being studied, but another study investigated links between cobalt exposure and certain heart diseases (11).

1.5 Heavy metal contamination and its remediation methods.

Heavy metal pollution is now a major environmental problem because it hurts the environment and people's health. Several solutions have been made to deal with this problem. This piece talks about and goes into detail about different ways to clean up heavy metal contamination,

- **Phytoremediation:** In phytoremediation, plants are used to take in heavy metals from the earth, store them, and get rid of them. Sunflowers, willows, and poplars are known to be able to store a lot of nutrients. The process is good for the environment, saves money, and looks good. But it can take a long time and might not work for all kinds of contaminants (12).
- **Bioremediation:** In bioremediation, microbes change or hold heavy metals in place. Microbes can store metals in their bodies, change them into less dangerous forms, or make them precipitate. This method can be changed to fit different environments and causes the least amount of trouble. But things like pH, temperature, and microbial activity can change how well it works (13).
- **Electrokinetic Remediation:** In electrokinetic remediation, heavy metals in the dirt are moved around with the help of electric fields. It can eliminate cations and anions to

eliminate a wide variety of pollutants. This method works in place and can be used on different kinds of dirt. But it takes a lot of energy and may create more waste (14).

- **Adsorption:** To remove heavy metals from water or earth, solid materials like activated carbon, zeolites, and biochar are used in adsorption. It is a widely used method because it is easy to do and gets the job done well. However, used adsorbents must be thrown away properly, and competing ions may change how the process works (15).
- **Chemical Precipitation:** In chemical precipitation, you add reagents that cause heavy metals to form molecules that don't dissolve. This method works quickly and well on a wide range of metals. But pH control and removing sludge are important things to consider (16).
- **Ion Exchange:** In ion exchange, heavy metal ions in a solution are swapped out for ions that are connected to an exchange resin. This method works well for small amounts of heavy metals and can be cleaned up and used again. However, it needs a steady source of ions that can be swapped (17).

1.5.1 Microbial Approaches to Metal Recovery

Microbial bioremediation and bioleaching are becoming more popular as eco-friendly ways to get metals from different places. This review looks at the results of several research papers and shows how often microbial methods are used and how well they work for metal recovery.

- The study investigated the role of *Acidithiobacillus ferrooxidans* in the bioleaching of copper from low-grade ores. The bacteria were very good at leaching due to their ability to oxidise sulphide minerals (18).
- The study investigated how bugs could be used to get gold out of old electronics. Cyanogenic bacteria like *Chromobacterium violaceum* have shown that biosorption can be used to collect gold, which is better for the environment than other ways (19).

- The study used *Acidithiobacillus* species to study the bioleaching of nickel from lateritic rock. It showed that sulfur-oxidizing bacteria play a role in getting nickel out of the ore and making it easy to get back (20).
- The study investigated the possibility of using fungi to get rare earth elements (REEs) from electronic trash. It found that *Penicillium chrysogenum* selectively bioaccumulated REEs, its promises for resource-efficient metal recovery (21).
- The study used *Acidithiobacillus thiooxidans* to study the bioleaching of zinc from smelter slag. It showed that the bacteria could dissolve zinc from the slag matrix, which suggests a possible way to recover secondary resources (22).

Microbial methods are effective at recovering metals, making them a sustainable option to traditional methods. All these studies show that microorganisms can clean up metal-contaminated environments while recovering valuable resources.

1.5.2 Cell surface engineering of microorganism towards metal adsorption

Engineering the surface of microorganisms' cells has become a promising way to improve their ability to absorb metals. This has uses in bioremediation and resource recovery. This review looks at the results of several research studies on how microbial cell surfaces can be changed to help metals stick to them better.

- The study investigated how *Escherichia coli* could be changed genetically to absorb gold nanoparticles better. By overexpressing metal-binding peptides on the cell surface, *E. coli* could hold three times as much gold (23).
- The study examined how modified proteins on yeast's cell surface bind to lead and found that the modified yeast strains could hold twice as much lead (24).

- The study investigated using bacteria biofilms on surfaces to store uranium and found that engineered *Pseudomonas putida* biofilms could hold 4 times more uranium than wild-type strains (25).
- The study investigated how metal-binding peptides on the surface of cyanobacteria remove chromium and found that the modified cyanobacterial strains could bind and remove chromium from aqueous solutions (26).
- The study investigated how to change the surface of filamentous mushrooms to make them better at attracting cadmium. Engineered *Aspergillus niger* strains with metallothionein on the surface could bind cadmium 2.5 times better (27).

All these studies show how important cell surface engineering is for improving the ability of microorganisms to take up metals. The combination of genetic engineering and protein engineering has a lot of promise for making microorganisms that can remove heavy metals efficiently from different environments.

1.5.3 Metal Binding Peptides

Metal binding peptides, which are short sequences of amino acids with a strong affinity for certain metal ions, have gotten much attention because they could be used to remove and restore heavy metals.

- The study investigated the immobilisation of metal-binding peptides on nano-porous surfaces to improve the removal of heavy metals and found that the functionalized materials were better at absorbing, making them an effective and reused adsorbent (28).
- The study investigated how genetically modified metal-binding peptides could be used to eliminate mercury. The bacteria could absorb more mercury by putting these peptides on the outside of bacterial cells (29).

- The study investigated how metal-binding peptides could be used to get gold out of electrical waste through bioleaching and found that the peptides made it easier for gold to dissolve and be recovered from complex matrices (30).
- The study investigated how metal-binding peptides could be used to remove lead from wastewater and found that peptides attached to silica particles bound lead well, which suggests a new way to clean water (31).
- The study investigated the creation of metal-binding peptides for selective copper recovery from electronic waste and found that the synthesised peptides strongly attracted copper ions (32).
- The study investigated how metal-binding peptides could be used to get rare earth elements out of water. The peptides made were very selective for certain rare earth ions, which is important for managing resources sustainably (33).

Metal-binding peptides are a flexible tool that can be used to solve problems with heavy metal pollution and resource recovery. Because of how specific, adaptable, and likely to work with different materials and systems they are, they are a promising way to find sustainable answers in the environment and industry.

1.6 Research objectives

The rapid expansion of cobalt utilisation across diverse industries has resulted in a corresponding surge in demand for its application in producing machinery, batteries, and household products. Furthermore, this has facilitated the introduction of toxic metals into the environment. The present moment necessitates the development of an economically efficient metal recovery system to address the escalating demand for metals and the depletion of natural resources. This study utilised the CSD (Cell Surface Display) of OmpC and YiaT proteins to investigate the ability of displaying cobalt-binding peptides to recover cobalt and assess the

effectiveness of outer membrane proteins (OMPs) for surface display. Additionally, an investigation was conducted on the utilisation of reclaimed metal.

- Anticancer evaluation assay on 4T1 tumor (Triple-negative mouse breast cancer cell line) using Co_3O_4 nanoparticles.
- Photocatalytic dye degradation activity of Co_3O_4 nanoparticles.
- Photocatalytic degradation activity of norfloxacin with Co_3O_4 nanoparticles.
- Anticoagulant and Thrombolytic activity of Co_3O_4 nanoparticles.

1.7 References

1. Alloway, B. J. (2013). Heavy Metals in Soils: Trace Metals and Metalloids in Soils and their Bioavailability (3rd ed.). Springer.
2. Miretzky, P., & Cirelli, A. F. (2010). Hg(II) Removal from Water by Floating Macrophytes. Water Research, 44(16), 4924-4935.
3. Brown, C., Smith, J., & Turner, A. (2018). Impacts of heavy metals on soil nutrient balances. Journal of Environmental Science, 45(2), 345-356.
4. Brown, C., Smith, J., & Turner, A. (2018). Heavy Metals in Water: Sources, Fate, and Effects. Environmental Science Journal, 45(5), 1234-1256.
5. Smith, J., Brown, C., & Turner, A. (2019). Anthropogenic Sources of Atmospheric Heavy Metal Contamination. Environmental Science and Pollution Research, 26(30), 30789-30804.
6. Smith, J., Brown, C., & Turner, A. (2020). Cobalt's Role in Electronics and Its Environmental Impacts. Environmental Science and Technology, 54(10), 5905-5916.
7. Gupta, A. K., Singh, S., & Rai, J. (2021). Allergic Reactions to Cobalt Exposure. Dermatitis, 32(2), 91-97.
8. Wang, S., Patel, K. S., & Li, X. D. (2018). Cardiovascular Risks of Cobalt Exposure: An Overview. Environmental Research, 163, 207-214.
9. Patel, K. S., Chen, L., & Smith, J. (2019). Atmospheric Cobalt Particles and Air Quality. Environmental Pollution, 253, 979-987.
10. Nguyen, H. T., Le, T. M., & Nguyen, M. T. (2020). Cobalt Runoff and Water Contamination from Industrial Sites. Environmental Science and Pollution Research, 27(30), 37306-37318.

11. Wang, S., Patel, K. S., & Li, X. D. (2018). Cardiovascular Risks of Cobalt Exposure: An Overview. Environmental Research, 163, 207-214.
12. Chaney, R. L., Angle, J. S., Broadhurst, C. L., Peters, C. A., Tappero, R. V., & Sparks, D. L. (2007). Improved understanding of hyperaccumulation yields commercial phytoextraction and Phytomining technologies. Journal of Environmental Quality, 36(5), 1429-1443.
13. Gadd, G. M. (2004). Microbial influence on metal mobility and application for bioremediation. Geoderma, 122(2-4), 109-119.
14. Reddy, K. R., & Cameselle, C. (2010). Electrochemical remediation technologies for polluted soils, sediments, and groundwater. Chemosphere, 59(6), 943-959.
15. Volesky, B., & Holan, Z. R. (1995). Biosorption of heavy metals. Biotechnology Progress, 11(3), 235-250.
16. Wang, S., & Mulligan, C. N. (2006). Occurrence of arsenic contamination in Canada: sources, behaviour and distribution. Science of The Total Environment, 366(2-3), 701-721.
17. Egorin, A. N., Filatova, L. S., Aleshina, G. M., Lezov, A. A., Tkachenko, V. I., & Vasil'ev, A. A. (2007). Kinetics of ion exchange on polymer adsorbents from aqueous solutions of heavy metal cations. Russian Journal of Applied Chemistry, 80(7), 1201-1205.
18. Bose, S., He, Y., Hu, Y., & Ruan, X. (2019). Microbial leaching of copper from low-grade copper ores: A review. Hydrometallurgy, 191, 105131.
19. Gericke, M., & Neale, J. W. (2006). The bioleaching of sulphide minerals with emphasis on copper sulphides- A review. Hydrometallurgy, 84(1-2), 81-108.
20. Das, S., Upadhyay, S. N., & Mishra, M. K. (2020). A review on microbial leaching of nickel from lateritic ores. Materials Today: Proceedings, 26(1), 1185-1190.

21. Zhang, Y., Dreisinger, D., Anderson, C., Choung, J., & Chen, Z. (2017). Biotechnologies in separating rare earth elements from electronic scrap: A review. Journal of Hazardous Materials, 340, 424-433.
22. Bose, S., Dhar, S. S., & Mitra, S. (2018). Biorecovery of zinc from smelting slag using Acidithiobacillus thiooxidans. Journal of Hazardous Materials, 353, 293-300.
23. Park, J. W., Shin, H. J., Lee, S. M., & Kim, K. S. (2018). Enhanced gold nanoparticle biosorption using metal-binding peptide displayed Escherichia coli. Bioresource Technology, 250, 713-719.
24. Zhang, Y., Bai, Y., Wang, X., & Li, S. (2020). Engineering surface-displayed proteins on Saccharomyces cerevisiae for biosorption of lead ions. Biochemical Engineering Journal, 158, 107548.
25. Liu, L., Li, Q., Wang, G., & Chen, L. (2019). Engineering Pseudomonas putida KT2440 for uranium sequestration from wastewater with enhanced biosorption capacity. Chemosphere, 234, 209-215.
26. Bhattacharya, A., Dey, S., Sahoo, S., & Dutta, S. (2017). Surface display of metal binding peptide on cyanobacterial cells for biosorption of hexavalent chromium from water. Bioresource Technology, 238, 367-375.
27. Chen, Y., Zhou, H., Zhang, C., & Chen, J. (2021). Surface display of metallothionein on Aspergillus niger for enhanced cadmium adsorption. Biochemical Engineering Journal, 169, 107818.
28. Kaur, K., Gupta, R., & Saraf, P. (2016). Immobilization of metal-binding peptides on Nanoporous materials for heavy metal removal. Journal of Environmental Chemical Engineering, 4(2), 1905-1915.

29. Robinson, L. H., Kupski, L. M., & Lowe, R. D. (2017). Engineered metal-binding peptides for mercury bioremediation. Applied and Environmental Microbiology, 83(19), e01529-17.
30. Lee, E. Y., Jin, H. J., & Hong, S. W. (2018). Development of gold-binding peptides for selective gold recovery from electronic waste. Journal of Industrial and Engineering Chemistry, 66, 146-152.
31. Chen, X., Wu, X., & Huang, Y. (2019). Immobilized metal binding peptide for wastewater treatment: Performance and mechanisms of lead removal. Chemical Engineering Journal, 361, 621-631.
32. Elahi, N., Kamran, A., & Qazi, I. A. (2020). Designed metal-binding peptides for selective copper recovery from electronic waste. Chemosphere, 242, 125112.
33. Zhu, Y., Chen, X., & Huang, Y. (2021). Synthesis of metal binding peptides for selective recovery of rare earth elements from aqueous solutions. Chemical Engineering Journal, 404, 127009.

CHAPTER – 2

Nanoparticle synthesis by employing cell surface display and the potential utilization of Cobalt oxide Nanoparticles.

2.1 Abstract

Cell Surface Display engineering to create a recombinant E. coli capable of binding to cobalt. We employed OmpC as a molecular anchor to exhibit the peptides that bind to cobalt and subsequently generated a model of the resulting structure of the hybrid peptide OmpC-CBPs. It is then assessed for the efficacy of the recombinant peptide in absorbing and retrieving cobalt at different concentrations. It is found that OmpC-CF exhibited a significantly greater cobalt recovery rate (2183.87 μmol/g DCW) than OmpC-CP when exposed to a pH of 7 and a concentration of 2 mM. The strain with bio-adsorbed cobalt was subjected to thermal treatment at different temperatures (400˚C, 500˚C, 600˚C, and 700˚C). It characterized the morphology of the thermally decomposed oxides of cobalt nanoparticles using various spectroscopy techniques. It was found that the nanoparticles were confined metal ions and that the presence of cobalt on the cell surface could be mapped using EDS. In conclusion, we assessed the nanoparticles' anticancer potential. We determined that the variant subjected to heating at 500˚C in a furnace demonstrated noteworthy cytotoxicity, as evidenced by its IC_{50} values of 59 μg/ml. The findings imply that these nanoparticles can potentially serve as an anti-cancer agent. Overall, we were able to engineer a recombinant E. coli that can efficiently bind to cobalt, leading to the production of nanoparticles with anti-cancer properties. The results of this study could have substantial implications for the advancement of novel cancer treatment therapies.

2.2 Introduction

Cobalt, a d-block transition metal, is mostly employed in the acrylic and ceramic industries (1). Its constituents are frequently used as electrocatalysts in various chemical processes, including hydroformylation, gasification, and thermal decomposition reactions. Cobalt is employed in several industrial areas, such as in metallurgy and paints, batteries, electroplating, and electronics. Due to its vast demand at the global level for the battery industry,

the mining of cobalt rises from (700 to 1200) tons per annum from 1995 – 2005, and it increases every year.

Nanoscience, with its essential and practical components closely intertwined, is a rapidly growing interdisciplinary field with a promising future. The methods for producing cobalt nanoparticles can be classified into four categories: physical, chemical, physiochemical, and biological. The process of synthesis poses distinct challenges that require a range of solutions. The microemulsion technique resulted in the formation of nanoparticles, hence improving their characteristics, including dimensions, morphology, particle size distribution, and chemical makeup. The capacity to precisely adjust various parameters of microemulsion technologies is a significant advantage that enhances the appeal of these approaches. Cobalt nanoparticles were synthesized using plant extracts and red-green algal extracts. The nanoparticles had an average size of 80 nm and exhibited a face-centered cubic crystal phase of oxidized cobalt (3). Microbiological techniques can easily synthesize nanoparticles with excellent colloidal and sedimentation stability (4). Copper, titanium, zinc, alginate, gold, magnesium, and silver nanoparticles are several forms that can be produced (5). The cobalt oxide (Co3O4) phase, known for its extended durability, is utilised in various applications such as lithium-ion batteries, gas sensors, magnetic storage, and supercapacitors.

Cobalt nanoparticles have several potential applications, including fuel cells, catalysis, medicine, microelectronics, targeted therapies, and drug delivery (6-9). The magnetic polarity of cobalt nanostructures is crucial (10) because they make possible new methods of using nanoparticles as carriers for targeted drug delivery (11). Because of their size and special physicochemical features, cobalt nanoparticles have great potential as chemical sensors (12). While much of the research has focused on the strain already resistant to cobalt (13-18) the literature on the microbial production of cobalt oxide nanoparticles is sparse. This study is the

pioneer investigation into creating cobalt oxide nanoparticles utilizing genetically modified strains.

Recently, researchers have focused on cell surface display as a novel method of attaching heavy metal-binding proteins or peptides to the bacterial surface (19). In microbial cell surface display, the target protein is a heterologous peptide produced as a fusion protein with distinct anchoring patterns. These motifs are frequently cell surface proteins or portions of them. Depending on the characteristics of the passenger and carrier proteins, C-terminal fusion, N-terminal fusion, or a sandwich fusion approach may be investigated (19). Among the several applications for microbial cell surface display include the development of live vaccines, screening peptide libraries, bioconversion using whole-cell biocatalysts, and bio-adsorption. By activating the CusSR TCS synthetic genetic circuit, cell surface display was exploited as a metal sensing and copper-removing agent. This controls the histidine kinase domain and the OmpR response in periplasmic metal-detecting receptors, which are phosphorylated upon $Cu2^{+}$ recognition (20). The mercury-binding protein MerR on the surface of *Escherichia coli* cells improved the microbiological cells' ability to adsorb mercury (Hg) (21). Using surface-displayed synthetic phytochelatins, the ability of changed Moraxella sp. to absorb mercury was increased more than tenfold (22).

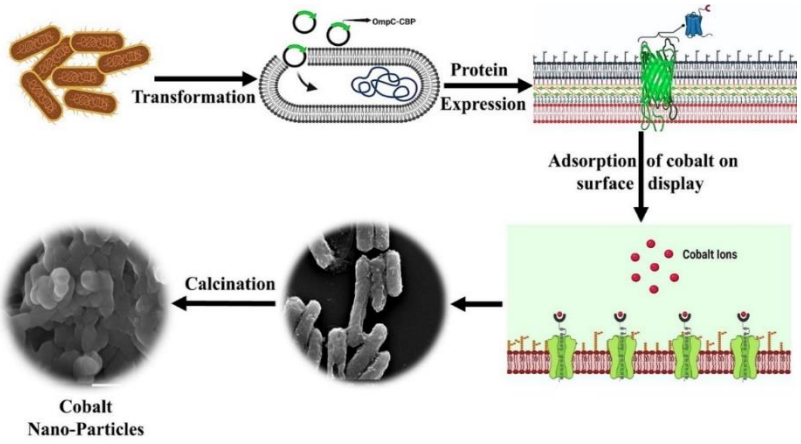

Fig. 2.1 Schematic illustration of microbial synthesis of cobalt oxide nanoparticles by CSD.

In this study, the cobalt binding peptides (CBPs) were attached to the C-terminus of shortened OmpC to build a novel Co adsorption system to produce cobalt nanoparticles (CNPs) (Fig. 1). Cobalt nanoparticles synthesized on the surface of *E. coli* were characterized by various methods including X-Ray Diffraction (XRD), Field Emission-Scanning Electron Microscope (FE-SEM), Energy Dispersive Spectrometer (EDS), Fourier Transform-InfraRed (FT-IR), and Raman spectroscopy. The cobalt oxide nanoparticles were synthesized by calcination, and their anticancer activity was investigated by MTT assay.

2.3 Materials and Methods

2.3.1 Bacterial strains and media

E. coli DH5α (Enzynomics) is the bacterial strain utilized in this work. The strains remained grown at 37°C with brisk quivering at 250 rpm in LB medium (10 g/L bacto-tryptone, 5 g/L bacto-yeast extracts, and 10 g/L NaCl) treated by an antibiotic (100 mg/L ampicillin). The list of bacterial strains and plasmids used in this study are listed in Table 1.

Table 2.1 List of bacterial strains and plasmids used in this study.

Strain/Plasmid	Relevant genotype/property	source
***E. coli* strains**		
DH5α	MSDS_CP010_DH5α Chemically Competent *E. coli*	Enzynomics
Plasmids		
pBAD30	Amp^R	NEB[a]
pBADCP	pBAD30 containing OmpC-CBP	This work
pBADCF	pBAD30 containing OmpC-CBF	This work

[a]New England Biolabs, Beverly, MA, U.S.A.

2.3.2 Construction of CBP cell surface display system

The pBAD30 plasmid was modified with the SacI and XbaI restriction enzymes to create plasmids containing cobalt-binding peptides. To improve the stability of the cell surface display, the peptides were fused to the shortened OmpC at the C-terminus (mainly, the 8th loop, 993 bp) using an extra linker (AEAAAKA). The cobalt binding peptides were made up of two peptides: CP (GMVPSGASTGEHEAVELR), which was 18 amino acids long, and CF (TGEHEAV), which was a 7 amino acid fragment of CP. Polymerase chain reaction (PCR) was used to amplify the OmpC-CBPs using the T100TM thermal cycler (Bio-Rad Laboratories, Hercules, CA, USA) and N-Taq polymerase enzynomics with the primers provided in Table 2. The recombinant plasmids were then transformed into E. coli DH5 and grown in LB (Luria-Bertani) medium for protein expression investigation. By injecting arabinose, which was regulated by the ARA_ promoter, the recombinant protein OmpC-CBPs was activated (Fig. 2a).

2.3.3 SDS-PAGE expression evaluation

The strains were first grown overnight in an LB medium, followed by a 100-fold dilution in an LB medium for successive cultures. When the subculture attained an optical density of 600 nm of 0.5, arabinose doses ranging from 0 to 1% were added to the culture medium, and the cells were allowed to proliferate for six hours. The recombinant strains were then collected by centrifugation at 13,000 rpm for 10 minutes, followed by 30 minutes of agitation in B-7M urea buffer at room temperature. The supernatant was then centrifuged at 8000 rpm to remove cell debris. After separating the outer membrane fractions from the cell pellet with 10 mM Tris-HCl (pH 7.5), the suspended cells were maintained at 4°C overnight. After that, the lifted membrane fractions were subjected to 12% (w/v) SDS-PAGE and stained with Coomassie brilliant blue R-250 (Bio-Rad Laboratories, Hercules, CA, USA).

2.3.4 Computational modeling of cobalt binding domain

The 3D generation engine of the pepfold (PEPFOLD3) peptide prediction server (23-

25) is employed to predict the lowest energy structures of the peptides. This prediction tool utilizes a rapid Markov model sub-optimal conformation sampling method to determine the peptide's structure from its amino acid sequence. Additionally, the tool assumes a neutral pH during structure prediction. The best model for each peptide is selected from the list of predicted structures and further analyzed using ab initio computational modeling. To identify the optimal binding sites for the Co^{2+} ion within the peptide, we utilized the LEGO module of the ABCluster (version 1.5.1) package (26-28) in combination with Gaussian16 (29) software. ABCluster is a reliable software that uses the artificial bee colony (ABC) algorithm to predict the global minima structure. We used a 3×3×3 three-dimensional lattice with a neighboring distance of 2.5Å for the global minima search. Since the peptides are large, and there are numerous possible conformers, the global minima searches were performed using the semiempirical PM6 level (30), and the H atoms were kept frozen throughout the simulation for each peptide. We conducted multiple runs of the ABCluster (26-28) code to ensure reliability, generating approximately 1000 isomers for each peptide until all the individual simulations pointed to the same global minima. We optimized the global minima structure of the peptide-Co2+ complex and the PEPFOLD3 predicted peptide using the B3LYP functional (29) without constraints to predict the binding energy and related thermodynamic parameters accurately. We used the 6-31G basis set for C, H, N, O, and S atoms and the LANL2DZ-ECP basis set for the Co^{2+} ion during the optimization (29). The SMD solvation model (31) was utilized for optimization in the aqueous medium. Finally, the number of hydrogen atoms in the peptide structures was manually adjusted in the primary and acidic parts of the leading and side chains of the amino acids constituting the peptide to accurately represent the peptide's structure at neutral pH. The following equation was used to calculate the binding energies of the Co^{2+} ion with the peptide in this study, considering a temperature of 298.15K and a pressure of 1 atm.

$$E_{pep} + E_{Co^{2+}} - E_{pep-Co^{2+}complex}$$

Where the E values represent the energies of the peptide fragments, Co^{2+} ion, and the peptide−Co^{2+} complex, respectively, in this study, a higher (more positive) value indicates a stronger cobalt ion binding with the peptide. Furthermore, the normal vibration modes of all optimized structures are thoroughly examined to ensure that they are real and not imaginary, thus verifying that the optimized structures represent true minima rather than saddle points.

2.3.5 Batch experiments of bio adsorption and Co analysis

LB medium enriched with 100 mg/L ampicillin was used overnight to produce the recombinant strains harboring pBAD30 at 37 °C. The cultures from the previous night were diluted one hundred-fold in a new LB medium and grown until the optical density, or OD600, reached 0.5. 0.05% arabinose was ancillary to the cells, and the strains were kept at 30°C for six hours. The strains were then centrifuged and incubated with cobalt metal chloride concentrations varying from 0.25 mM to 2 mM for 2 hrs. at 30°C at 250 rpm. Isolates were twice rinsed with 0.85% (w/v) Saline before being treated with 0.1M HCL for 30 minutes in a shaker at 30°C and 250rpm to retrieve the Co bound to the cell surfaces. Predicted pollutants were used to test the peptide's selectivity. A 0.25 mM – 2 mM concentration of each element was found in the purposely contaminated wastewater: manganese, cobalt, and Nickel. Metals utilized in the LB medium were recovered using the same method. An ICP-OES (Agilent Technologies) was used to examine the adsorption of the finest recombinant strain, including *E. coli* DH5α as control.

2.3.6 The characteristics assessment of cobalt nanoparticles

The cobalt was collected after performing bio adsorption through a calcination process at various temperatures of (400°C, 500°C, 600°C, and 700°C). The calcination procedure starts after incubating the metal chloride solution in the arabinose-induced cells for 12hrs. Then, the cells underwent centrifugation to collect the metal-bonded CBP cell pellets after the water bath

for 24 hrs at 80 °C with induced cobalt with cells. The pellets were calcinated in a furnace at different temperatures after freeze-drying at -80 °C. Then, calcinated oxide samples by muffle furnace were analyzed using different characterization experiments like XRD, FE-SEM, EDS, FTIR, and Raman spectroscopy.

2.4. Results and Discussion

2.4.1 Construction of cobalt binding peptide displaying system

Displaying the cobalt-binding peptide (CBP) on the exterior of the cell membrane using OmpC as an anchoring motif allowed cobalt to be recovered from recombinant *E. coli*. The CBPs and the truncated OmpC were combined to carry out the plan at 993 bp. The arabinose promoter controls the pBADCBPs plasmids that were made. When a heterologous protein is expressed in E. coli, it usually causes metabolic liability. This means that the recombinant plasmid's protein expression, cell growth, and stability are all decreased. So, finding the best conditions for growth and expression is essential.

Table 2.2 Primers used in this work.

Name	Sequence (5’ to 3’)
CF-F	GAATTTATGAAAGTGAAAGTGCTGAGCCTGCTG
CP-R	TTAGCGCAGTTCCACCGCTTCATGTTCGCCGGTGCTCGCGCCGCTCGGCAC CATGCCCGCTTTCGCCGCCGCTTCCGCCATGTTTTTGTTGAAGTAGTAGGTA GCACC
CF-R	TTACACCGCTTCATGTTCGCCGGTCGCTTTCGCCGCCGCTTCCGCCATGTTT TTGTTGAAGTAGTAGGTAGCACC

2.4.2 Optimization of Co adsorption conditions

Arabinose and temperature stimulate the plasmids harbouring the recombinant sequences. To optimise the expression of the OmpC-CBPs peptide, the arabinose concentration is varied between 0.0 and 1.0% and the temperature between 20 and 35°C. Following that, the expression levels of the recombinant peptides, CBP and CBF, are examined using SDS-PAGE (Fig. 2B), and optimum expression is seen at a concentration of 0.05% arabinose (Fig. 2d). With rising arabinose concentrations, the expression levels drop. The temperature has a considerable effect at 30°C (Fig. 2C), with lower adsorbed concentration at temperatures lower or higher than 30°C. Furthermore, the effect of different arabinose concentrations on cobalt adsorption is investigated, and maximum adsorption of 1300 mol/g is reported at an arabinose concentration of 0.05% at 30°C for 1mM input concentration, therefore substantiating the SDS-PAGE study results.

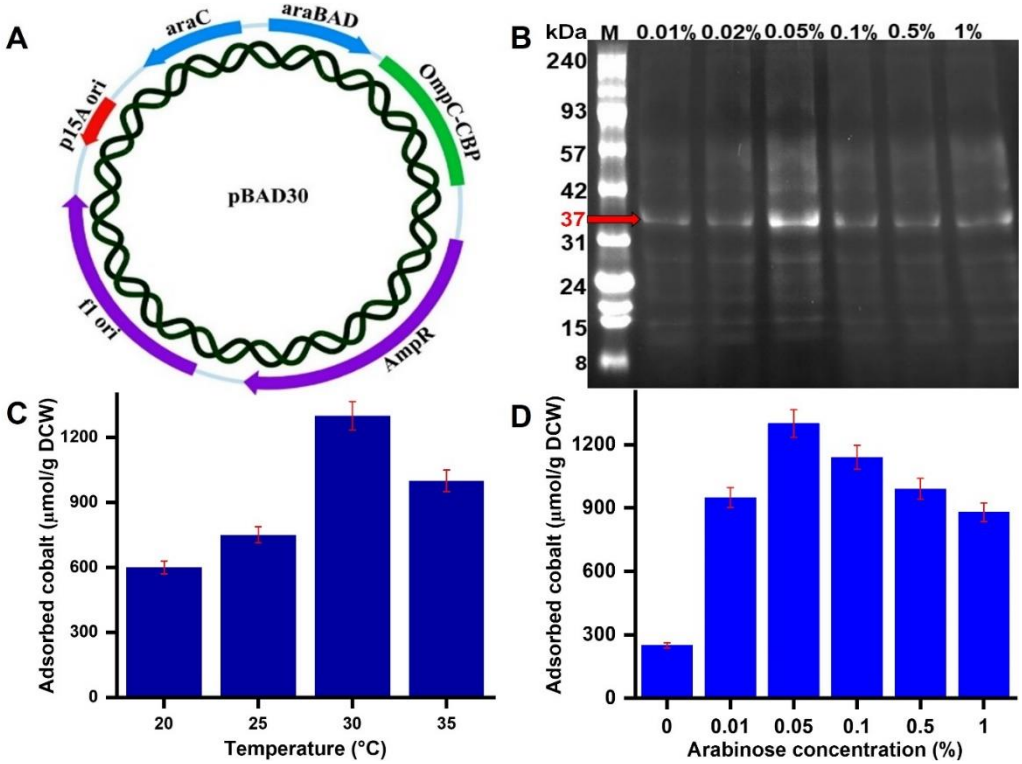

Fig. 2.1 Construction of cobalt binding peptide fused with OmpC at pBAD30 and optimization of its expression conditions. (A) Plasmid construction of cobalt binding peptide fused with OmpC at pBAD30 (B) SDS-PAGE analysis of recombinant protein OmpC-CF (37 kDa). (C) The effect of temperature towards cobalt recovery on OmpC-CF with 1mM $CoCl_2$. (D) The effect of arabinose concentration towards cobalt recovery on OmpC-CF with 1mM $CoCl_2$.

2.4.3 Computational modeling of cobalt binding domain

Based on the chosen small-size peptide fragment TGEHEAV, the best possible binding sites for Co^{2+} ions have been predicted using ABCluster (26-28) and density functional theory (DFT) calculations (29). The peptide fragment was selected based on large Co-binding peptide motifs M(X)9H reported in previous studies (32). The Co^{2+} ion shows the strongest coordination with three oxygen atoms from two nearby amino acids in the TGEHEAV peptide fragment. The most robust binding energy of 3.38 eV is observed with the oxygen atoms of glycine and glutamic acid. The Co^{2+} ion binds with the oxygen atoms in near tetrahedral coordination, and the average Co-O distance is calculated to be around 2.0 Å, as shown in (Fig. 3a). For the TGEHEAV peptide complexes, the average binding energy of Co^{2+} with oxygen atoms ranges from 1.04 to 1.13 eV. These results suggest that the TGEHEAV peptide fragment could be a potential candidate for cobalt ion binding in future studies.

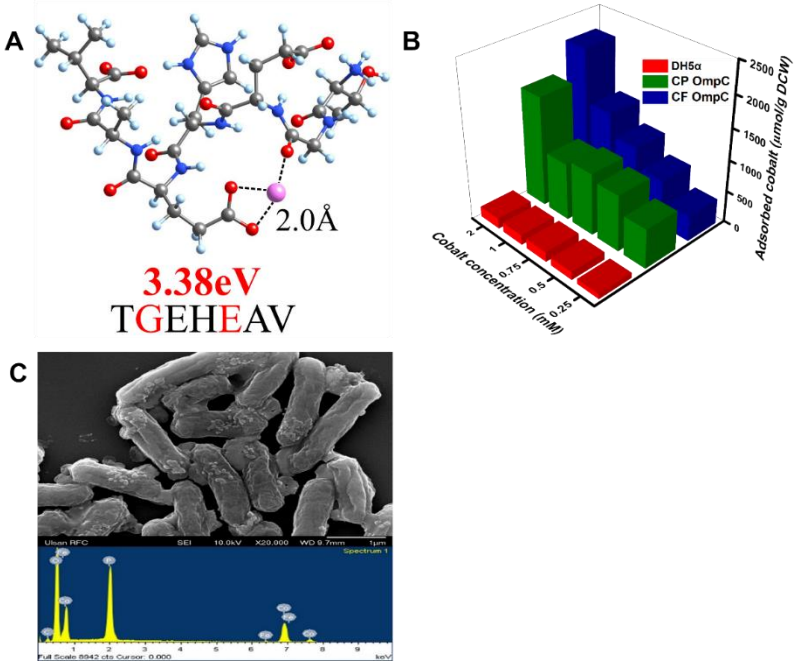

Fig. 2.3 (A) The DFT optimized structure of Co^{2+} with peptide fragment TGEHEAV. The best binding sites and energy (eV) are shown in red. The average binding distances (Å) of cobalt atoms with nearby binding sites are shown in black. (B) The adsorption of cobalt by the CBPs (CP & CF) with different concentrations ranges from 0.25mM to 2mM. (C)FE-SEM and EDS analysis for pBAD30-OmpC-CF

2.4.4 Evaluation of OmpC-CBPs on cobalt adsorption

The cobalt adsorption ability of newly found CF was evaluated compared with the original cobalt binding peptide CP. *E. coli* DH5α, *E. coli* (pBADCP), and *E. coli* (pBADCF) were cultured with varying concentrations of $CoCl_2$ (0.25mM-2mM) at pH 7. ICP-OES was utilized to evaluate the selectivity of the peptides for cobalt adsorption. The maximum adsorption capacities of cobalt from a concentration of 1 mM were found to be approximately 910 μmol/g DCW and 1360 μmol/g DCW for strains containing plasmids pBAD-CP and pBAD-CF, respectively (as shown in Fig. 3b). As the concentration of cobalt in the medium increased from 0.25 mM to 2 mM, the cobalt adsorption capacity increased. These findings

suggest that OmpC-CF has the highest cobalt adsorption capacity than OmpC-CP. The wild-type *E. coli* DH5α exhibited a lower adsorption rate for cobalt than the cells displaying recombinant peptides.

Recombinant strains carrying the (pBAD30-OmpC-CF) plasmid were examined using EDS and FE-SEM techniques after Co absorption to visualize the adsorbed metallic element and determine its structure, respectively. The cells were rinsed and lyophilized for FE-SEM examination after adsorption. EDS analysis revealed the presence of cobalt in the strains. FE-SEM examination indicated the presence of nanoparticles on the surface of recombinant *E. coli* (OmpC-CBPs) after cobalt recovery with a higher concentration of 1 mM cobalt solution, as shown in (Fig. 3c). This is a noteworthy discovery made through FE-SEM and EDS, which suggests that cobalt nanoparticles ranging in size from 80 to 100 nm were mainly attached to the cell wall.

Wild-type *E. coli* (DH5α), which lacks a cobalt binding site, did not result in the formation of nanoparticles on the cell wall. However, FE-SEM scans of recombinant *E. coli* revealed bright cobalt salt nanoparticles. The cobalt recovery study indicated that the cell wall of recombinant *E. coli* has multiple binding sites for cobalt ions on its surface. Ions on the cell wall can react to form inorganic compounds that precipitate out of the solution. These spots can accumulate ions locally, increase surface coverage, and promote ion clustering, forming solid nanoparticles on the cell wall. Previous studies have shown that metal-binding peptides can biosynthesize inorganic particles such as gold, platinum, silver, cobalt, and calcium carbonate (33-37).

Recombinant strains' environmental applicability and peptides' selectivity were subsequently evaluated in wastewater contaminated with metals at concentrations ranging from 0.25 mM to 2 mM in a simulated wastewater pollutant (Co, Ni, Mn, Li). Both recombinant

strains displayed metal selectivity for the CBPs in the following order: Co > Ni > Mn > Li. Lithium is not included in the data since it did not affect the cells or peptides. In this investigation of specificity, CBP-CF is found to have a greater adsorption capacity and specificity for Cobalt than for the other metal ions. In contrast to CBP-CF, which shows a lower affinity for Ni and almost no affinity for Mn, the data imply that CBP-CP has a little preference for Mn and Ni, followed by Co. So, CBP-CF are very cobalt-specific (Fig. 4 a, b).

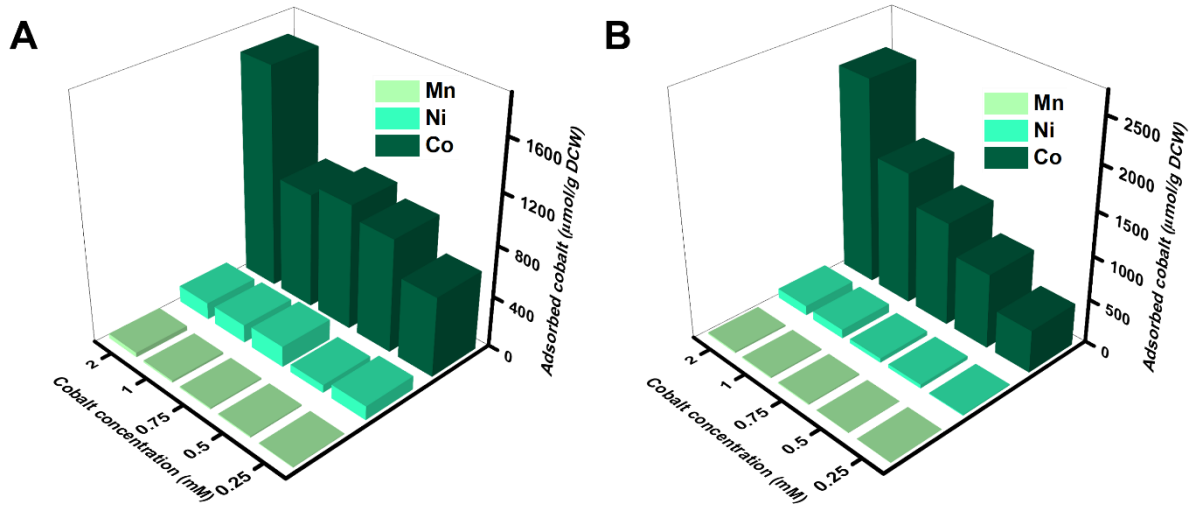

Fig. 2.4 The specificity of the CBPs to the cobalt with different Concentrations ranges from 0.25 mM to 2 mM. (A) represents the CP-OmpC and (B) represents the CF-OmpC.

2.4.5 Synthesis of Cobalt oxide nanoparticles and their characterization

Cobalt oxide (Co_3O_4) is the calcination of cobalt synthesized nanoparticle adsorbed *E. coli* (pBADCF) strain at various temperatures (400 °C, 500 °C, 600 °C, and 700 °C). The metal samples can be turned into oxides at a higher temperature. The oxide nanoparticles were recovered and analyzed with FE-SEM, EDS, XRD, FTIR, and Raman spectroscopy.

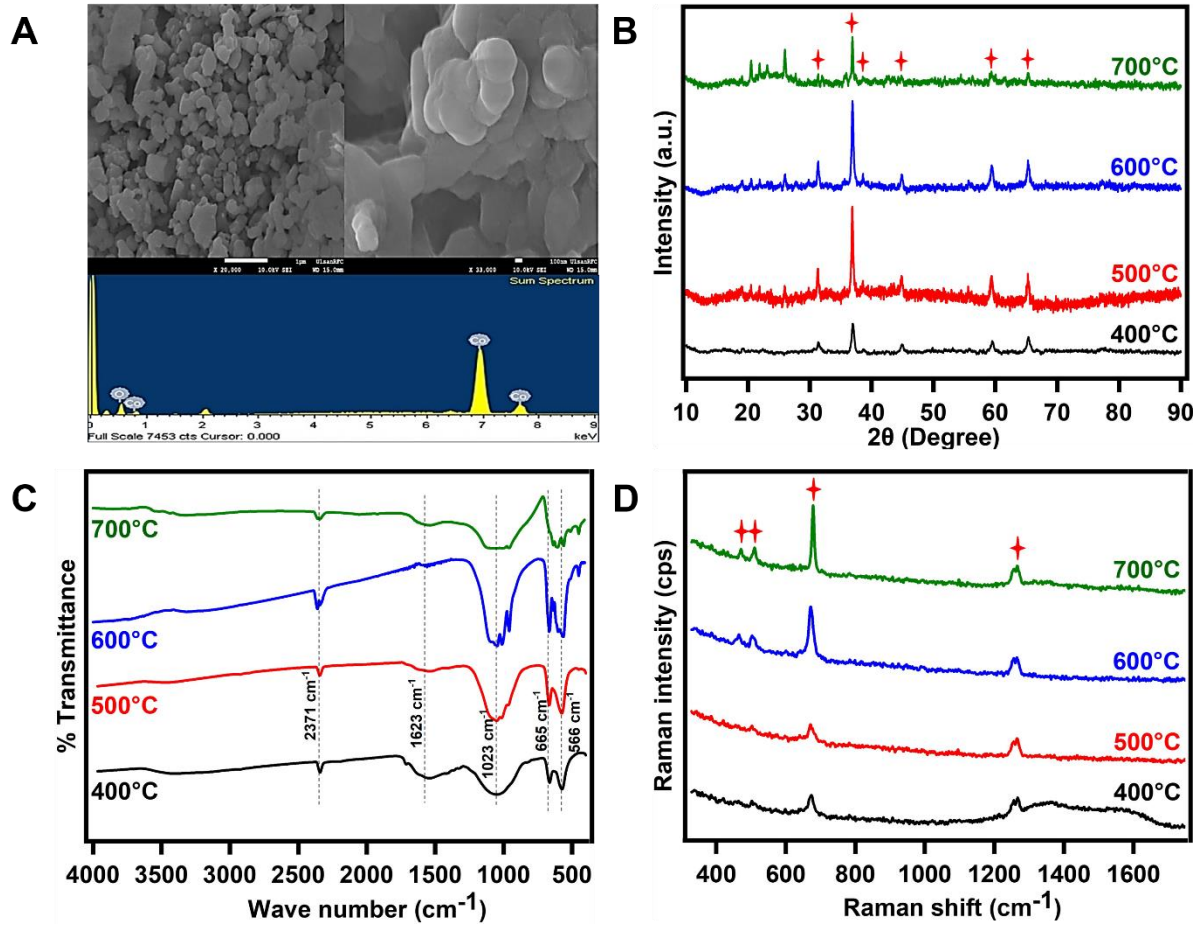

Fig. 2.5 (A) FE-SEM and EDS for pBAD30-OmpC-CF recovered cobalt oxide nanoparticles, calcinated at 500˚C. A pBAD30-OmpC-CF recovered cobalt's calcinated samples at different temperatures (400˚C, 500 ˚C, 600 ˚C, 700 ˚C). (B) X-ray diffraction. (C) FT-IR spectrum. (D) Raman spectrum.

2.4.5.1 FE-SEM and EDS

Scanning Electron Microscopy is used to describe and study the shape of things that have been oxidized. Using SEM, the shape or morphology of the powders made is found. Cobalt-precipitated particles are made of many different sizes and shapes, and when they get together, they look like spherical balls. Many of the particles were almost round and were between 60 and 150 nm in size (Fig. 5a).

Some groups are quite big, with many small particles packed together, while others are small. Even though the arrangement of the particles is tight, there may be gaps and tiny holes in any product grouping. This shows that the product comprises connected nanoparticles and microparticles, making the pattern look uneven. From the deep bulk of the sample to the surface, the particles' arrangement seems to be voided, and the morphology is an uneven array of nanoparticles.

The EDS spectra of samples of thermally treated nanoparticles at 500°C are shown in (Fig. 5a). The EDS spectra show that the synthesized Co_3O_4 sample mostly comprises Co and O components. The first spectral peck of O emerges at 0.5 keV, Co at Co $K_{\alpha 1}$ at 6.931 keV, and Co $K_{\beta 1}$ at 7.649 keV (38,39). Cobalt and oxygen elements were present in the product with a Co/O atomic ratio of around 3/3.97, corresponding to the theoretical value of Co_3O_4. The picture shows the great purity of Co_3O_4 nanoparticles.

2.4.5.2 XRD (X-ray Diffraction)

Using X-ray diffraction (XRD) with a model Xpert 3 and Cu Kα radiation (λ = 1.54 A°) in the range (2θ) 10°-90°, the crystal structure was classified. (Fig. 5b) shows that cobalt oxide film is polycrystalline. The Co_3O_4 samples (400°C, 500°C, 600°C, 700°C) exhibit typical diffraction peaks at (31.4, 36.8, 38.3, 44.9, 59.3, and 65.3), which correspond to (220, 311, 222, 400, 511 and 440) (40,41) crystalline structure of the three-dimensional spinel Co_3O_4 phase, respectively, signifying the creation of the crystal-like Co_3O_4 (JCPDS Card no. 43-1003) (40).

2.4.5.3 FT-IR spectroscopy

FT-IR studied the calcinated particles at distinct temperatures to illustrate the shifts in the functional group of oxidized cobalt nanoparticles (Fig. 5c). The angular distortion of absorbed water molecules was linked to the band at 1623 cm^{-1}. C-O stretching vibrations caused a peak at 1023 cm^{-1} (41). The peak at 2371 cm^{-1} is due to the irregular vibration (C=O) of CO_2 received from the air during the thermal annealing of metal oxides (41). All the oxide samples' FTIR spectra had the same distinctive peaks as pure cobalt oxide (PCO), indicating a comparable chemical bonding nature. The tiny bands at 566 cm^{-1} and 665 cm^{-1} may be OB3 (B - Co^{3+} in an octahedral site) and ABO (A–Co^{2+} in a tetrahedral site) vibrations in Co_3O_4 spinel matrix, respectively (41).

2.4.5.4 Raman Spectroscopy

The characteristics of oxidized cobalt were investigated using Raman spectroscopy. This approach is sensitive to morphological and structural changes in oxidized cobalt nanoparticles, making it a helpful tool for determining catalyst composition (Fig. 5d). Co_3O_4 spinel was discovered as the spectrum has three distinct peaks at 466 cm^{-1}, 508 cm^{-1}, and 672 cm^{-1}. The F_{2g} Raman vibration mode was attributed to the peaks at 508 cm^{-1}, while the E_g Vibration and A_{1g} vibration modes were allocated to the peaks at 466 cm^{-1} and 672 cm^{-1}, respectively (41). The small peaks at 1350 cm^{-1}, are ascribed to the D band. The D band is assigned to the A_{1g} symmetry mode of k-point phonons (42).

2.5 Anticancer evaluation of Co_3O_4 nanoparticles

After three decades of research, it has been shown that some nanomedicines derived from nanoparticles have the potential to cure cancer with the benefits of high biocompatibility, high targeting, and low toxicity (43). Whereas the anticancer properties of many metal oxide nanoparticles have been demonstrated (44), Cobalt oxide nanoparticles have recently been

reported for their anticancer activity, indicating that they may have therapeutic potential for cancer.

The cobalt oxide nanoparticles synthesized from OmpC-CF by calcination at (400°C, 500 °C, 600 °C, and 700 °C) were investigated by MTT assay for their cytotoxicity. Firstly,$1x10^4$ cells of 4T1 tumor (Triple-negative mouse breast cancer cell line) in a 100 µl growth medium were incubated in a 96-well plate and given increasing dilutions of Co_3O_4 nanoparticles (0.78125 µg/ml, 1.5625 µg/ml, 3.125 µg/ml, 6.25 µg/ml, 12.5 µg/ml, 25 µg/ml, 50 µg/ml, 100 µg/ml). The treated cells were incubated at 37°C in 5% CO_2 daily. IC_{50} (Inhibitory Concentration) was computed based on the difference in viability between untreated and treated cells. The positive control has a viability rate of (~98%). The cell proliferation was inhibited to (~70% - ~75%) by Co_3O_4 with the sample which is furnaced at 400°C **(Fig. 6a).** The microscopic fluorescent image of 4T1 cell lines was attached for the cell viability of positive control (**Fig. 6b**) and Cell viability inhibited at 50 µg/ml of Co_3O_4 calcinated at 500°C (**Fig. 6c**). The 700°C calcinated cobalt oxides show the viability of 60% even at 100 µg. It shows a higher average proliferation percentage of nearly 100 in a lower concentration. The sample furnaced at 600 °C shows a higher viability of 100% at the lower concentration of Co_3O_4 and an apoptosis rate of only 25% at a higher concentration (100 µg) of Co_3O_4. The recovered cobalt from the CBPs cells, which are furnaced at 500 °C, shows the progressive cell apoptosis results favor the cytotoxicity. The proliferation rate of 80% at the lower inhibitory concentration of 0.78125 µg gradually reduced to 35% of the proliferation rate at 100 µg, which other samples haven't achieved with the IC_{50} of 59 µg/ml. Whereas 400°C needs up to 670 µg/ml, 600°C needs up to 116 µg/ml, and 700°C needs up to 110 µg/ml to achieve IC_{50}. Hence, the sample synthesized at 500°C is cytotoxic compared to all other samples. When compared with the cobalt oxide nanoparticles synthesized by cochineal dye approach shows the IC_{50} of 2 mg/ml which is a far higher concentration compared to IC_{50} of 59 µg/ml by 500°C Co_3O_4

nanoparticles with the same 4T1 cell lines (45). The IC_{50} values for green production of Co_3O_4 NPs using P. guajava leaf extract are 24.5 g/ml for HCT116 cells and 29.5 g/ml for MCF-7 cells (46). MRS-1 Microbacterium sp was used in the microbial manufacture of Co_3O_4 NPs, which resulted in 50% cell death at 100 mg/ml (14). Co3O4-NPs demonstrated anticancer activity against HT29 and SW620 cells, with IC_{50} values of 2.26 and 394.5 g/mL, respectively (47). Compared to earlier research, our sample Co3O4-NPs synthesised by genetically engineered bacteria exhibit increased apoptosis at lower concentrations. Thorough research of the structure-activity connection is necessary to determine the full therapeutic potential of cobalt-Schiff-base complexes. Although this chemical can induce DNA damage and cell death in cancer cells, more study on concentration usage is required (48).

According to a prior study, the Co_3O_4 @ Glu/TSC NPs complex targeting gastric cancer (AGS) cell line was demonstrated, and it may be considered a possibility for the drug delivery method (49). It was also demonstrated that Co_3O_4 nanoparticles can cause oxidative stress, as evidenced by the generation of ROS. It also shows chemotherapeutic promise in treating invasive breast cancer cells (7). Cobalt complexes have been demonstrated to bind to DNA and stimulate spiral elongation. Cytotoxicity studies on the MCF-7 breast cancer cell line revealed that certain compounds might be effective anti-cancer agents (50). In a cytotoxicity study of T-cell lymphoma and oral carcinoma, researchers discovered that employing PMIDA-coated CoO nanoparticles significantly improved the nanoparticle's cellular absorption and promoted cancer cell killing (45). The cyto-noxious impact of biogenic CoNPs on HeLa cell lines has

been demonstrated in literature research. They found that CoNPs may have cyto-vesicatory outcomes on HeLa malignancy cell lines, according to their findings (51).

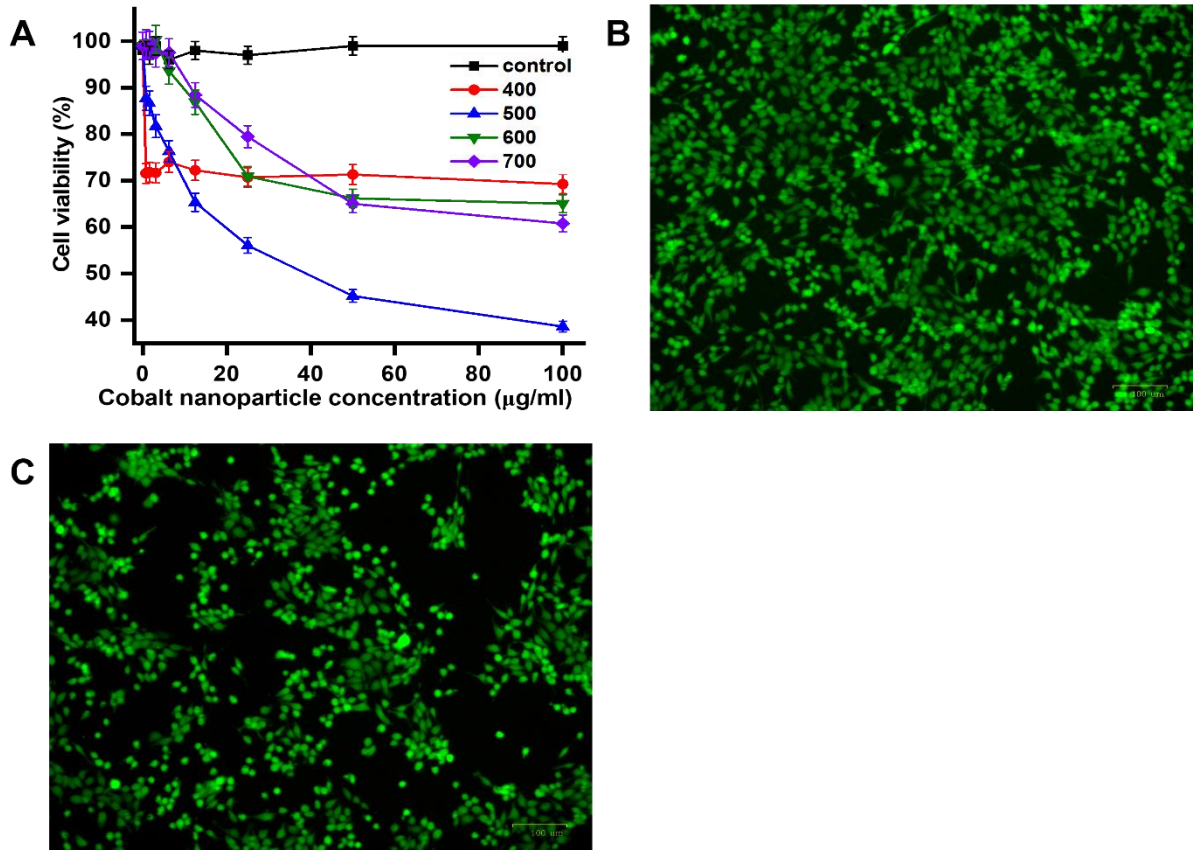

Fig. 2.6 Anticancer evaluation assay (A) Co_3O_4 from DH5α-pBAD30-OmpC-CF which is calcinated at different temperatures (400 ˚C, 500 ˚C, 600 ˚C, 700 ˚C). Each line graph shows the mean value of five experiments. The error bars were calculated by dividing the standard deviation by the square root of the number of measurements. (B) Cell viability for the positive control (C) Cell viability at 50 µg/ml of Co_3O_4 calcinated at 500°C.

2.6 Conclusion

Co is an essential mineral in the manufacturing sector. Industrial metal alloys, notably battery manufacture, relied heavily on Co. The importance of Co has grown as battery manufacturing technology has advanced. Creating a cell-surface display system for whole-cell bio-catalysis remains valuable for environmental applications. Molecule modelling and wet lab analysis must be used to ensure the display system is optimized for the optimal activity of a certain protein or peptide on the surface of cells. The cell surface display of synthesized cobalt binding peptides was used in this work to produce a high cobalt recovery technique. The anchoring motif OmpC was used to display CBP-CF on the cell surface, and the peptide recovered more cobalt than the other peptides, with an average of ≥1360 μmol/g DCW at pH 7 and 1mM Co concentration. Furthermore, FE-SEM was used to examine the morphological characteristics of cobalt attached to recombinant cells. There were reports on the characterization and prospective use of cobalt oxide nanoparticles, which were recovered from peptides, and the best oxide, which exhibited a progressive mortality rate of cancer cells. Still, the concentration for biomedical use must be researched further.

2.7 REFERENCES

1. Pourret, O. and M.-P. Faucon, Cobalt. 2018. p. 291-294.
2. Prathna, T.C., et al., Biomimetic Synthesis of Nanoparticles: Science, Technology & Applicability, in Biomimetics, M. Amitava, Editor. 2010, IntechOpen: Rijeka. p. Ch. 1.
3. Ismat, D., et al., Green and eco-friendly synthesis of cobalt-oxide nanoparticle: Characterization and photo-catalytic activity. Advanced Powder Technology, 2017. 28.
4. Jang, E., et al., Adsorption of microbial esterases on Bacillus subtilis-templated cobalt oxide nanoparticles. International Journal of Biological Macromolecules, 2014. 65: p. 188-192.
5. AbdelRahim, K., et al., Extracellular biosynthesis of silver nanoparticles using Rhizopus stolonifer. Saudi Journal of Biological Sciences, 2017. 24(1): p. 208-216.
6. Dong, H., et al., Magnetic Nanocomposite for Potential Ultrahigh Frequency Microelectronic Application. Journal of Electronic Materials, 2007. 36(5): p. 593-597.
7. Jarestan, M., et al., Preparation, characterization, and anticancer efficacy of novel cobalt oxide nanoparticles conjugated with thiosemicarbazide. 3 Biotech, 2020. 10(5): p. 230.
8. Puche, M., et al., Tuning the Catalytic Performance of Cobalt Nanoparticles by Tungsten Doping for Efficient and Selective Hydrogenation of Quinolines under Mild Conditions. ACS Catalysis, 2021. 11(13): p. 8197-8210.
9. Parkes, L.M., et al., Cobalt nanoparticles as a novel magnetic resonance contrast agent—relaxivities at 1.5 and 3 Tesla. Contrast Media & Molecular Imaging, 2008. 3(4): p. 150-156.

10. Farkaš, B., U. Terranova, and N.H. de Leeuw, The mechanism underlying the functionalisation of cobalt nanoparticles by carboxylic acids: a first-principles computational study. Journal of Materials Chemistry B, 2021. 9(24): p. 4915-4928.
11. De, D., et al., Studies on cancer cell death through delivery of dopamine as anti-cancer drug by a newly functionalized cobalt ferrite nano-carrier. Colloids and Surfaces A: Physicochemical and Engineering Aspects, 2021. 627: p. 127202.
12. Jincy, C.S. and P. Meena, Synthesis, characterization, and NH3 gas sensing application of Zn doped cobalt oxide nanoparticles. Inorganic Chemistry Communications, 2020. 120: p. 108145.
13. Vijayanandan, A.S. and R.M. Balakrishnan, Biosynthesis of cobalt oxide nanoparticles using endophytic fungus Aspergillus nidulans. Journal of Environmental Management, 2018. 218: p. 442-450.
14. Sundararaju, S., M. Arumugam, and P. Bhuyar, Microbacterium sp. MRS-1, a potential bacterium for cobalt reduction and synthesis of less/non-toxic cobalt oxide nanoparticles (Co3O4). Beni-Suef University Journal of Basic and Applied Sciences, 2020. 9(1): p. 44.
15. Mubraiz, N., et al. Microbial and Plant Assisted Synthesis of Cobalt Oxide Nanoparticles and Their Antimicrobial Activities. Agronomy, 2021. 11, DOI: 10.3390/agronomy11081607.
16. Jang, E., et al., Preparation of cobalt nanoparticles from polymorphic bacterial templates: A novel platform for biocatalysis. International Journal of Biological Macromolecules, 2015. 81: p. 747-753.
17. Iravani, S. and R.S. Varma, Sustainable synthesis of cobalt and cobalt oxide nanoparticles and their catalytic and biomedical applications. Green Chemistry, 2020. 22(9): p. 2643-2661.

18. Marimuthu, S., et al., Eco-friendly microbial route to synthesize cobalt nanoparticles using Bacillus thuringiensis against malaria and dengue vectors. Parasitology Research, 2013. 112(12): p. 4105-4112.

19. Lee, S.Y., J.H. Choi, and Z. Xu, Microbial cell-surface display. Trends in Biotechnology, 2003. 21(1): p. 45-52.

20. Ravikumar, S., et al., Construction of Copper Removing Bacteria Through the Integration of Two-Component System and Cell Surface Display. Applied Biochemistry and Biotechnology, 2011. 165(7): p. 1674-1681.

21. Bae, W., et al., Enhanced Mercury Biosorption by Bacterial Cells with Surface-Displayed MerR. Applied and Environmental Microbiology, 2003. 69(6): p. 3176-3180.

22. Bae, W., A. Mulchandani, and W. Chen, Cell surface display of synthetic phytochelatins using ice nucleation protein for enhanced heavy metal bioaccumulation. Journal of Inorganic Biochemistry, 2002. 88(2): p. 223-227.

23. Lamiable, A., et al., PEP-FOLD3: faster de novo structure prediction for linear peptides in solution and in complex. Nucleic Acids Res, 2016. 44(W1): p. W449-54.

24. Shen, Y., et al., Improved PEP-FOLD Approach for Peptide and Miniprotein Structure Prediction. Journal of Chemical Theory and Computation, 2014. 10(10): p. 4745-4758.

25. Thévenet, P., et al., PEP-FOLD: an updated de novo structure prediction server for both linear and disulfide bonded cyclic peptides. Nucleic Acids Research, 2012. 40(W1): p. W288-W293.

26. Zhang, J. and M. Dolg, ABCluster: the artificial bee colony algorithm for cluster global optimization. Physical chemistry chemical physics : PCCP, 2015. 17(37): p. 24173-24181.

27. Zhang, J. and M. Dolg, Global optimization of clusters of rigid molecules using the artificial bee colony algorithm. Physical Chemistry Chemical Physics, 2016. 18(4): p. 3003-3010.

28. Zhang, J. and V.-A. Glezakou, Global optimization of chemical cluster structures: Methods, applications, and challenges. International Journal of Quantum Chemistry, 2021. 121(7): p. e26553.

29. Frisch, M.J., et al., Gaussian 16 Rev. C.01. 2016: Wallingford, CT.

30. Stewart, J.J.P., Optimization of parameters for semiempirical methods V: Modification of NDDO approximations and application to 70 elements. Journal of Molecular Modeling, 2007. 13(12): p. 1173-1213.

31. Marenich, A.V., C.J. Cramer, and D.G. Truhlar, Universal Solvation Model Based on Solute Electron Density and on a Continuum Model of the Solvent Defined by the Bulk Dielectric Constant and Atomic Surface Tensions. The Journal of Physical Chemistry B, 2009. 113(18): p. 6378-6396.

32. Sun, X., et al., Putative copper- and zinc-binding motifs in Streptococcus pneumoniae identified by immobilized metal affinity chromatography and mass spectrometry. Proteomics, 2011. 11(16): p. 3288-3298.

33. Lee, H., et al., Peptide sequence-driven direct electron transfer properties and binding behaviors of gold-binding peptide-fused glucose dehydrogenase on electrode. iScience, 2021. 24(11): p. 103373.

34. Pramounmat, N., et al., Platinum-binding peptides: understanding of selective binding and multifunctionality. Multifunctional Materials, 2022. 5(1): p. 012002.

35. Hughes, Z.E., et al., Tuning Materials-Binding Peptide Sequences toward Gold- and Silver-Binding Selectivity with Bayesian Optimization. ACS Nano, 2021. 15(11): p. 18260-18269.

36. Cho, Y., et al. Development of Cobalt-Binding Peptide Chelate from Human Serum Albumin: Cobalt-Binding Properties and Stability. International Journal of Molecular Sciences, 2022. 23, DOI: 10.3390/ijms23020719.

37. Finney, A.R., et al., Amino Acid and Oligopeptide Effects on Calcium Carbonate Solutions. Crystal Growth & Design, 2020. 20(5): p. 3077-3092.

38. Pal Singh, R.P., I.S. Hudiara, and S. Bhushan Rana, Effect of calcination temperature on the structural, optical and magnetic properties of pure and Fe-doped ZnO nanoparticles. Materials Science-Poland, 2016. 34(2): p. 451-459.

39. Yin, X., et al., Chemical insights into the roles of nanowire cores on the growth and supercapacitor performances of Ni-Co-O/Ni(OH)2 core/shell electrodes. Scientific Reports, 2016. 6(1): p. 21566.

40. Liu, F., et al., Facile synthesis of ultrafine cobalt oxide nanoparticles for high-performance supercapacitors. Journal of Colloid and Interface Science, 2017. 505: p. 796-804.

41. Naveen, A.N. and S. Selladurai, Investigation on physiochemical properties of Mn substituted spinel cobalt oxide for supercapacitor applications. Electrochimica Acta, 2014. 125: p. 404-414.

42. Wang, X., et al., Cobalt oxide/graphene composite for highly efficient CO oxidation and its application in reducing the fire hazards of aliphatic polyesters. Journal of Materials Chemistry, 2012. 22(8): p. 3426-3431.

43. Li, W., et al., Hierarchical drug release designed Au @PDA-PEG-MTX NPs for targeted delivery to breast cancer with combined photothermal-chemotherapy. Journal of Nanobiotechnology, 2021. 19(1): p. 143.

44. Vinardell, M.P. and M. Mitjans, Antitumor Activities of Metal Oxide Nanoparticles. Nanomaterials, 2015. 5(2).

45. Goudarzi, M. and M. Salavati-Niasari, Synthesis, characterization and evaluation of Co3O4 nanoparticles toxicological effect; synthesized by cochineal dye via environment friendly approach. Journal of Alloys and Compounds, 2019. 784: p. 676-685.

46. Govindasamy, R., et al. Green Synthesis and Characterization of Cobalt Oxide Nanoparticles Using Psidium guajava Leaves Extracts and Their Photocatalytic and Biological Activities. Molecules, 2022. 27, DOI: 10.3390/molecules27175646.

47. Khan, S., et al., In vitro evaluation of anticancer and antibacterial activities of cobalt oxide nanoparticles. JBIC Journal of Biological Inorganic Chemistry, 2015. 20(8): p. 1319-1326.

48. Munteanu, C.R. and K. Suntharalingam, Advances in cobalt complexes as anticancer agents. Dalton Transactions, 2015. 44(31): p. 13796-13808.

49. Thamilarasan, V., et al., Cobalt(III) complexes as potential anticancer agents: Physicochemical, structural, cytotoxic activity and DNA/protein interactions. Journal of Photochemistry and Photobiology B: Biology, 2016. 162: p. 558-569.

50. Chattopadhyay, S., et al., Surface-modified cobalt oxide nanoparticles: new opportunities for anti-cancer drug development. Cancer nanotechnology, 2012. 3(1-6): p. 13-23.

51. Koyyati, R., K.R. Kudle, and P.R.M.J.I.j.o.p.r. Padigya, Evaluation of antibacterial and cytotoxic activity of green synthesized cobalt nanoparticles using Raphanus sativus var. longipinnatus leaf extract. 2016. 9(3): p. 466-472.

CHAPTER 3

Cobalt oxide nanoparticle synthesis by cell surface engineered recombinant *Escherichia coli* and the potential application on photocatalytic degradation of different dyes.

3.1 Abstract

The technique of Cell Surface Display engineering was employed to construct a hybrid strain of *E. coli* with the ability to bind to cobalt. The study utilised OmpC as a molecular tether to demonstrate the peptides that have an affinity for cobalt, leading to the development of a model for the resultant structure of the hybrid peptide OmpC-CBPs. The efficacy of the recombinant peptide in absorbing and retrieving cobalt at varying concentrations is subsequently evaluated. The results of the study indicate that *E. coli* (OmpC-CF2) demonstrated a notably higher cobalt recovery rate (1395 μmol/g DCW) compared to *E. coli* (OmpC-CP) under conditions of pH 7 and a metal concentration of 2 mM. The sample containing cobalt nanoparticles that were bio-adsorbed underwent thermal decomposition at a temperature of 500˚C. The morphology of the resulting thermally decomposed oxides of the cobalt nanoparticles was analysed using a variety of spectroscopy methodologies. The study revealed that the nanoparticles were restricted to metallic ions and that the utilisation of Energy Dispersive Spectroscopy (EDS) enabled the cartography of cobalt on the cellular membrane. In summary, our evaluation of the photocatalytic properties of nanoparticles has demonstrated a significant capacity for the degradation of dyes. The results suggest that the nanoparticles exhibit promising characteristics for the process of photocatalytic degradation of dyes. In summary, we successfully designed a recombinant strain of *E. coli* with high affinity towards cobalt. This resulted in synthesising nanoparticles that possess remarkable photocatalytic capabilities for dye degradation. The findings of this investigation may have significant ramifications for the progress of wastewater treatment methodologies.

3.2 Introduction

The increasing rate of urbanization and industrial expansion in the modern era has acquired drinkable water, a critical resource for the sustenance of living beings, a serious issue. The textile industry's usage of cancer-causing organic dyes has been steadily rising over the past few years, and with it, the industry's pollution of aquatic habitats through the release of effluents. (1-5)

Textile wastewater poses a significant environmental threat due to the large variety of chemicals used in the textile industry, such as dyes and additives. Most of the contaminants in textile wastewater come from the dyeing and finishing processes. Many kinds of chemicals and dyestuffs are employed in these processes. Water is commonly used as the medium for applying dyes and chemical treatments. Since they are not used in the full production process, they are discarded and cause problems with waste management. The most frequent types of pollution detected in textile wastewaters include suspended particles, chemical oxygen demand (COD), colour, acidic nature, and other soluble substances. Contaminants such as nitrogen, heavy metals, and dyestuffs are frequently found in textile effluent. (6-7)

More than 10,000 dyes are used in the fabric-making industry, but about 70% are azo dyes. In recent years, reducing the quantity of dye that remains in textile effluent after the aqueous dyeing process has been increasingly important, a major source of colour release into the environment. Because of their -N=N- chromophore, azo dyes harm plants and animals and have difficulty decomposing in nature. (8-9)

There is a growing need to find methods of processing and degrading these dyes into less hazardous substances. One of the most recent and frequently used techniques for the degradation or decolorization of organic dyes is heterogeneous advanced oxidation technology (HET.AOT) (10-13). The technique relies heavily on transferring electrons from the valence

band (VB) to the conduction band (CB) on the surface of semiconductor metal oxide nanoparticles when exposed to light of a certain wavelength. When these excitons encounter oxygen or water, they form reactive oxygen species (ROS), such as superoxide anions and hydroxyl radicals (14,15). These substances have a high oxidizing potential, making them hazardous to many materials.

The unique qualities of transition metal oxide nanoparticles inspire various cutting-edge uses (16-18). Cobalt oxide has several key applications, including as a catalyst, a gas sensor, a magnetic material, an electrochromic film substrate, a battery cathode, a heterogeneous catalytic material, a rechargeable battery, a carbon monoxide abatement catalyst, and a gas sensor (19-23). Several techniques, including physical vapour deposition, inert gas condensation, molecular beam epitaxy, chemical vapour deposition (CVD), laser ablation, the sol-gel process, and cathode sputtering, have been used to synthesise nanocrystalline materials (24). Due to its unusual characteristics, chemical stability, and simple synthesis procedure, spinel-tricobalt tetroxide (Co_3O_4), often written as CoO or Co_2O_3, has quickly become one of the most common spinel materials (26,27). In addition, CoO (rock salt) and Co_2O_6 (hexagonal cobalt oxide) are the other two families to which Co_3O_4 belongs. In the spinel structure of Co_3O_4, the p-type semiconducting Co^{2+} ions are found in the tetragonal 8(a) sites, the p-type Co^{3+} ions are found in the octahedral 16(d) sites, and the p-type O^{2-} ions are situated in the 32(e) sites in a cubic close-packed arrangement (25,28). Due to their unique physicochemical characteristics and small size, cobalt nanoparticles show significant promise as sensors for various chemical compounds (29). Literature on the microbial generation of cobalt oxide nanoparticles is limited, and most studies have only looked at the strain that is already resistant to cobalt (30-35). This is the first research to use genetically modified strains to produce cobalt oxide nanoparticles for the dye degradation application.

Cell surface display has recently been investigated as a potential new approach for tethering heavy metal-binding proteins or peptides to the exterior of bacteria. Using this method, a foreign peptide is expressed as a fusion protein with different anchoring patterns, most commonly found in proteins on the surface of cells or their fragments. *Escherichia coli* OmpC is a frequently occurring and extensively researched entity. The OmpC β-barrel structure comprises 16 antiparallel β-strands located in the transmembrane membrane. These β-strands are connected by seven internal loops and eight exterior loops, ultimately forming a large channel encircled by the structure **(16).** Although *E. coli* possesses multiple types of Omps, it is noteworthy that only the trimeric porin protein OmpC plays a crucial role in preserving the structural integrity of the cell's outer membrane. OmpC was recommended as a favorable option for CSD due to its elevated copy level of $2x10^5$ molecules per cell **(31).** The properties of the passenger and carrier proteins determine whether a C-terminal fusion, N-terminal fusion, or sandwich fusion is the best option.

This study developed a novel cobalt adsorption system by fusing cobalt-binding peptides to the C-terminus of a truncated version of the OmpC protein. The technique was used to fabricate nanoparticles of cobalt. Different methods, such as X-ray diffraction, scanning electron microscopy, energy dispersive spectroscopy, and Fourier transform infrared spectroscopy, were used to examine the cobalt nanoparticles synthesised on the surface of E. coli. Dye degradation was accomplished with the help of calcined cobalt oxide nanoparticles.

3.3 Materials and Methods

3.3.1 Bacterial strains and media

Cobalt adsorption and genetic engineering were performed using *E. coli* DH5α (Enzynomics). The bacterial strains were cultured at a temperature of 37 °C with agitation at

250 rpm in Luria-Bertani (LB) medium containing 10 g/L bacto-tryptone, 5 g/L bacto-yeast extracts, and 10 g/L sodium chloride, supplemented with an antibiotic (100 mg/L ampicillin). Table 1 contains a comprehensive inventory of the bacterial strains and plasmids employed in the present investigation.

Table 3.1 List of bacterial strains and plasmids used in this study.

Strain/Plasmid	Relevant genotype/property	source
***E. coli* strains**		
TOP 10	One Shot™ TOP10 Chemically Competent *E. coli*	Enzynomics
Plasmids		
pBAD30	Amp^R	NEB[a]
pBADCP	pBAD30 containing OmpC-CBP	This work
pBADCF2	pBAD30 containing OmpC-CBF2	This work

[a]New England Biolabs, Beverly, MA, U.S.A.

3.3.2 Cobalt Binding Domain Computational Modelling

To determine which peptide structures, have the least energy, we use the 3D generation engine of the pepfold (PEPFOLD3) peptide prediction service. This prediction tool employs a quick Markov model sub-optimal conformation sampling approach to deduce the peptide structure from the amino acid sequence. When predicting structures, the program also considers only a neutral pH. Each peptide has a set of predicted structures, and the best model is chosen for further analysis using ab initio computer modelling. We used the LEGO module of the ABCluster (version 1.5.1) package in conjunction with Gaussian16 software to locate the most favourable binding sites for the Co^{2+} ion within the peptide. You can rely on ABCluster, a program that employs the artificial bee colony (ABC) algorithm for accurate predictions of the global minimum structure. We employed a 3x3x3 three-dimensional lattice for the global

minimum search with a neighboring distance of 2.5Å. Due to the size and diversity of peptides, global minima searches were carried out at the semi-empirical PM6 level, and H atoms were held steady for the duration of the simulation. We generated around a thousand isomers of each peptide using numerous iterations of the ABCluster code until all the results converged on the same global minimum. We further optimized the global minimum structure of the peptide Co^{2+} complex and the PEPFOLD3 predicted peptide using the B3LYP functional without limitations to estimate the binding energy and related thermodynamic parameters accurately. For C, H, N, O, and S atoms, we optimized using the 6-31G basis set, while for the Co^{2+} ion, we used the LANL2DZ-ECP basis set. Optimization in water was performed using the SMD solvation model. Finally, to precisely depict the peptide's structure at neutral pH, the number of hydrogen atoms in the basic and acidic sections of the main and side chains of the amino acids forming the peptide was manually modified. In this study, the binding energies of the Co^{2+} ion with the peptide were calculated using the following equation at 298.15K and 1 atm.

$$E_{pep} + E_{Co^{2+}} - E_{pep-Co^{2+}complex}$$

The E values denote the energies of the peptide fragments, the Co^{2+} ion, and the peptide-Co^{2+} complex. The present investigation demonstrates that an elevated (favourable) numerical value denotes an intensified interaction between the cobalt ion and the peptide. In addition, a comprehensive analysis is conducted on the normal vibration modes of all optimised structures to ascertain their authenticity and eliminate any possibility of them being imaginary. This process confirms that the optimised structures are true minima, not saddle points.

3.3.3 Construction of CBP cell surface display system

The pBAD30 plasmid was modified to exhibit cobalt-binding peptides through the utilization of restriction enzymes. The C-terminus of Truncated OmpC was merged with cobalt-binding peptides. The fusion process was executed by utilising a polymerase chain

reaction (PCR) and N-Taq polymerase obtained from Enzynomics, which was conducted on a T100TM thermal cycler manufactured by Bio-Rad Laboratories located in Hercules, CA, USA. Table 2 enumerates the primers employed in the present investigation. After obtaining the recombinant plasmids, the transformation of plasmids into *E. coli* TOP10 and subsequent bacterial culture growth in LB (Luria-Bertani) medium was performed. The induction of recombinant protein OmpC- cobalt-binding peptides production was achieved through the addition of arabinose, which serves to activate the ARA_promoter.

Table 3.2 Primers used in this work.

Name	Sequence (5' to 3')
CF-F	GAATTTATGAAAGTGAAAGTGCTGAGCCTGCTG
CP-R	TTAGCGCAGTTCCACCGCTTCATGTTCGCCGGTGCTCGCGCCGCTCGGCAC TTATTTCTGCCAGCTATGAAATTCTTCCACGCCCGGATCGCGCATATAGGTC GGGTTCTGCGCGCCCGCTTTCGCCGCCGCTTCCGCCATGTTTTTGTTGAAG TAGTAGGTAGCACC
CF2-R	TTACTGCCAGCTATGAAATTCTTCCGCTTTCGCCGCCGCTTCCGCACGATCA ATCATCGGGCT

3.3.4 SDS-PAGE expression evaluation

The recombinant strain underwent overnight cultivation in an LB medium and was subsequently subjected to a 100-fold dilution in LB media for subculture. Upon reaching an OD600 nm of 0.5, varying concentrations of arabinose, ranging from 0 to 1%, were introduced into the culture medium, followed by a 6-hour incubation period. Following this, the strains that had undergone recombination were retrieved via centrifugation at a rate of 13,000 rpm for 10 mins. Subsequently, these strains were agitated in B-7M urea buffer at ambient temperature

for 30 mins. Subsequently, the supernatant underwent a process of cellular debris removal via centrifugation at a rate of 8000 rpm. The process of isolating the outer membrane fractions involved the addition of 10 mM Tris-HCl (pH 7.5) to the cell pellet, followed by overnight incubation of the suspended cells at a temperature of 4°C. Subsequently, the elevated membrane fractions underwent analysis via 12% (w/v) Sodium dodecyl-sulfate polyacrylamide gel electrophoresis (SDS-PAGE). They were subjected to staining with Coomassie brilliant blue R-250 (Bio-Rad Laboratories, Hercules, CA, USA).

3.3.5 Batch experiments of bio adsorption and Co analysis

Recombinant strains containing pBAD30 were produced at 37 °C using LB medium supplemented with 100 mg/L ampicillin and incubated overnight. The cultures that were incubated overnight were subjected to a 100-fold dilution in newly prepared LB media and were subsequently cultured until the optical density at 600 nm reached a value of 0.5. The cells were supplemented with 0.5% arabinose and maintained at 30°C for 6 hrs. Subsequently, the strains underwent centrifugation and were exposed to cobalt metal chloride solutions with concentrations varying from 0.25 mM to 2 mM. The incubation lasted 30 mins at a temperature of 30 °C while being agitated at 250 rpm. To retrieve the cobalt that was adsorbed onto the cell surface, the strains underwent a washing process using a solution of 0.85% (w/v) NaCl, followed by treatment with 0.1M HCL for 30 minutes at a temperature of 30 °C while being agitated at a speed of 200 rpm. The peptide's selectivity was evaluated through the utilisation of anticipated pollutants. The adsorption of the superior recombinant strain was analysed using an ICP-OES, while *E. coli* TOP10 was employed as a control.

3.3.6 The assessment of the attributes of cobalt nanoparticles.

The cobalt was obtained via bio adsorption and subsequently subjected to a calcination process at a temperature of 500°C. The calcination process commences after a 12-hour incubation period of arabinose-induced cells in a metal chloride solution. Subsequently, the cells are subjected to a 24 hrs water bath at 80 °C in the presence of cobalt-bound cells, followed by centrifugation to obtain the metal-bound cell pellets. The sample underwent freeze-drying at a temperature of -80°C, followed by calcination of the resulting pellets in a furnace at 500°C. Subsequently, calcined oxide specimens were subjected to various characterization techniques, including FE-SEM, XRD, EDS, and FTIR.

3.3.7 Photocatalytic Studies

Assessing the photocatalytic efficacy of synthesised cobalt oxide nanoparticles involved the degradation of dyes in an aqueous solution while being exposed to visible light irradiation. Approximately 10 mg of catalyst was introduced into a dye solution of 100 ml, with a concentration of 10 ppm. The suspension comprising of dyes and catalyst underwent stirring for 20 mins under dark conditions to attain adsorption-desorption equilibrium of the dyes on the material's surface. Subsequently, the suspension underwent exposure to visible light irradiation while continuously agitated at predetermined intervals. Approximately 3 ml of the solution was extracted and centrifuged at 10000 rpm for 5 mins to eliminate the catalysts. The resulting supernatant clear solution was subsequently analysed using a UV–vis spectrophotometer, with absorbance λmax being recorded for the respective dyes. The calculation of the degradation percentage (%D) was performed utilising the following formula: $\%D = ((A_0 - A_t) / A_0) * 100$. Here, A_0 represents the initial concentration of the dye before irradiation, while A_t denotes the concentration of the dye at the time of illumination. Time was denoted as “t”.

3.4 Results and Discussion

3.4.1 Computational modelling of cobalt binding domain

To predict the most favourable sites for cobalt ion (Co^{2+}) binding, two small peptide fragments, CF1 (PTYMRDP) & CF2 (EEFHSWQ), were chosen from the M(X)8H motifs (GAQNPTYMRDPGVEEFHSWQK) present in the CP peptide. The most favourable binding sites for individual peptide fragments were determined using ABCluster and density functional theory (DFT) calculations Figure 1. The sulphur atom of methionine exhibits the highest binding energy for Co^{2+} in the CF1 peptide fragment. The measured binding energies are situated within the range of 1.3 eV. The range of 2.5 Å has been identified as the optimised distance between the S and Co atoms. The CF2 peptide fragment demonstrates a significant inclination for coordination with Co^{2+}. This coordination is most pronounced when Co^{2+} interacts with three oxygen atoms from two adjacent amino acids. The CF2 peptide fragment exhibits a notable binding energy (3.12 eV) with a pair of glutamic acid constituents, particularly with the Co^{2+}. The peptide fragments under consideration demonstrate the ability to bind with the Co^{2+} ion through the oxygen atoms in a nearly tetrahedral coordination. The mean separation distance of Co-O has been estimated to be around 2.1 Å. The peptide complex CF2 demonstrates an average binding energy between Co^{2+} and oxygen atoms within the 1.04 - 1.13 eV range.

3.4.2 Developing cobalt-binding peptide-displaying system

The pBAD30 plasmid was utilised to construct pBADCP and pBADCF2 using cloning the OmpC-C) and OmpC-CF2, respectively, with SacI and XbaI restriction enzymes. The truncated OmpC protein was used as a fusion partner for the peptides attached to the protein's C-terminus of the 8th loop (993 bp). An extra linker (AEAAAKA) was incorporated to improve

the cell surface display's stability. The peptides CP (GAQNPTYMRDPGVEEFHSWQK) and CF2 (EEFHSWQ) were conjugated to OmpC via the polymerase chain reaction. The pBADCP plasmids were regulated by the arabinose promoter. In general, the expression of a heterologous protein in E. coli results in metabolic instability. Consequently, the expression of proteins, cellular proliferation, and durability of the recombinant plasmid are all diminished. Identifying optimal growth and expression conditions is a crucial factor. The impact of varying arabinose concentrations and culture temperatures was assessed. The optimisation of OmpC-CP peptide expression involves adjusting the arabinose concentration within the range of 0.0 - 1.0% and the temperature within 20°C – 35°C. The expression levels of the recombinant peptides, OmpC-CP, were subsequently assessed through SDS-PAGE analysis (as shown in Fig. 2B). The most favourable expression was observed at an arabinose concentration of 0.05%. A negative correlation was observed between the levels of expression and the concentrations of arabinose while conducting cobalt adsorption experiments at different temperatures, revealing that a higher temperature resulted in greater adsorption of cobalt. The maximum cobalt adsorption was recorded at 30°C with a cobalt chloride concentration of 1 mM, yielding 1050 µmol/g DCW.

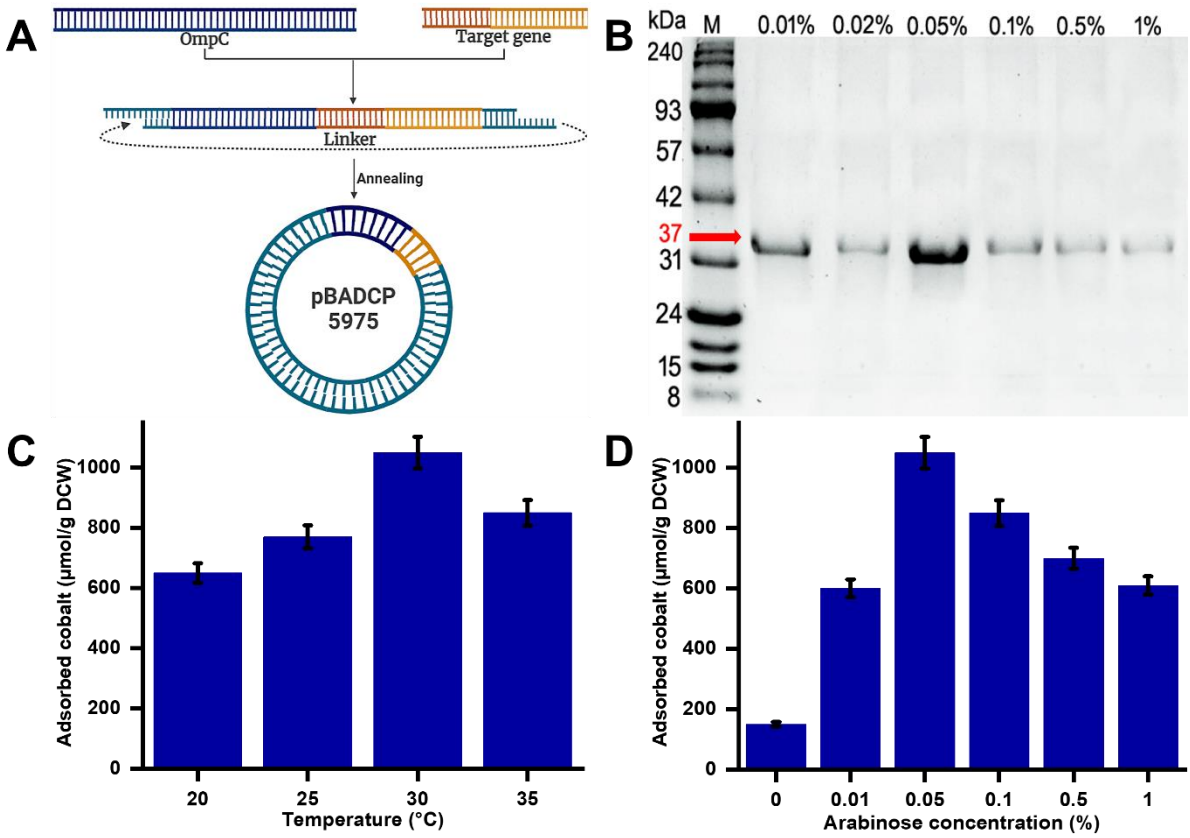

Fig. 3.2 Construction of cobalt binding peptide fused with OmpC at pBAD30 and optimization of its expression conditions. (A) Plasmid construction of cobalt binding peptide fused with OmpC at pBAD30 (B) SDS-PAGE analysis of recombinant protein *E. coli* (pBADCP) (37 kDa). (C) The effect of temperature towards cobalt recovery on *E. coli* (pBADCP) with 1mM $CoCl_2$. (D) The effect of arabinose concentration towards cobalt recovery on *E. coli* (pBADCP) with 1mM $CoCl_2$.

3.4.3 Cobalt bio-adsorption and analysis

An evaluative comparison of the adsorption capacity between the original cobalt binding peptide CP and the recently discovered cobalt binding peptide CF2 was conducted. The bacterial strains *E. coli* DH5α, *E. coli* (pBADCP), and *E. coli* (pBADCF2) were subjected to culture under different concentrations of $CoCl_2$ (ranging from 0.25 mM to 2 mM) at a pH of 7. Upon incubation of strains in a 2mM cobalt solution, it was observed that the recombinant

E. coli (pBADCF2) exhibited an absorption of 1395 μmol/g DCW of cobalt, whereas *E. coli* (pBADCP) exhibited an absorption of 1124 μmol/g DCW of cobalt, as depicted in Figure 3C. The adsorption of cobalt increased as the concentration of cobalt in the medium was raised from 0.25 mM to 2 mM. The results indicate that the cobalt adsorption capacity of *E. coli* (pBADCF2) is superior to that of *E. coli* (pBADCP). The *E. coli* DH5α of the wild-type array exhibited minimal cobalt adsorption.

The present study involved the analysis of recombinant strain *E. coli* (pBADCF2) using FE-SEM and EDS techniques after cobalt absorption. The primary objective of this analysis was to visualise the adsorbed metallic element and determine its structural characteristics. Following adsorption, the cells underwent a rinsing and lyophilization process for examination via FE-SEM. The utilisation of FE-SEM analysis revealed the existence of nanoparticles on the surface of recombinant *E. coli* (pBADCF2) after cobalt adsorption at a concentration of 2 mM cobalt solution, as depicted in Figure 3D. According to the findings obtained from the FE-SEM analysis, it can be inferred that the cobalt nanoparticles, which exhibited a size distribution within the range of 10 to 50 nm, were predominantly adhered to the cellular wall.

Identifying cobalt nanoparticles in the strains was possible by detecting Co Kα1 and Co Kβ1 spectral peaks at 6.931 keV and 7.649 keV, respectively, using EDS. The wild-type strain of *E. coli* (TOP10) did not exhibit the formation of nanoparticles on the cell wall. Conversely, the recombinant *E. coli* strain displayed the presence of bright cobalt salt nanoparticles on the surface of its membrane. The findings of the cobalt adsorption investigation suggest that the surface of the cell wall of recombinant *E. coli* contains numerous binding sites for cobalt ions. Ionic species present on the cellular membrane have the potential to undergo chemical reactions leading to the formation of inorganic compounds that exhibit precipitation from the surrounding solution. These locations have the potential to mass ions in a confined area,

augment surface coverage, and facilitate ion clustering, ultimately resulting in the generation of solid nanoparticles on the cellular membrane.

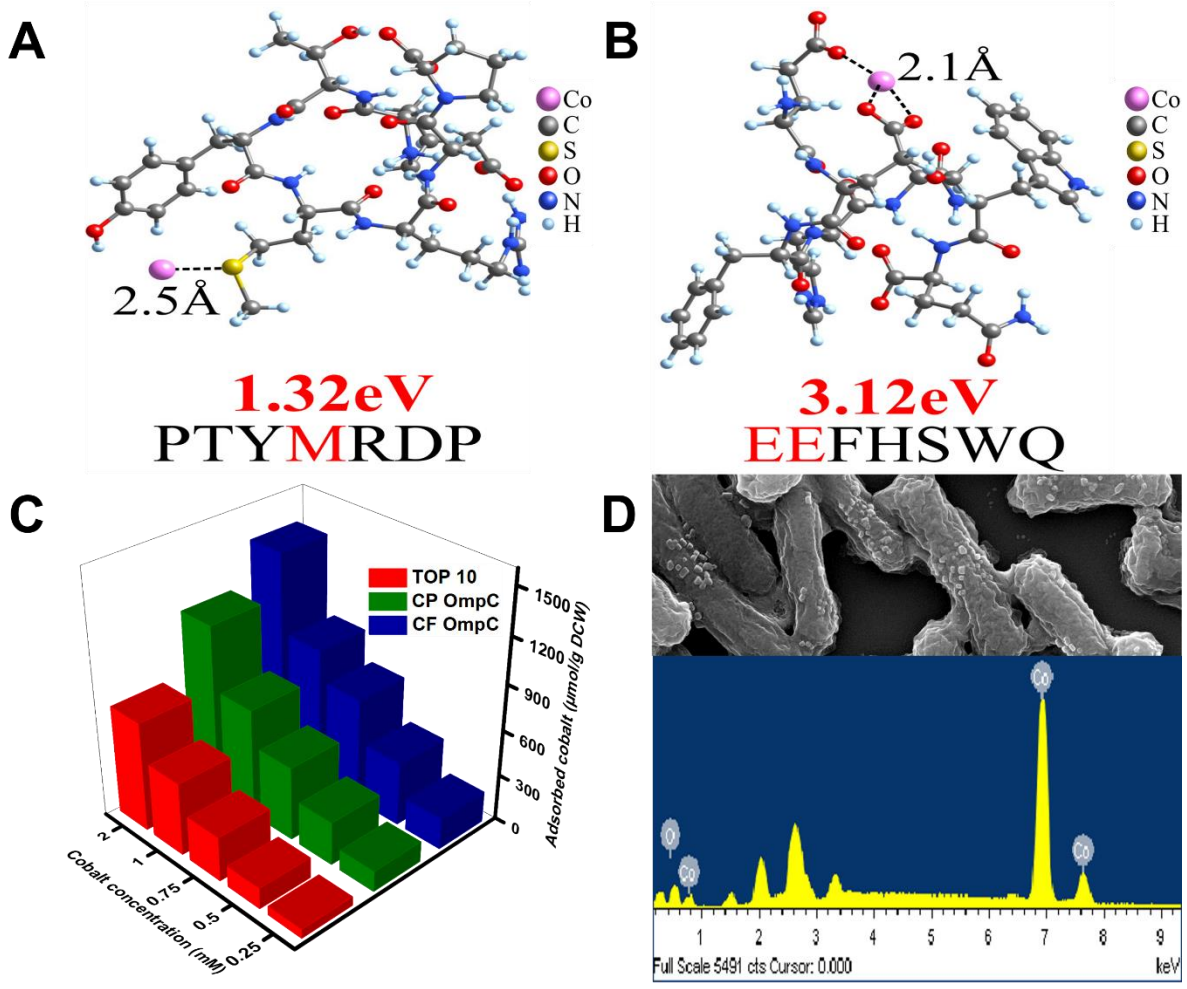

Fig. 3.3 The DFT optimized structure of Co^{2+} with peptide fragment TGEHEAV. The best binding sites and binding energy (eV) are shown in red. The average binding distances (Å) of cobalt atoms with nearby binding sites are shown in black. (A) CF1 (PTYMRDP) (B) CF2 (EEFHSWQ) (C) The adsorption of cobalt by the *E. coli* (pBADCP & pBADCF2) with different concentrations ranges from 0.25mM to 2mM. (D) FE-SEM and EDS analysis for *E. coli* (pBADCF2)

3.4.4 Synthesis of Cobalt oxide nanoparticles and their characterization

Cobalt oxide nanoparticles were produced at a temperature of 500 °C by calcining a cobalt-adsorbed *E. coli* (pBADCF2) strain. This was done to eliminate any impurities or volatile compounds. At a higher temperature, the metal samples can be converted into oxides. After that process, the oxide nanoparticles can be collected and examined using FE-SEM, EDS, XRD, and FTIR.

3.4.4.1 FE-SEM and EDS

The technique of Scanning Electron Microscopy (SEM) is employed for the characterization and analysis of the morphology of oxidized materials. The morphology of the produced powders can be determined through the utilization of SEM. The cobalt-precipitated particles exhibit a heterogeneous morphology characterized by diverse sizes and shapes. Upon aggregation, these particles manifest a spherical morphology. A significant proportion of the particles exhibited a near-spherical morphology with a diameter ranging from 100 to 150 nm. Certain groups exhibit a substantial size, characterized by a dense aggregation of diminutive particles, whereas others are comparatively diminutive. Despite the compact arrangement of particles, it is possible for there to exist interstices and minuscule apertures within any given product grouping. The observed pattern irregularity indicates the presence of both nanoparticles and microparticles interlinked within the product. The observed sample exhibits a lack of particle arrangement from its deep bulk to the surface, resulting in an uneven array of nanoparticles in its morphology.

The energy-dispersive X-ray spectroscopy (EDS) spectra of thermally treated nanoparticles are depicted in Figure 4A. According to the EDS spectra, the Co_3O_4 sample that was synthesized is predominantly composed of Co and O constituents. The initial spectral peak of element O is detected at an energy level of 0.5 keV, while the emergence of Co is observed at Co Kα1 with an energy level of 6.931 keV and Co Kβ1 with an energy level of 7.649 keV

[38][39]. The product under investigation exhibited cobalt and oxygen elements, with an observed Co/O atomic ratio of approximately 3/3.97. This ratio aligns with the anticipated value for Co_3O_4. The image depicts the high level of purity exhibited by Co_3O_4 nanoparticles.

3.4.4.2 XRD (X-ray Diffraction)

The crystal structure was classified through the employment of X-ray diffraction (XRD) utilizing a model Xpert 3 and Cu Kα radiation (λ = 1.54 A°) within the 10°-90° range of 2θ. The polycrystalline nature of the cobalt oxide film is demonstrated in Figure 4B. The diffraction patterns of the Co_3O_4 samples display characteristic peaks at specific angles, namely (18.73, 31.4, 36.8, 38.3, 44.9, 55.66, 59.3, and 65.3), which correspond to the (220, 311, 222, 400, 422, 511 and 440) crystalline structure of the Co_3O_4 phase with a three-dimensional spinel configuration. This observation indicates the successful formation of the Co_3O_4 cubic phase with a crystal-like structure.

3.4.4.3 FT-IR spectroscopy

The functional group shifts of oxidized cobalt nanoparticles were illustrated by studying the calcinated particles at various temperatures using FT-IR, as depicted in Figure 4C. The peak observed at 3431 cm^{-1} is attributed to the stretching vibration mode of the O–H functional group. The band observed at 1623 cm^{-1} was found to be associated with the angular distortion of water molecules upon absorption. The peak observed at 1023 cm^{-1} was attributed to the C-O stretching vibrations. The observed peak at 2371 cm^{-1} can be attributed to the anomalous vibration of the (C=O) bond in CO_2, which was acquired from the surrounding atmosphere during the thermal annealing of metal oxides. The Fourier-transform infrared (FTIR) spectra of all oxide samples exhibited identical characteristic peaks to those of pure cobalt oxide (PCO), suggesting a similar chemical bonding behaviour. The spectral features observed at 566 cm^{-1} and 665 cm^{-1} are likely attributed to OB3 and ABO vibrations,

respectively. These vibrations correspond to B - Co^{3+} in an octahedral site and A–Co^{2+} in a tetrahedral site within the Co_3O_4 spinel matrix.

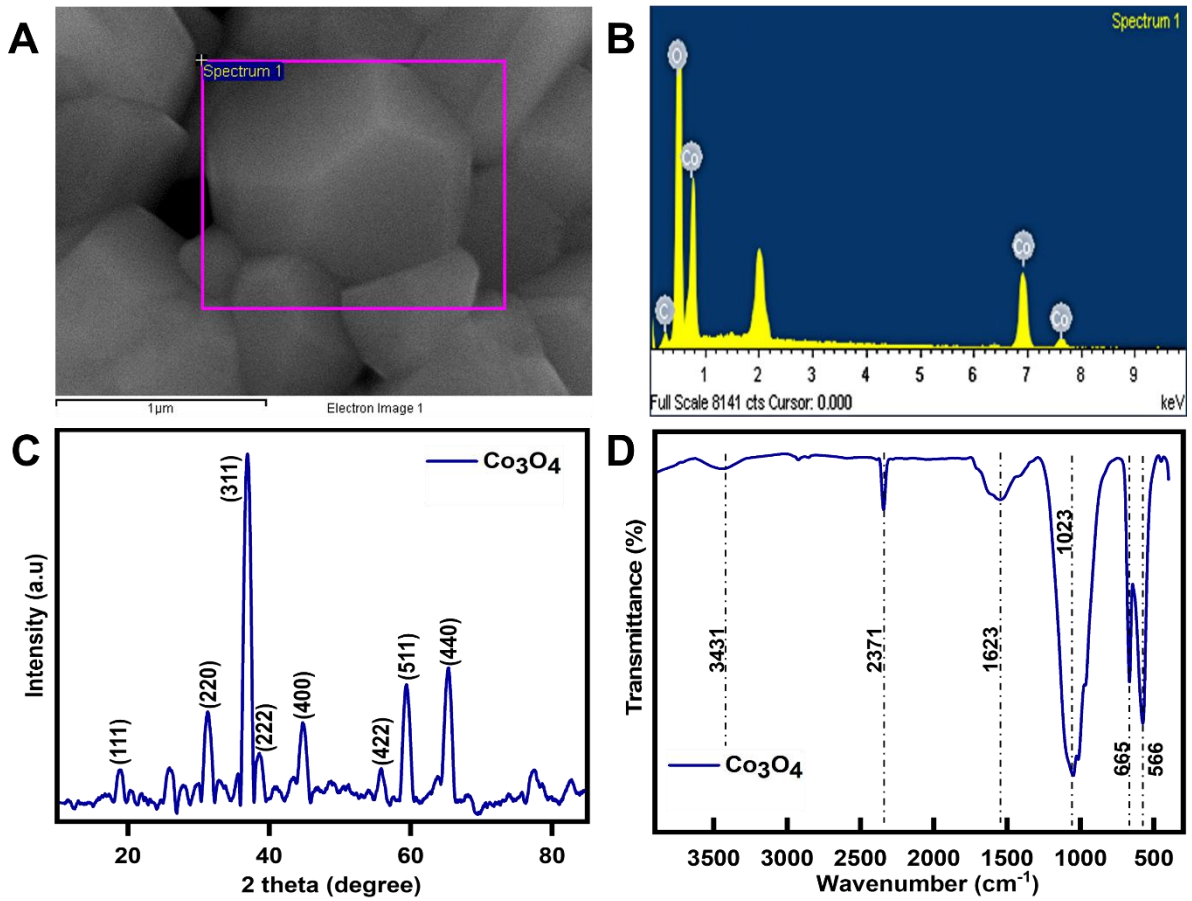

Fig. 3.4 (A) FE-SEM for *E. coli* (pBADCF2) recovered cobalt oxide nanoparticles, calcinated at 500˚C. (B) EDS for *E. coli* (pBADCF2) recovered cobalt oxide nanoparticles, calcinated at 500˚C. An *E. coli* (pBADCF2) recovered cobalt's calcinated samples at 500 ˚C. (C) X-ray diffraction. (D) FT-IR spectrum.

Photocatalytic dye degradation activity of Co_3O_4 nanoparticles.

3.5 Dye degradation mechanism

The utilization of dyes is a prevalent practice in various industries, such as textile, leather goods, and furniture, among others, to produce items. Approximately 12% of the dye is lost during the manufacturing process, specifically during the dying stage, with approximately

20% of this waste being released into the environment. During the process of dye degradation, the chemical breakdown of the comparatively large dye molecules results in the formation of smaller molecules. The procedure is employed to decontaminate perilous waste. The original dye's colour is attributed to the by-products of water, carbon dioxide, and minerals produced during the process, and in the process of dying, it is observed that not all the dye molecules are consumed. During industrial release, a certain proportion of dye molecules are present in the wastewater. The molecules' colouration underwent a permanent alteration. Photocatalysis is a contemporary technique that is extensively utilized for disintegrating dye during the degradation process. The process primarily entails the conversion of electrons from the valence band to the conduction band of the semiconductor surface upon exposure to a suitable wavelength of visible light.

3.5.1 Photocatalytic dye degradation activity of Co_3O_4 nanoparticles on Rhodamine B, Methyl violet 2B, Methylene blue tetrahydrate, Coomassie Brilliant Blue G-250 and Trypan blue.

The present study investigated the degradation of Rhodamine B (RhB) (λ = 568 nm), Methyl violet (MV) (λ = 587 nm), Methylene blue tetrahydrate (MBT) (λ = 670 nm), Coomassie Brilliant blue G-250 (CBB) (λ = 595 nm) and Trypan blue (TB) (λ = 600 nm) dyes using Co3O4 nanoparticles as a photocatalyst under visible light irradiation. The results presented in Figure 5 indicate that the absorbance of RhB, MV, MBT, CBB, and TB dyes decreased the duration of visible light irradiation in the presence of photocatalyst. After 120 mins of irradiation, the degradation percentages of RhB, MV, MBT, CBB, and TB were determined to be 93.83%, 92.68%, 90.84%, 78.64%, and 76.64%, respectively. The degradation efficiency is primarily contingent upon the crystalline structure, distinct splitting of charges, and surface pattern.

The Co_3O_4 photocatalyst exhibits photocatalytic activity upon exposure to visible light. The process of the reaction mechanism commences with the excitation of electrons from the valence band (VB) towards the conduction band (CB), thereby creating a vacancy in the VB. The VB-generated perforations concomitantly engage with the surface-bound water molecule or hydroxyl ion, forming hydroxyl radicals ($^{\bullet}OH$). Upon immediate contact, the electrons in the conduction band situated on the surface of the nanoparticles undergo a reaction with the dissolved oxygen molecule, forming superoxide radicals ($^{\bullet}O_2^-$). The electron-hole pair recombination was avoided through the involvement of $^{\bullet}O_2^-$ in the oxidation process, thereby preserving electron neutrality within the photocatalyst. The production of hydrogen peroxide (H_2O_2) occurred through the process of protonation of hydroperoxyl radicals, followed by the dissociation of H_2O_2, which subsequently generated $^{\bullet}OH$ radicals. The Co_3O_4 nanoparticles generate a potent oxidizing agent in the form of reactive species that proceeds to initiate an attack on the dye molecules. The reactive species attack the organic dye molecules, leading to their mineralization and subsequent water molecules and carbon dioxide formation. The photodegradation mechanism of RhB, MV, MBT, CBB, and TB dyes is primarily governed by the reactive species $^{\bullet}OH$ and $^{\bullet}O_2^-$. The findings indicate that the Co_3O_4 nanoparticles that were prepared demonstrate favourable photocatalytic efficacy of approximately 90% upon exposure to visible light for RhB, MV, and MBT dyes, and 70% for CBB and TB dyes.

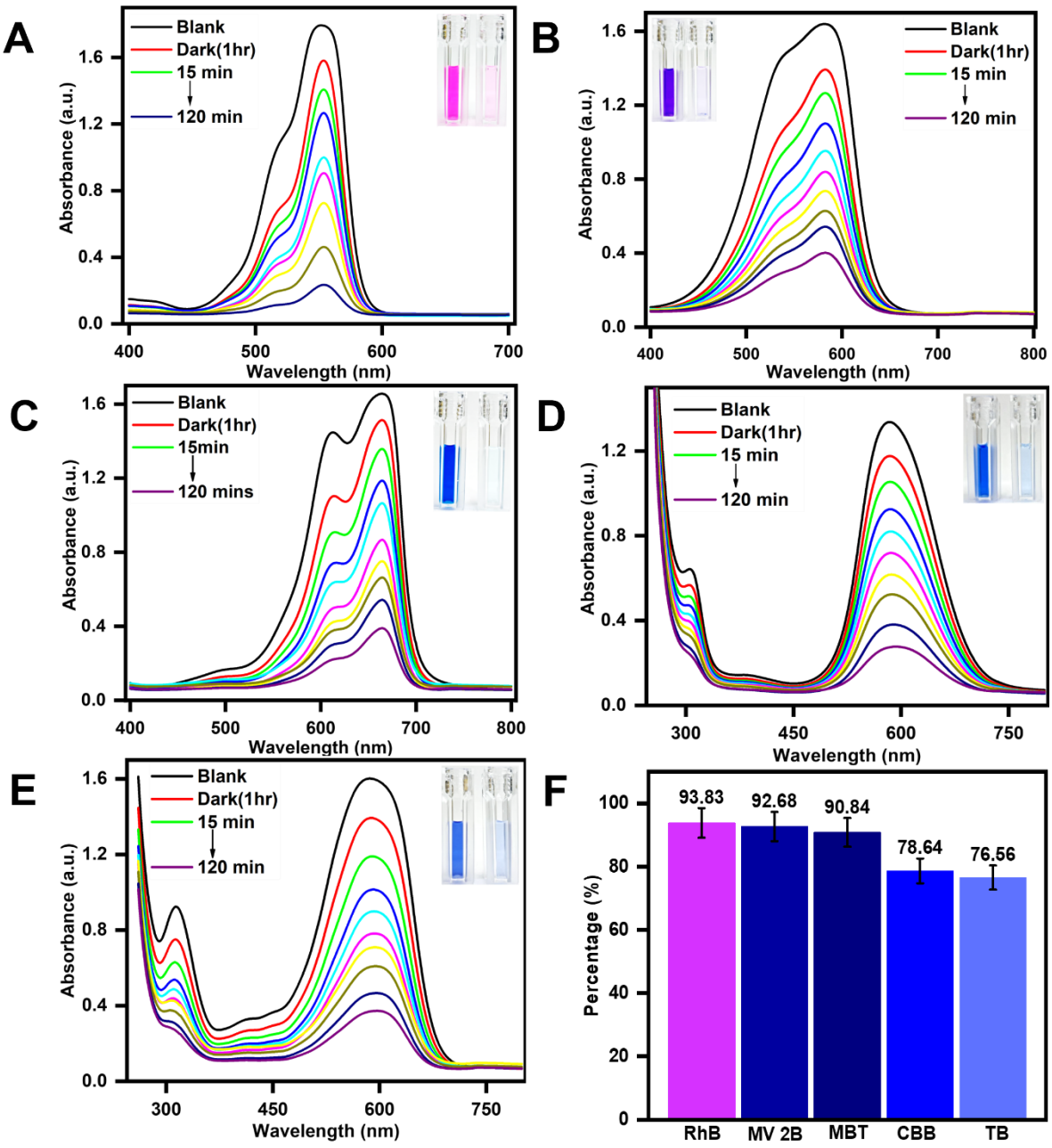

Fig. 3.5 Photocatalytic dye degradation activity of Co_3O_4 nanoparticles from *E. coli* (pBADCF2) oxidised at 500 ˚C. (A)Rhodamine B (B)Methyl violet 2B (C)Methylene blue tetrahydrate (D) Coomassie Brilliant Blue G 250 (E)Trypan blue (F) Percentage of dye degradation.

3.6 Conclusion

The synthesis of cobalt oxide nanoparticles using recombinant bacteria has been found to have various applications, including but not limited to photocatalytic degradation of dye, catalysts for batteries, and utilisation in medical sectors. Using whole-cell biocatalysts to produce cobalt oxide nanoparticles with a cell-surface display system holds significant value in environmental applications. The optimisation of a peptide's activity on cell surfaces was ensured through the utilisation of both molecular modelling and wet lab analysis techniques. In this study, cobalt-binding peptides were synthesised and displayed on the cell surface using the anchoring motif OmpC. The displayed peptides were used to display *E. coli* pBADCF2 on the cell surface, resulting in a higher cobalt recovery compared to other peptides. The average cobalt recovery was 1395 μmol/g DCW at a pH of 7 and a concentration of 2 mM cobalt chloride solution. In addition, Field Emission Scanning Electron Microscopy (FE-SEM) and EDS were employed to investigate the morphological features of cobalt affixed to genetically modified cells. The present study focused on the characterization and potential application of cobalt oxide nanoparticles obtained through the calcination of peptides. The optimal oxide was identified at a temperature of 500 °C and exhibited a gradual degradation of various dyes.

References

1. A.C. Pradhan, T. Uyar, Morphological Control of Mesoporosity and Nanoparticles within Co3O4–CuO Electrospun Nanofibers: Quantum Confinement and Visible Light Photocatalysis Performance, ACS Applied Materials & Interfaces, 9 (2017) 35757-35774.
2. S. Vadivel, B. Saravanakumar, M. Kumaravel, D. Maruthamani, N. Balasubramanian, A. Manikandan, G. Ramadoss, B. Paul, S. Hariganesh, Facile solvothermal synthesis of BiOI microsquares as a novel electrode material for supercapacitor applications, Materials Letters, 210 (2018) 109-112.
3. S. Asiri, M. Sertkol, S. Guner, H. Gungunes, K.M. Batoo, T.A. Saleh, H. Sozeri, M.A. Almessiere, A. Manikandan, A. Baykal, Hydrothermal synthesis of CoyZnyMn1-2yFe2O4 nanoferrites: Magneto-optical investigation, Ceramics International, 44 (2018) 5751-5759.
4. A.T. Ravichandran, J. Srinivas, R. Karthick, A. Manikandan, A. Baykal, Facile combustion synthesis, structural, morphological, optical and antibacterial studies of Bi1−xAlxFeO3 ($0.0 \leq x \leq 0.15$) nanoparticles, Ceramics International, 44 (2018) 13247-13252.
5. R. Ahmadi, M. Imani, A. Tadjarodi, Microwave assisted synthesis of CoFe₂O₄ nanoparticles by utilizing organic promoters and evaluation of its properties, 2020.
6. S. Erdemoğlu, S.K. Aksu, F. Sayılkan, B. İzgi, M. Asiltürk, H. Sayılkan, F. Frimmel, Ş. Güçer, Photocatalytic degradation of Congo Red by hydrothermally synthesized nanocrystalline TiO2 and identification of degradation products by LC–MS, Journal of Hazardous Materials, 155 (2008) 469-476.

7. J. Wang, T. Ma, Z. Zhang, X. Zhang, Y. Jiang, D. Dong, P. Zhang, Y. Li, Investigation on the sonocatalytic degradation of parathion in the presence of nanometer rutile titanium dioxide (TiO2) catalyst, Journal of Hazardous Materials, 137 (2006) 972-980.
8. K. Melghit, M.S. Al-Rubaei, I. Al-Amri, Photodegradation enhancement of Congo red aqueous solution using a mixture of SnO2·xH2O gel/ZnO powder, Journal of Photochemistry and Photobiology A: Chemistry, 181 (2006) 137-141.
9. H. Lachheb, E. Puzenat, A. Houas, M. Ksibi, E. Elaloui, C. Guillard, J.-M. Herrmann, Photocatalytic degradation of various types of dyes (Alizarin S, Crocein Orange G, Methyl Red, Congo Red, Methylene Blue) in water by UV-irradiated titania, Applied Catalysis B: Environmental, 39 (2002) 75-90.
10. S. Jessl, J. Rongé, D. Copic, M.A. Jones, J. Martens, M. De Volder, Honeycomb-shaped carbon nanotube supports for BiVO4 based solar water splitting, Nanoscale, 11 (2019) 22964-22970.
11. C.V. Reddy, I.N. Reddy, K.R. Reddy, S. Jaesool, K. Yoo, Template-free synthesis of tetragonal Co-doped ZrO2 nanoparticles for applications in electrochemical energy storage and water treatment, Electrochimica Acta, 317 (2019) 416-426.
12. K.R. Reddy, C.H.V. Reddy, M.N. Nadagouda, N.P. Shetti, S. Jaesool, T.M. Aminabhavi, Polymeric graphitic carbon nitride (g-C3N4)-based semiconducting nanostructured materials: Synthesis methods, properties and photocatalytic applications, Journal of Environmental Management, 238 (2019) 25-40.
13. N.L. Reddy, V.N. Rao, M. Vijayakumar, R. Santhosh, S. Anandan, M. Karthik, M.V. Shankar, K.R. Reddy, N.P. Shetti, M.N. Nadagouda, T.M. Aminabhavi, A review on frontiers in plasmonic nano-photocatalysts for hydrogen production, International Journal of Hydrogen Energy, 44 (2019) 10453-10472.

14. E. Haque, Y. Yamauchi, V. Malgras, K.R. Reddy, J.W. Yi, M.S.A. Hossain, J. Kim, Nanoarchitectured Graphene-Organic Frameworks (GOFs): Synthetic Strategies, Properties, and Applications, Chemistry – An Asian Journal, 13 (2018) 3561-3574.
15. C. Zhang, Y. Li, D. Shuai, Y. Shen, W. Xiong, L. Wang, Graphitic carbon nitride (g-C3N4)-based photocatalysts for water disinfection and microbial control: A review, Chemosphere, 214 (2019) 462-479.
16. P. Durán, J. Tartaj, C. Moure, Fully Dense, Fine-Grained, Doped Zinc Oxide Varistors with Improved Nonlinear Properties by Thermal Processing Optimization, Journal of the American Ceramic Society, 86 (2003) 1326-1329.
17. J. Wang, L. Gao, Photoluminescence Properties of Nanocrystalline ZnO Ceramics Prepared by Pressureless Sintering and Spark Plasma Sintering, Journal of the American Ceramic Society, 88 (2005) 1637-1639.
18. M. Mazaheri, A.M. Zahedi, M.M. Hejazi, Processing of nanocrystalline 8mol% yttria-stabilized zirconia by conventional, microwave-assisted and two-step sintering, Materials Science and Engineering: A, 492 (2008) 261-267.
19. M.I. Shliomis, A.F. Pshenichnikov, K.I. Morozov, I.Y. Shurubor, Magnetic properties of ferrocolloids, Journal of Magnetism and Magnetic Materials, 85 (1990) 40-46.
20. C. Bergemann, D. Müller-Schulte, J. Oster, L. à Brassard, A.S. Lübbe, Magnetic ion-exchange nano- and microparticles for medical, biochemical and molecular biological applications, Journal of Magnetism and Magnetic Materials, 194 (1999) 45-52.
21. C.-B. Wang, C.-W. Tang, S.-J. Gau, S.-H. Chien, Effect of the surface area of cobaltic oxide on carbon monoxide oxidation, Catalysis Letters, 101 (2005) 59-63.
22. C.-B. Wang, H.-K. Lin, C.-W. Tang, Thermal Characterization and Microstructure Change of Cobalt Oxides, Catalysis Letters, 94 (2004) 69-74.

23. F. Grillo, M.M. Natile, A. Glisenti, Low temperature oxidation of carbon monoxide: the influence of water and oxygen on the reactivity of a Co3O4 powder surface, Applied Catalysis B: Environmental, 48 (2004) 267-274.
24. S.A. Needham, G.X. Wang, H.K. Liu, Synthesis of NiO nanotubes for use as negative electrodes in lithium ion batteries, Journal of Power Sources, 159 (2006) 254-257.
25. X. Wang, W. Tian, T. Zhai, C. Zhi, Y. Bando, D. Golberg, Cobalt(ii,iii) oxide hollow structures: fabrication, properties and applications, Journal of Materials Chemistry, 22 (2012) 23310-23326.
26. N.M. Basith, J.J. Vijaya, L.J. Kennedy, M. Bououdina, S. Jenefar, V. Kaviyarasan, Co-Doped ZnO Nanoparticles: Structural, Morphological, Optical, Magnetic and Antibacterial Studies, Journal of Materials Science & Technology, 30 (2014) 1108-1117.
27. L.F. Liotta, H. Wu, G. Pantaleo, A.M. Venezia, Co3O4 nanocrystals and Co3O4–MOx binary oxides for CO, CH4 and VOC oxidation at low temperatures: a review, Catalysis Science & Technology, 3 (2013) 3085-3102.
28. H. Singh, A.K. Sinha, M.N. Singh, P. Tiwari, D.M. Phase, S.K. Deb, Spectroscopic and structural studies of isochronally annealed cobalt oxide nanoparticles, Journal of Physics and Chemistry of Solids, 75 (2014) 397-402.
29. C.S. Jincy, P. Meena, Synthesis, characterization, and NH3 gas sensing application of Zn doped cobalt oxide nanoparticles, Inorganic Chemistry Communications, 120 (2020) 108145.
30. A.S. Vijayanandan, R.M. Balakrishnan, Biosynthesis of cobalt oxide nanoparticles using endophytic fungus Aspergillus nidulans, Journal of Environmental Management, 218 (2018) 442-450.
31. S. Sundararaju, M. Arumugam, P. Bhuyar, Microbacterium sp. MRS-1, a potential bacterium for cobalt reduction and synthesis of less/non-toxic cobalt oxide

nanoparticles (Co3O4), Beni-Suef University Journal of Basic and Applied Sciences, 9 (2020) 44.

32. N. Mubraiz, A. Bano, T. Mahmood, N. Khan, Microbial and Plant Assisted Synthesis of Cobalt Oxide Nanoparticles and Their Antimicrobial Activities, in: Agronomy, 2021.
33. E. Jang, H.-W. Shim, B.H. Ryu, D.R. An, W.K. Yoo, K.K. Kim, D.-W. Kim, T.D. Kim, Preparation of cobalt nanoparticles from polymorphic bacterial templates: A novel platform for biocatalysis, International Journal of Biological Macromolecules, 81 (2015) 747-753.
34. S. Iravani, R.S. Varma, Sustainable synthesis of cobalt and cobalt oxide nanoparticles and their catalytic and biomedical applications, Green Chemistry, 22 (2020) 2643-2661.
35. S. Marimuthu, A.A. Rahuman, A.V. Kirthi, T. Santhoshkumar, C. Jayaseelan, G. Rajakumar, Eco-friendly microbial route to synthesize cobalt nanoparticles using Bacillus thuringiensis against malaria and dengue vectors, Parasitology Research, 112 (2013) 4105-4112.
36. S.Y. Lee, J.H. Choi, Z. Xu, Microbial cell-surface display, Trends in Biotechnology, 21 (2003) 45-52.
37. P.-S. Li, H.-C. Tao, Cell surface engineering of microorganisms towards adsorption of heavy metals, Critical Reviews in Microbiology, 41 (2015) 140-149.
38. I.A. Rodionova, Y. Gao, J. Monk, Y. Hefner, N. Wong, R. Szubin, H.G. Lim, D.A. Rodionov, Z. Zhang, M.H. Saier, B.O. Palsson, A systems approach discovers the role and characteristics of seven LysR type transcription factors in Escherichia coli, Scientific Reports, 12 (2022) 7274.
39. X.-m. Lin, M.-j. Yang, H. Li, C. Wang, X.-X. Peng, Decreased expression of LamB and Odp1 complex is crucial for antibiotic resistance in Escherichia coli, Journal of Proteomics, 98 (2014) 244-253.

40. M. Vahed, F. Ramezani, V. Tafakori, V.S. Mirbagheri, A. Najafi, G. Ahmadian, Molecular dynamics simulation and experimental study of the surface-display of SPA protein via Lpp-OmpA system for screening of IgG, AMB Express, 10 (2020) 161.
41. M. Lukas, R. Schwidetzky, A.T. Kunert, E.H.G. Backus, U. Pöschl, J. Fröhlich-Nowoisky, M. Bonn, K. Meister, Interfacial Water Ordering Is Insufficient to Explain Ice-Nucleating Protein Activity, The Journal of Physical Chemistry Letters, 12 (2021) 218-223.
42. B. Liang, L. Han, Displaying of acetylcholinesterase mutants on surface of yeast for ultra-trace fluorescence detection of organophosphate pesticides with gold nanoclusters, Biosensors and Bioelectronics, 148 (2020) 111825.
43. D.-Y. Tsai, Y.-J. Tsai, C.-H. Yen, C.-Y. Ouyang, Y.-C. Yeh, Bacterial surface display of metal binding peptides as whole-cell biocatalysts for 4-nitroaniline reduction, RSC advances, 5 (2015) 87998-88001.
44. Z. Xu, S.Y. Lee, Display of polyhistidine peptides on the Escherichia coli cell surface by using outer membrane protein C as an anchoring motif, Applied and Environmental Microbiology, 65 (1999) 5142-5147.
45. N. Cruz, S. Le Borgne, G. Hernández-Chávez, G. Gosset, F. Valle, F. Bolivar, Engineering the Escherichia coli outer membrane protein OmpC for metal bioadsorption, Biotechnology Letters, 22 (2000) 623-629.

CHAPTER 4

Cobalt oxide nanoparticle synthesis by cell surface engineered recombinant *Escherichia coli* and the potential application on photocatalytic degradation of Norfloxacin.

4.1 ABSTRACT

This research will examine the binding affinity of peptides interacting with cobalt ions and their practical applications. Four peptide sequences showed cobalt ion binding selectivity. Computer modeling and density functional theory simulations found the best peptide binding locations. Note that methionine-containing peptides bind cobalt ions, forming strong coordination complexes. Experimentally, these peptides and their source sequences were examined for cobalt adsorption. E. coli peptides adsorb cobalt differently. The species with the highest cobalt adsorption potential was E. coli (YiaT-CF4). The recent investigation also shown that these peptides favor cobalt over nickel and manganese. In E. coli cultures that expressed these peptides, cobalt levels were consistently greater than nickel and manganese. The study characterized cobalt oxide nanoparticles calcined from cobalt-ingested E. coli cells. FE-SEM, EDS, XRD, and UV-DRS showed that Co3O4 nanoparticles with well-defined crystalline structures were produced. The study also examined norfloxacin photocatalytic degradation with Co3O4. The catalyst broke norfloxacin well in the study. This efficiency depends on catalyst concentration and pH. The findings illuminate cobalt-binding peptides, their specific affinity for cobalt, and the prospective use of cobalt-absorbing nanoparticles in environmental and biotechnological settings. This study advances our understanding of metal-specific peptide interactions and their potential effects in industrial and environmental settings.

Keywords: Adsorption, cobalt binding peptides, selectivity, nanoparticles, drug degradation.

4.2 Introduction

In recent years, the issue of emerging contaminants (ECs) in wastewater has garnered increasing attention within the scientific community and environmental sector. These ECs represent a novel category of pollutants, encompassing various substances such as medicinal chemicals, illegal drugs, and surfactants [1,2]. Among the ECs, antibiotics have emerged as a significant concern due to their extensive use in modern medicine. Antibiotics, including

norfloxacin (NOX), are now recognized as the third most prescribed pharmaceuticals, constituting over 6% of the general prescription medications [3]. Their widespread application extends across various species, from humans to fowl, cattle, fish, and swine, making them a ubiquitous component of wastewater effluents. In wastewater treatment plant effluents, norfloxacin concentrations are typically measured in (mg/L), while it is detected in surface water, groundwater, and drinking water at levels as low as (ng/L) [4–6]. The indiscriminate release of antibiotics into the natural environment has increased their prevalence in aquatic ecosystems, resulting in profound consequences for marine organisms. These consequences encompass alterations in developmental patterns and survival rates among aquatic species [7,8]. Moreover, antibiotics in wastewater have raised a critical concern about developing bacterial resistance. This phenomenon poses significant implications not only for human health but also for the overall ecological balance of aquatic ecosystems [9].

Among the antibiotics, norfloxacin (NOX) belongs to the class of fluoroquinolones and is extensively employed in both human and veterinary medicine. NOX finds widespread use in treating Gram-positive and Gram-negative bacterial infections, notably for conditions such as prostatitis and urinary tract infections [10,11]. Consequently, NOX has become a prominent pharmaceutical agent in the medical field. Given the prevalent use of antibiotics, including NOX, in healthcare facilities, animal husbandry, and wastewater treatment systems, their release into the environment has become unavoidable [12]. Consequently, detecting NOX in sedimentary deposits and waterways has become a concerning issue [13]. The challenges posed by the widespread presence of antibiotics, including NOX, in wastewater are compounded by the fact that most conventional wastewater treatment facilities are ill-equipped to remove these pharmaceutical compounds effectively. Consequently, a significant proportion of NOX-contaminated effluents can be released into water bodies and the surrounding environment as post-treatment effluent [8]. This uncontrolled discharge has raised alarm bells within the

scientific community and the environmental sector, highlighting the urgent need for viable removal strategies.

The escalating concern over NOX contamination in aquatic environments has galvanized researchers, particularly those working in aquatic science and environmental protection, to explore innovative approaches for removing NOX from aqueous solutions. The necessity of addressing this issue is underscored by its potential adverse effects on aquatic ecosystems and its implications for human health. As such, developing and implementing effective NOX removal techniques have become paramount in safeguarding our natural surroundings and ensuring the sustainability of water resources.

Removing NOX from wastewater has emerged as a critical research focus, exploring diverse wastewater treatment methods. These methodologies encompass various techniques, each aiming to degrade or eliminate NOX to mitigate its presence in aquatic environments. Notable among the methods investigated for NOX removal from wastewater are adsorption [14,15], membrane filtration [16], adsorption-photocatalytic processes [17], coagulation [18], electrocoagulation [19–21], photo-Fenton processes [22], electro-Fenton techniques [23], photocatalyst-based approaches [24], and sonocatalytic methods [25].

Furthermore, biomaterials and biological methods have garnered considerable attention for their potential to reclaim water contaminated with pharmaceuticals, including NRFX [26-29]. Among these approaches, the most promising advanced oxidation process is photocatalytic degradation [30-33], which relies on various innovative composite nano-photocatalysts, proving to be highly effective and sustainable for the removal and mineralization of persistent organic contaminants [34-36]. The photocatalytic degradation technique has demonstrated exceptional efficacy in treating norfloxacin-contaminated water media [37].

Photocatalysis, as a method, is particularly favourable for eliminating pharmaceutical pollutants due to its environmentally friendly, clean, and efficient nature [38]. This technique holds promise in addressing the persistent challenge of antibiotic contamination in wastewater, offering a sustainable and effective solution.

Nanotechnology has revolutionized various fields of science and technology, with transition metal oxide nanoparticles emerging as a focal point of research due to their distinctive properties and versatile applications [39-41]. Cobalt oxide (Co_3O_4) is notable for its wide array of applications, including catalysts, gas sensors, magnetic materials, electrochromic film substrates, battery cathodes, heterogeneous catalytic materials, rechargeable batteries, carbon monoxide abatement catalysts, and gas sensors [42-46]. Researchers have utilised various synthesis approaches to create nanocrystalline cobalt oxide materials. These techniques include physical vapour deposition, inert gas condensation, molecular beam epitaxy, chemical vapour deposition, laser ablation, sol-gel procedures, and cathode sputtering [47]. This study focuses on spinel-tricobalt tetroxide (Co_3O_4), denoted as CoO or Co_2O_3. This compound is important due to its distinctive characteristics, notable chemical stability, and easily reproducible synthesis methods, contributing to its widespread use as a spinel material [48,49].

In addition, it is worth noting that Co_3O_4 is a member of the spinel family, which includes CoO (rock salt) and Co_2O_6 (hexagonal cobalt oxide) [50]. The crystal structure of Co_3O_4 consists of Co^{2+} ions, which exhibit p-type semiconducting behaviour, occupying tetragonal 8(a) sites. Additionally, p-type Co^{3+} ions are in octahedral 16(d) sites, while p-type O^{2-} ions are grouped in a cubic close-packed arrangement within the 32(e) sites [51]. Cobalt nanoparticles provide notable promise as sensors for various chemical substances due to their distinctive physicochemical properties and nanoscale size [52]. It is worth noting that literature about the microbial synthesis of cobalt oxide nanoparticles is scarce. Most existing studies have

concentrated on investigating naturally occurring cobalt-resistant strains [53-58]. The current investigation signifies a groundbreaking endeavour in employing genetically engineered strains to produce cobalt oxide nanoparticles, specifically focusing on their potential use in degrading dyes.

Recently, there has been a growing interest in utilising cell surface display (CSD) technology as an innovative method for immobilising heavy metal-binding proteins or peptides on the outer surface of bacterial cells. The methodology employed involves the expression of exogenous peptides as fusion proteins, commonly utilising cell surface proteins or fragments as anchoring motifs. The outer membrane protein (YiaT) of *Escherichia coli*, a commonly encountered bacteria, is a possibility for comprehensive investigation in CSD. Significantly, within the assortment of outer membrane proteins found in *E. coli*, the trimeric porin protein YiaT is crucial in upholding the structural integrity of the cell's outer membrane. The selection of C-terminal fusion, N-terminal fusion, or sandwich fusion is contingent upon the characteristics of the passenger and carrier proteins, as each arrangement presents unique benefits in the context of cell surface display.

This study devised a novel cobalt adsorption system by integrating cobalt-binding peptides onto the C-terminus of a shortened form of the YiaT protein. The aforementioned methodology was employed in the production of cobalt nanoparticles. Various analytical techniques were employed to investigate the cobalt oxide nanoparticles derived from the calcinated cobalt product on the surface of *E. coli*. These techniques included X-ray diffraction, scanning electron microscopy, energy dispersive spectroscopy, and Fourier transform infrared spectroscopy. The breakdown of NOX was achieved by using calcined cobalt oxide nanoparticles.

4.3 Materials and Methods

4.3.1 Bacterial strains and media

The Cobalt adsorption and genetic engineering experiments utilized the *E. coli* DH5α (Enzynomics) bacterial strain. The cultivation of these bacterial strains took place at a temperature of 37 °C with continuous agitation at 250 rpm. The culture medium employed for this purpose was Luria-Bertani (LB) medium, which consisted of 10 g/L bacto-tryptone, 5 g/L bacto-yeast extracts, and 10 g/L sodium chloride. An antibiotic (100 mg/L ampicillin) was added to the medium to ensure appropriate selection pressure. A detailed list of the bacterial strains and plasmids employed in this study can be found in Table 1.

Table 1 List of bacterial strains and plasmids used in this study.

Strain/Plasmid	Relevant genotype/property	source
***E. coli* strains**		
DH5α	One Shot™ DH5α Chemically Competent *E. coli*	Enzynomics
Plasmids		
pBAD30	Amp^R	NEB[a]
pBADCP1	pBAD30 containingYiaT-CBP1	This work
pBADCP2	pBAD30 containingYiaT-CBP2	This work
pBADCF1	pBAD30 containingYiaT-CBF1	This work
pBADCF2	pBAD30 containing YiaT-CBF2	This work
pBADCF3	pBAD30 containingYiaT-CBF3	This work
pBADCF4	pBAD30 containingYiaT-CBF4	This work

[a]New England Biolabs, Beverly, MA, U.S.A.

4.3.2 Cobalt Binding Domain Computational Modelling

The pepfold (PEPFOLD3) (59-61) peptide prediction server's 3D generation engine is used to predict the lowest energy structures of peptides. PEPFOLD3 employs a rapid Markov model sub-optimal conformation sampling method to forecast peptide structures based on their amino acid sequences, assuming a neutral pH. Among the predicted structures, the most suitable model for each peptide is selected for further analysis through ab initio computational modeling. To identify the optimal binding sites for the Co^{2+} ion within the peptide, the LEGO module of the ABCluster (version 1.5.1) package (62-64), in conjunction with Gaussian16 software (65), is employed. The ABCluster package utilizes the artificial bee colony (ABC) algorithm, known for its reliability in predicting global minima structures. A 3×3×3 three-dimensional lattice with a neighboring distance of 2.5Å is used for global minima search. Given the peptide's size and the possible conformers, global minima searches are conducted using the semiempirical PM6 level (66), with H atoms fixed throughout each simulation. For reliability, multiple runs of the ABCluster code are performed until a substantial number of total isomers (approximately 1000 for each peptide) are generated, and all simulations converge to the same global minima.

To accurately predict binding energy and related thermodynamic parameters, the global minima structure of the peptide-Co^{2+} complex and the PEPFOLD3-predicted peptide are optimized using the B3LYP functional (65) without constraints. The optimization employs the 6-31G basis set for C, H, N, O, and S atoms, while the LANL2DZ-ECP basis set is selected for the Co^{2+} ion. The SMD solvation model (67)is applied for optimization in an aqueous medium. The number of hydrogen atoms in the peptide structures is manually adjusted in both the basic and acidic regions of the main and side chains of the constituent amino acids to describe the peptide's structure at a neutral pH. The binding energies of the Co2+ ion with the peptide, as

reported here, are calculated at a temperature of 298.15K and a pressure of 1 atm using the following equation:

$$E_{pep} + E_{Co^{2+}} - E_{pep-Co^{2+}complex}$$

The E values represent the energy levels associated with the peptide fragments, the Co^{2+} ion, and the peptide-Co^{2+} complex. The current study illustrates that a higher numerical value indicates a greater interaction between the cobalt ion and the peptide. Furthermore, a thorough examination is performed on the normal vibration modes for all optimised structures to verify their validity and exclude any potential existence of fictitious modes. This procedure aims to validate that the optimised structures are global minima rather than transition states.

4.3.3 Construction of CBP cell surface display system

The pBAD30 plasmid was subjected to genetic modification to include cobalt-binding peptides in its structure, employing restriction enzymes to facilitate this process. The C-terminus of Truncated YiaT was fused with cobalt-binding peptides. The fusion procedure used a polymerase chain reaction (PCR) and N-Taq polymerase sourced from Enzynomics. The PCR was carried out on a T100TM thermal cycler produced by Bio-Rad Laboratories in Hercules, CA, USA. Table 2 presents a comprehensive list of the primers utilized in the current study. Following the acquisition of the recombinant plasmids, introducing these plasmids into E. coli DH5α cells, known as transformation, was carried out. Subsequently, the bacterial culture was cultivated in LB (Luria-Bertani) medium to facilitate growth. The creation of recombinant protein YiaT-cobalt-binding peptides was induced by the presence of arabinose, which functioned as an activator for the ARA_promoter.

Table 2 Primers used in this work.

Name	Sequence (5' to 3')
CF-F	GAATTTATGAAAGTGAAAGTGCTGAGCCTGCTG
CP1_R	TTAGCGCAGTTCCACCGCTTCATGTTCGCCGGTGCTCGCGCCGCTCGGCAC TCTAGATTTCTGCCAGCTATGAAATTCTTCCACGCCCGGATCGCGCATATAG GTCGGGTTCTGCGCGCCACGATCAATCATCGGG
CF1_R	TCTAGATTACGGATCGCGCATATAGGTCGGCGCTTTCGCCGCCGCTTCCGCA CGATCAATCATCGGGCT
CF2_R	TCTAGATTACTGCCAGCTATGAAATTCTTCCGCTTTCGCCGCCGCTTCCGCA CGATCAATCATCGGGCT
CP2_R	TCTAGAGCGCAGTTCCACCGCTTCATGTTCGCCGGTGCTCGCGCCGCTCGG CACCATG
CF3_R	TCTAGATTAGCTCGGCACCATGCCCGCTTTCGCCGCCGCTTCCGCACGATC AATCATCGGGCT
CF4_R	TCTAGATTACACCGCTTCATGTTCGCCCGCTTTCGCCGCCGCTTCCGCACGA TCAATCATCGGGCT

4.3.4 SDS-PAGE expression evaluation

The recombinant strain was subjected to an overnight incubation in an LB medium, after which it was diluted 100-fold in LB medium for subsequent cultivation. After attaining an optical density (OD) of 0.5 at a wavelength of 600 nm, diverse amounts of arabinose (ranging from 0% to 1%) were introduced to the culture. Subsequently, the culture was incubated for 5 hr, subjecting it to temperatures ranging from 20 °C to 35 °C. Subsequently, the strains that underwent recombination were segregated using centrifugation at a speed of 13,000 rpm for 10 min. The chosen strains were afterward combined with a B-7M urea buffer

and subjected to agitation at ambient temperature for 30 min. Subsequently, the liquid fraction was centrifuged at 8000 rpm to eliminate cellular debris. To obtain the outer membrane fractions, a 10 mM Tris-HCl (pH 7.5) solution was added to the cell pellet and incubated overnight at 4 °C. Afterwards, the membrane fractions were subjected to analysis using a 12% (w/v) Sodium dodecyl-sulfate polyacrylamide gel electrophoresis (SDS-PAGE) method and afterward stained with Coomassie brilliant blue R-250 (Bio-Rad Laboratories, Hercules, CA, USA).

4.3.5 Batch experiments of bio adsorption and Co analysis

Recombinant strains harbouring the pBAD30 plasmid were cultivated at 37 °C in a Luria-Bertani (LB) medium supplemented with 100 mg/L of ampicillin. The cultures were cultured for an extended period, expressly overnight. The cultures that underwent incubation for one night were diluted by a factor of 100 in freshly prepared LB media. These diluted cultures were then cultivated until the optical density at a wavelength of 600 nm reached a value of 0.5. The cells were provided with a 0.5% arabinose supplement and incubated at 30 °C for 6 hr. Following this, the bacterial strains were centrifugated and treated to solutions containing cobalt metal chloride at different concentrations ranging from 0.25 mM to 3 mM. The incubation period lasted for 30 min, at a temperature of 30 °C, with continuous agitation at a speed of 250 rpm. To recover the cobalt that had been adsorbed onto the surface of the cells, the strains were subjected to a washing procedure utilising a solution containing 0.85% (w/v) sodium chloride (NaCl). This was followed by treatment with hydrochloric acid (HCl) at a concentration of 0.1 M for 30 min, at a temperature of 30 °C, with agitation at 200 rpm. The adsorption intensity of the peptide was assessed by employing expected contaminants. The adsorption of the high-quality recombinant strain was analysed using an Inductively Coupled Plasma Optical Emission Spectroscopy (ICP-OES) technique, with *E. coli* DH5α being utilised as a control. The selectivity of recombinant strains was assessed by subjecting them to varying

doses (ranging from 0.25mM to 1mM) of cobalt (Co), nickel (Ni), and manganese (Mn) at a pH of 7.

4.3.6 The assessment of the attributes of cobalt nanoparticles.

The cobalt was acquired through bio adsorption and calcinated at a temperature of 500 °C. The calcination process initiates during a 12 hr incubation period of arabinose-induced cells in a metal chloride solution. Following this, the cells are exposed to a 24-hour immersion in a water bath at a temperature of 80 °C, in the company of cobalt-attached cells. Subsequently, centrifugation is performed to acquire the cell pellets bound to the metal. The provided sample was subjected to freeze-drying at -80 °C, followed by the calcination of the resultant pellets in a furnace operating at 500 °C. Following that, the calcined oxide samples underwent a range of characterisation procedures, such as field emission scanning electron microscopy (FE-SEM), energy-dispersive spectroscopy (EDS), X-ray diffraction (XRD), and UV-DRS analysis.

4.3.7 Photocatalytic Studies

The photocatalytic degradation of NOX was conducted within a glass vessel, utilising a 50 mg catalyst in a 50 mL solution containing 10 mg/L of NOX. The experiment was performed under ambient atmospheric conditions. Each instance of photocatalytic degradation experimentation was performed under uninterrupted magnetic stirring and exposure to a pair of tungsten-halogen lamps. The mixed suspension was subjected to stirring in a dark environment for 60 min to establish an equilibrium state of adsorption and desorption before exposure to light. At regular intervals, an approximate volume of 5 mL of the suspension was collected and afterwards subjected to centrifugation at a speed of 5000 revolutions per minute for 10 mins. The obtained clear suspension was subsequently analysed using a UV–vis spectrophotometer to determine the absorbance of NOX at its peak wavelength of 278 nm.

4.4 Results and Discussion

4.4.1 Computational modelling of cobalt binding domain

Four reduced-sized peptide fragments were initially selected to anticipate the optimal locations for cobalt ion (Co^{2+}) binding. All four pieces are selected based on two major co-binding peptide motifs, specifically CP1 (M(X)8H) and CP2 (M(X)9H) (68) documented. The initial pair of peptides, specifically CF3 (GMVPSGA) and CF4 (TGEHEAV), are segments derived from M(X)9H, while the subsequent pair, namely CF1 (PTYMRDP) and CF2 (EEFHSWQ), constitute components of the M(X)8H motifs. **Figure 1** illustrates the optimal binding locations for four peptide segments, as determined using our ABCluster4–6 and density functional theory (DFT) calculations. The two peptide segments containing methionine, GMVPSGA and PTYMRDP **(Figure 1a-b),** exhibit the highest binding energy of Co^{2+} with the sulphur atom of methionine. The binding energies fall within the range of approximately 1.2-1.3 eV. The figure presented in **Figure 1a-b** demonstrates that the optimal spacing between S and Co atoms is within the range of 2.5-2.7 Å. The peptide segments TGEHEAV and EEFHSWQ exhibit a notable affinity for Co^{2+} ions, as their strong coordination with three oxygen atoms derived from adjacent amino acids. The oxygen atoms of glycine and glutamic acid have the highest binding energy (3.38 eV) in the case of TGEHEAV. In the context of EEFHSWQ, it is seen that the cobalt ion exhibits the most significant binding energy (3.12 eV) when interacting with two glutamic acid components. In the case of both peptide segments, the Co^{2+} ion forms coordination bonds with the oxygen atoms in a near tetrahedral arrangement. The average distance between the cobalt ion and the oxygen atoms is around 2.0 Å, as depicted in **Figure 1 c-d**. The average binding energy of Co^{2+} with oxygen atoms in TGEHEAV and EEFHSWQ peptide complexes falls within the 1.04−1.13 eV range.

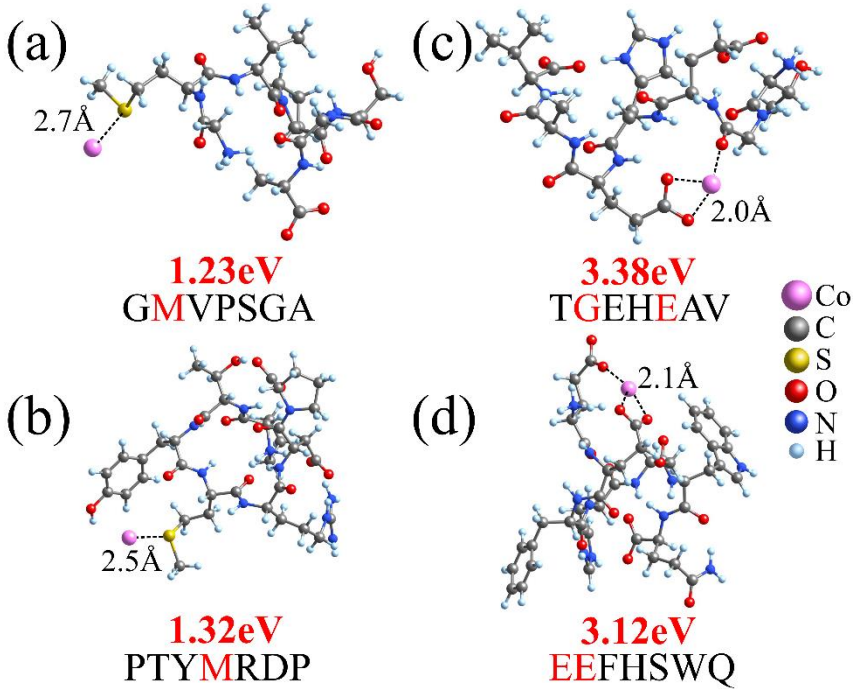

Fig 4.2. The DFT optimized structure of Co^{2+} with peptide fragments a) GMVPSGA b) PTYMRDP c) TGEHEAV and d) EEFHSWQ. The best binding sites and binding energy (eV) are shown in red. The average binding distances (Å) of cobalt atoms with nearby binding sites are shown in black.

4.4.2 Developing cobalt-binding peptide-displaying system

The pBAD30 plasmid was utilized to construct pBADCP and pBADCP2 by cloning the YiaT-CP1 and YiaT-CP2 and its fragments with SacI and XbaI restriction enzymes. The truncated YiaT protein was used as a fusion partner for the peptides attached to the protein's C-terminus. An extra linker (AEAAAKA) was incorporated to improve the cell surface display's stability. The peptides CP peptides and their fragments were conjugated to YiaT via the polymerase chain reaction. The pBADCP plasmids were regulated by the arabinose promoter. In general, the expression of a heterologous protein in *E. coli* results in metabolic instability. Consequently, the expression of proteins, cellular proliferation, and durability of

the recombinant plasmid are all diminished. Identifying optimal growth and expression conditions is a crucial factor. The impact of varying arabinose concentrations and culture temperatures was assessed. The optimisation of YiaT-CP peptide expression involves adjusting the arabinose concentration within the range of 0.0 - 1.0% and the temperature within 20 °C – 35 °C. The expression levels of the recombinant peptides, YiaT-CP, were subsequently assessed through SDS-PAGE analysis (as shown in Fig. 2B). The most favourable expression was observed at an arabinose concentration of 0.05%. A negative correlation was observed between the levels of expression and the concentrations of arabinose while conducting cobalt adsorption experiments at different temperatures, revealing that a higher temperature resulted in greater adsorption of cobalt. The maximum cobalt adsorption was recorded at 30 °C with a cobalt chloride concentration of 1 mM, yielding 1050 µmol/g DCW.

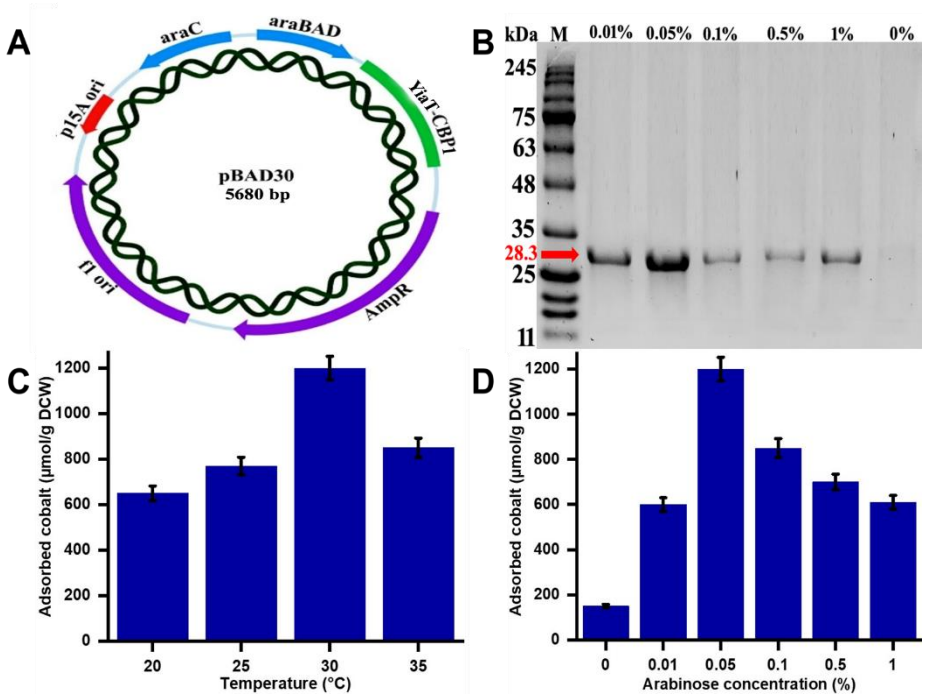

Fig. 4.2 Construction of cobalt binding peptide fused with YiaT at pBAD30 and optimization of its expression conditions. (A) Plasmid construction of cobalt binding peptide fused with OmpC at pBAD30 (B) SDS-PAGE analysis of recombinant protein *E.*

***coli* (pBADCP1) (37 kDa). (C) The effect of temperature towards cobalt recovery on *E. coli* (pBADCP1) with 1mM $CoCl_2$. (D) The effect of arabinose concentration towards cobalt recovery on *E. coli* (pBADCP1) with 1mM $CoCl_2$.**

4.4.3 Cobalt bio-adsorption and analysis

A comparative evaluation was carried out to assess the adsorption capability of the original cobalt binding peptide CP1 and CP2 and the subsequently identified cobalt binding fragments CF1, CF2, CF3, and CF4. The bacterial strains *E. coli* (DH5α), *E. coli* (YiaT-CP1), *E. coli* (YiaT-CF1), *E. coli* (YiaT-CF2), *E. coli* (YiaT-CP2), *E. coli* (YiaT-CF3), and *E. coli* (YiaT-CF4) were subjected to induction using varying amounts of $CoCl_2$ (ranging from 0.25 mM to 3 mM) at a pH of 7.

When comparing the cobalt adsorption capacities of *E. coli* (YiaT-CF1) and *E. coli* (YiaT-CF2) with *E. coli* (YiaT-CP1), it is apparent that *E. coli* (YiaT-CP1) YiaT demonstrates a cobalt adsorption capacity of 1267 μmol/g DCW, whereas *E. coli* (YiaT-CF1) YiaT exhibits a slightly lower cobalt adsorption capacity of 1223 μmol/g DCW at a cobalt concentration of 2 mM. This implies that the cobalt adsorption capability of *E. coli* (YiaT-CF1) YiaT is slightly lower than its *E. coli* (YiaT-CP1) counterpart. Comparably, it has been observed that *E. coli* (YiaT-CP2) exhibits a greater capacity for adsorbing cobalt, reaching 1524 μmol/g DCW at a cobalt concentration of 2 mM. This performance surpasses *E. coli* (YiaT-CF2), demonstrating a slightly lower cobalt adsorption rate of 1464 μmol/g DCW at the exact cobalt dosage of 2 mM. When comparing the cobalt adsorption rates of *E. coli* (YiaT-CF3) and *E. coli* (YiaT-CF4) in the presence of *E. coli* (YiaT-CP2), it was seen that *E. coli* (YiaT-CF3) exhibited a cobalt adsorption rate of 1471 μmol/g DCW for a cobalt concentration of 2 mM. This finding suggests that *E. coli* (YiaT-CF3) is highly effective in binding cobalt. Nevertheless, it is worth noting that among all strains, *E. coli* (YiaT-CF4) has the maximum cobalt adsorption capacity at a concentration of 2 mM cobalt, with a value of 1865 μmol/g DCW. This finding highlights the

superior ability of *E. coli* (YiaT-CF4) to adsorb cobalt ions. Upon careful evaluation of all strains, it becomes apparent that *E. coli* (YiaT-CF4) is the most efficient strain, demonstrating the maximum cobalt adsorption capacity. Conversely, *E. coli* (YiaT-CF1) displays the lowest potential for cobalt adsorption. In addition, it has been observed that *E. coli* (YiaT-CP2) exhibits superior cobalt adsorption capabilities compared to *E. coli* (YiaT-CP1), potentially influencing the choice of strains for diverse applications.

This work examines the affinity of peptides for cobalt compared to other elements, specifically nickel and manganese, by examining their specificity. The focus of our inquiry revolves around four discrete strains of *E. coli* (YiaT-CF1), *E. coli* (YiaT-CF2), *E. coli* (YiaT-CF3), and *E. coli* (YiaT-CF4). The cobalt concentration for *E. coli* (YiaT-CF1) is measured at 745 µmol/g DCW, whilst the quantities of nickel and manganese are recorded as 50 µmol/g DCW and 28 µmol/g DCW, respectively. In the instance of *E. coli* (YiaT-CF2), it is shown that the concentration of cobalt significantly rises to 985 µmol/g DCW, suggesting a greater affinity for cobalt in comparison to nickel (41 µmol/g DCW) and manganese (14 µmol/g DCW). The *E. coli* strain YiaT-CF3 demonstrates a cobalt concentration of 895 µmol/g DCW, which exceeds nickel concentrations (60 µmol/g DCW) and manganese (20 µmol/g DCW). This finding further highlights the selectivity of these peptides towards cobalt. The most notable finding arises from the study of *E. coli* (YiaT-CF4), in which the cobalt concentration reaches 1177 µmol/g DCW. This indicates a significant preference for cobalt compared to other elements, as seen by the lower concentrations of nickel (46 µmol/g DCW) and manganese (16 µmol/g DCW). In brief, it can be concluded that the four strains, namely *E. coli* (YiaT-CF1), *E. coli* (YiaT-CF2), *E. coli* (YiaT-CF3), and *E. coli* (YiaT-CF4), demonstrate a discernible preference for cobalt in comparison to nickel and manganese. The results of this study shed light on the unique capacity of these peptides, with a specific emphasis on *E. coli* (YiaT-CF4), to selectively absorb cobalt rather than nickel and manganese. The results highlight the

potential practicality of these strains in situations where there is a need for targeted metal absorption or elimination. As a result, they represent intriguing contenders for further investigation in the realms of biotechnology and environmental research.

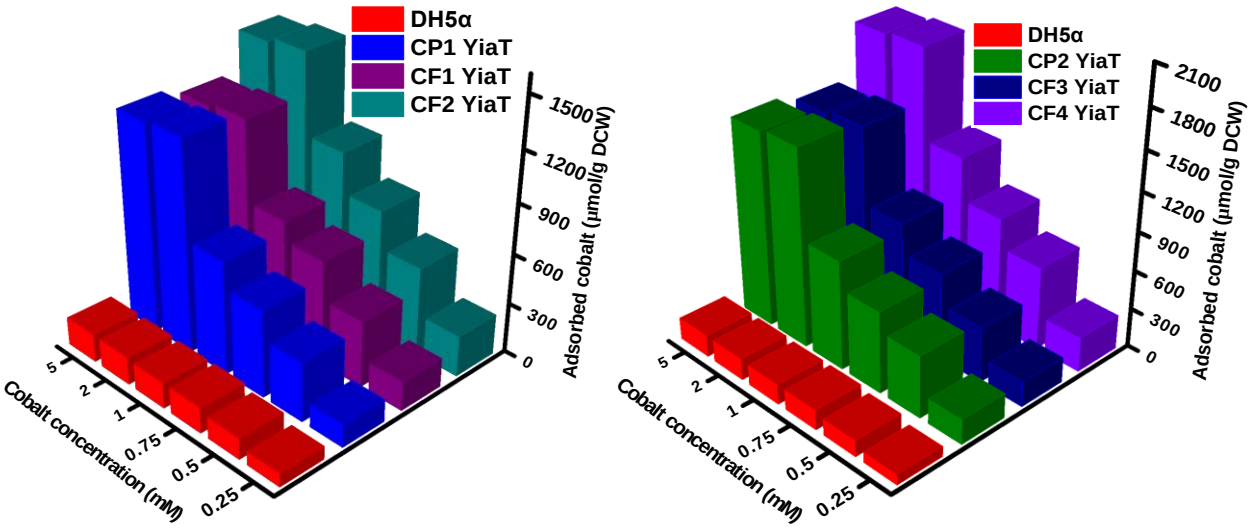

Fig. 4.3 The adsorption of cobalt by the *E. coli* (YiaT-CP1, YiaT-CP2, YiaT-CF1, YiaT-CF2, YiaT-CF3, YiaT-CF4) with different concentrations ranges from 0.25mM to 5mM.

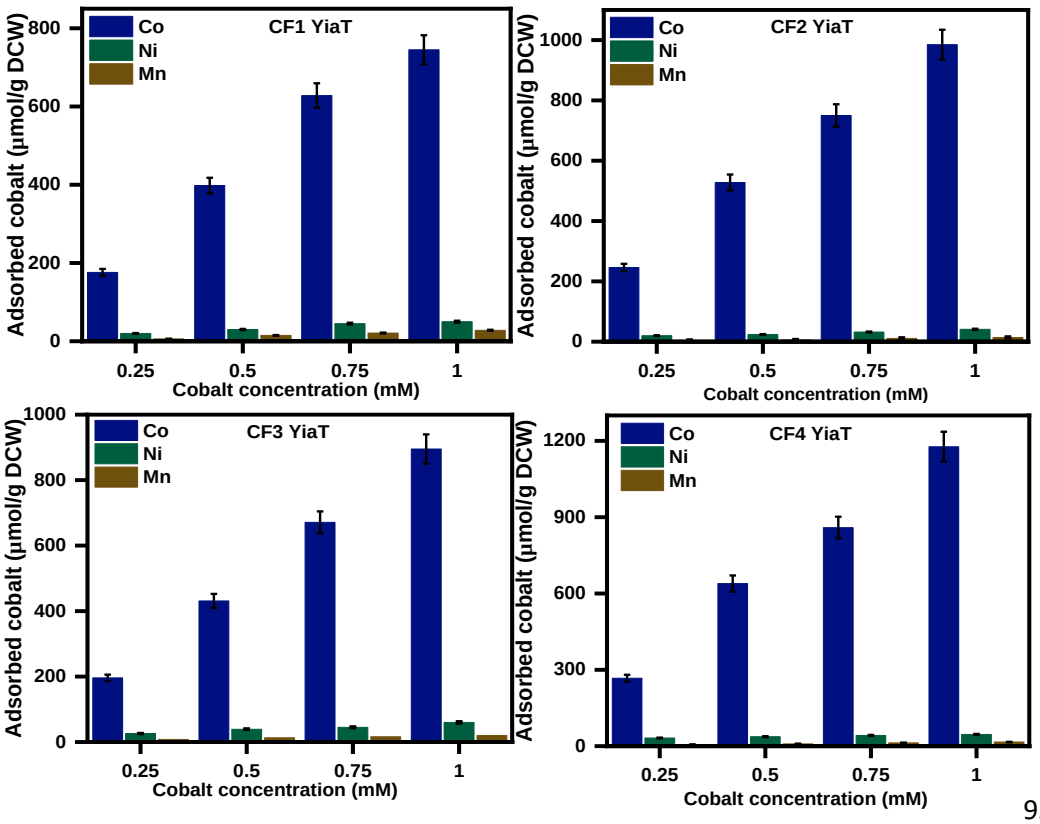

Fig. 4.4 The selectivity of cobalt over nickel and manganese by the *E. coli* (YiaT-CF1, YiaT-CF2, YiaT-CF3, YiaT-CF4) with different concentrations ranges from 0.25mM to 1mM.

In this study, an examination was conducted on the recombinant *E. coli* (YiaT-CF4) strain using FE-SEM and EDS techniques after cobalt absorption. The principal aim was to visualize the adsorbed metallic element and discern its structural attributes. Following adsorption, the cells underwent a thorough rinsing and lyophilization procedure for FE-SEM analysis. This examination, employing FE-SEM, unveiled nanoparticles adhering to the surface of recombinant *E. coli* (YiaT-CF4) after cobalt adsorption at 2 mM cobalt solution, as depicted in Figure 3D. The results from the FE-SEM analysis suggest that the cobalt nanoparticles, featuring a size distribution ranging from 10 to 50 nm, were predominantly affixed to the cellular wall. Identifying cobalt nanoparticles within the strains was made feasible by detecting spectral peaks corresponding to Co Kα1 and Co Kβ1 at energy levels of 6.931 keV and 7.649 keV, respectively (69,70) using EDS, as illustrated in Figure 3D. In contrast, the wild-type *E. coli* strain (DH5α) did not exhibit the formation of nanoparticles on its cell wall. Conversely, the recombinant *E. coli* strain exhibited the presence of conspicuous cobalt salt nanoparticles on the surface of its membrane. The observations stemming from the investigation of cobalt adsorption imply that the cell wall surface of the recombinant *E. coli* harbors numerous binding sites for cobalt ions. Ionic species localized on the cellular membrane possess the potential to engage in chemical reactions leading to the formation of inorganic compounds that subsequently precipitate from the surrounding solution. These sites can accumulate ions in a confined region, enhance surface coverage, and promote ion clustering, ultimately culminating in the generation of solid nanoparticles on the cellular membrane.

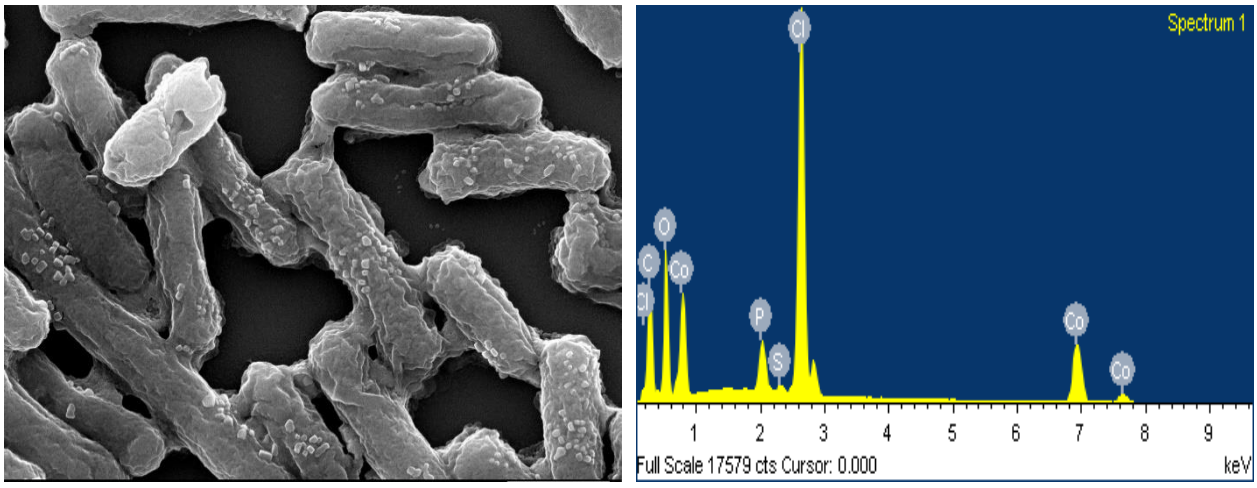

Fig. 4.5 FE-SEM and EDS analysis for *E. coli* (pBADCF2)

4.4.4 Synthesis of cobalt oxide nanoparticles and their characterization

Cobalt oxide nanoparticles were synthesised using the process of calcination at a temperature of 500 °C, utilising a strain of *E. coli* YiaT-CF4 that had adsorbed cobalt. The action was carried out to remove contaminants and volatile chemicals. At elevated temperatures, the metal samples transform oxides. Subsequently, the resulting oxide nanoparticles can be gathered and analysed using FE-SEM, EDS, XRD, and UV-DRS techniques.

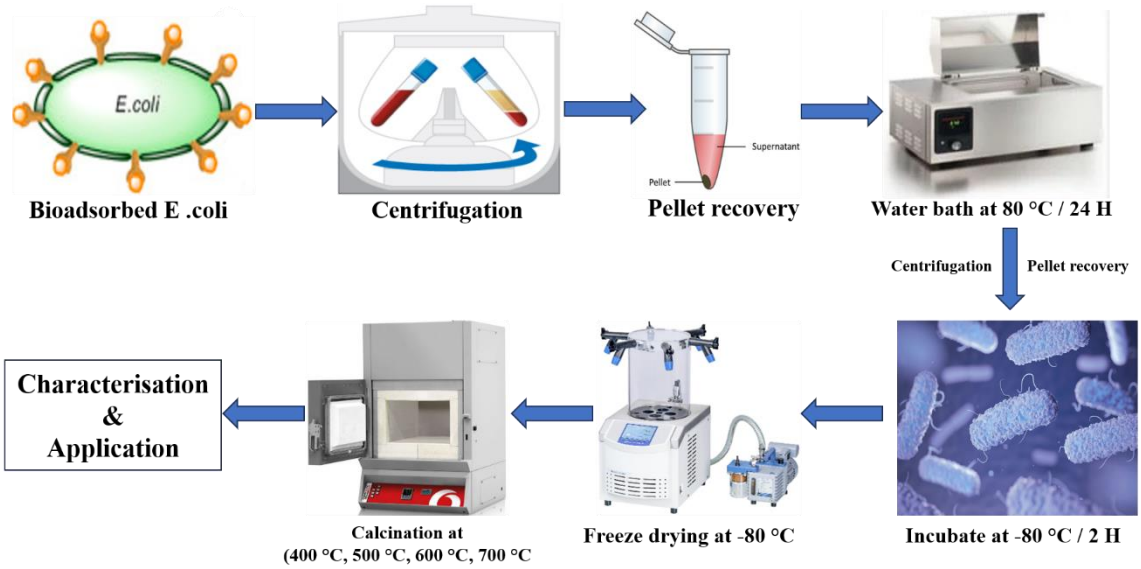

Fig. 4.6 Schematic representation of the synthesis of cobalt oxide nanoparticle

4.4.4.1 FE-SEM and EDS

The utilisation of Scanning Electron Microscopy (SEM) is employed to characterise and analyse the morphology of oxidised materials. The generated powders' morphology can be determined using Field Emission Scanning Electron Microscopy (FE-SEM). The particles precipitated by cobalt demonstrate a heterogeneous morphology, characterised by a diverse range of sizes and forms. Upon aggregation, these particles assume a spherical form. Figure 5A demonstrates that a considerable proportion of the particles display a nearly spherical morphology, with diameters spanning from 150 to 1000 nm. Certain groups exhibit bigger sizes, distinguished by a compact arrangement of tiny particles, while others are comparatively smaller. Although the particles are densely packed, it is possible for there to be small gaps and apertures inside the product grouping. The observed deviation from the expected pattern indicates the coexistence of nanoparticles and microparticles within the product, with interconnections between them. The observed sample has a non-uniform arrangement of particles, evident across its whole volume, including the surface. Consequently, there is an uneven distribution of nanoparticles in its morphology.

Figure 5B displays the Energy-Dispersive X-ray Spectroscopy (EDS) spectra of nanoparticles subjected to heat treatment. Based on the analysis of the Energy Dispersive X-ray Spectroscopy (EDS) spectra, it can be determined that the Co_3O_4 sample that was synthesised predominantly consists of cobalt (Co) and oxygen (O) elements. The first spectral peak of the oxygen element (O Kα1) is discovered at an energy level of 0.5 keV, whereas the presence of cobalt is detected at Co Kα1 (6.931 keV) and Co Kβ1 (7.649 keV) (69,70). The investigated product demonstrates cobalt and oxygen elements, as evidenced by an observed Co/O atomic ratio of roughly 3/3.97. This ratio aligns with the anticipated value for Co_3O_4.

The observation highlights the exceptional level of purity exhibited by the Co_3O_4 nanoparticles, as visually represented in the accompanying image.

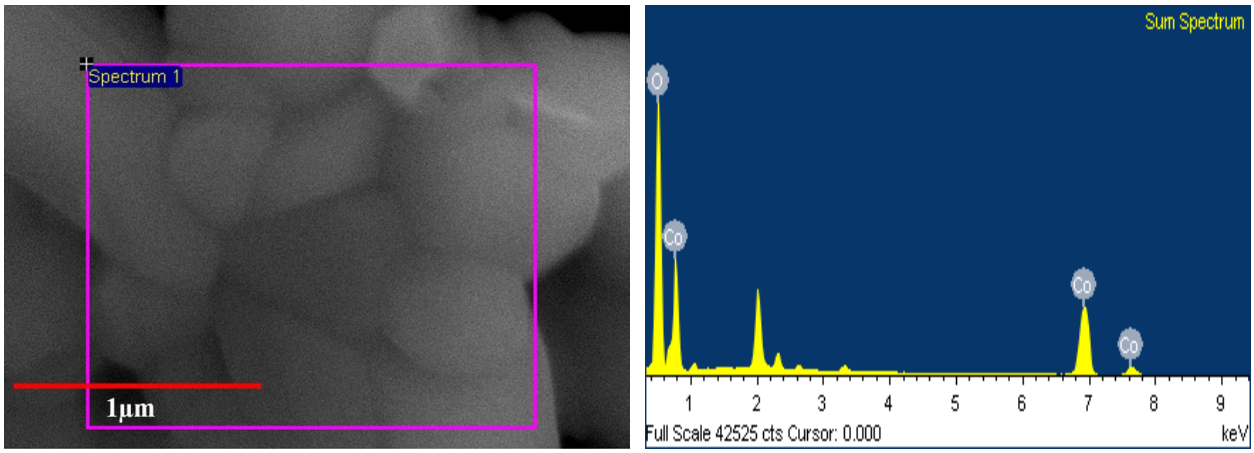

Fig. 4.7 A) FE-SEM for *E. coli* (pBADCF2) recovered cobalt oxide nanoparticles, calcinated at 500˚C. (B) EDS for *E. coli* (pBADCF2) recovered cobalt oxide nanoparticles, calcinated at 500˚C.

4.4.4.2 XRD (X-ray Diffraction)

The crystallographic characterisation was conducted using X-ray diffraction (XRD) with an Xpert 3 model and Cu Kα radiation (λ = 1.54 A°) within the 10°-90° 2θ range. The X-ray diffraction (XRD) pattern depicted in Figure 5C provides unambiguous evidence of the polycrystalline characteristics exhibited by the cobalt oxide nanoparticles. The diffraction patterns of the Co_3O_4 samples exhibit distinct peaks at specific angles (18.73, 31.4, 36.8, 38.3, 44.9, 55.66, 59.3, and 65.3), which correspond to the crystalline planes (111, 220, 311, 222, 400, 422, 511, and 440) of the Co_3O_4 phase. These peaks align with the Co_3O_4 phase's three-dimensional spinel configuration. The results presented in this study provide evidence for the effective production of the Co_3O_4 cubic phase, which is distinguished by its clearly defined crystalline structure (71).

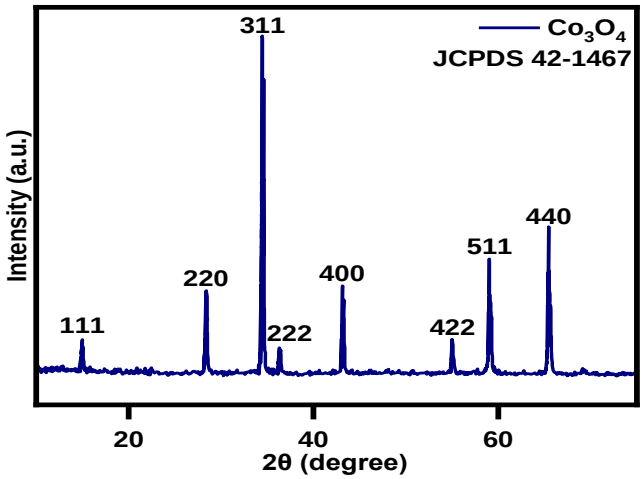

Fig. 4.8 X-ray diffraction of cobalt oxide nanoparticles.

4.4.4.3 UV-DRS Analysis

The absorbance spectra of Co_3O_4 nanoparticles mediated by microbes are shown in Figure 3. The establishment of Co_3O_4 nanoparticles through microbial mediation was determined by analysing the absorbance peaks at 390 nm and 690 nm [72,73]. The shift of charges from oxygen (O) to cobalt (Co) orbitals was revealed by observing the broad two peaks produced by microbial-mediated cobalt oxide (Co_3O_4) nanoparticles. The movement of orbital electrons of Co^{2+} and Co^{3+} towards O^{2-} signifies the presence of cobalt ions in a twofold oxidation state [72,73].

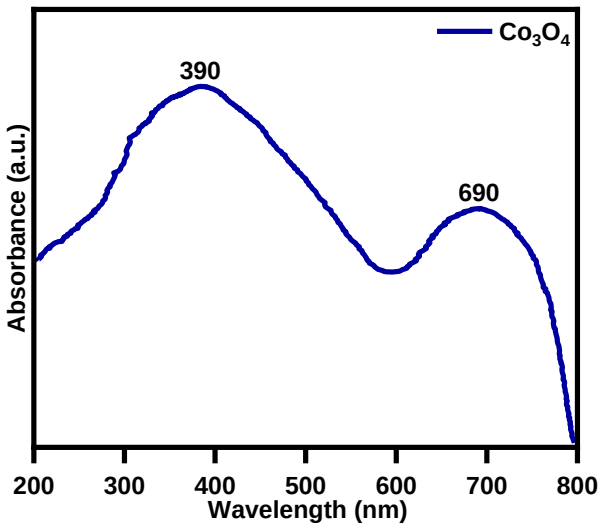

Fig. 4.9 UV-DRS Analysis of cobalt oxide nanoparticles.

4.5 Photocatalytic degradation of norfloxacin

The photocatalytic degradation of NOX utilising Co_3O_4 as a catalyst is a multifaceted phenomenon encompassing various interconnected pathways. The intricacies of this mechanism can be expounded upon extensively within the context of this study. The process commences with the absorption of visible light by nanoparticles of Co_3O_4. The process of absorption leads to the creation of electron-hole pairs (e^-/h^+), wherein the electrons undergo excitation from the valence band (VB) to the conduction band (CB), thereby leaving positively charged holes in the VB. The Norfloxacin molecules inside the solution exhibit an affinity towards the Co_3O_4 surface, primarily driven by electrostatic interactions, Vander Waals forces, and hydrogen bonding. The drug molecules undergo adsorption onto the surface of the catalyst.

The electrons generated during photoexcitation in the conduction band (CB) of Co_3O_4 exhibit reducing properties, while the holes in the valence band (VB) have oxidising characteristics. The electrons in an excited state could engage in interactions with oxygen and water molecules present in the immediate vicinity. These interactions form hydroxyl radicals (•OH) and superoxide radicals ($O2•^-$). These radicals are of utmost importance in the process of degradation. The hydroxyl radicals (•OH) and superoxide radicals ($O2•^-$) exhibit significant reactivity as they engage in the assault on the adsorbed norfloxacin molecules. The degradation process can be initiated by •OH radicals, which target different functional groups in the norfloxacin molecule, including the fluorine atoms and the piperazinyl ring.

The impact of reactive oxygen species (ROS) on NOX leads to the fragmentation of chemical bonds within the molecular structure of the medication. This process may result in the generation of intermediate products and smaller organic fragments. The intermediate products that arise during the degradation process undergo additional oxidation by reactive

oxygen species (ROS), ultimately resulting in the conversion of NOX into simpler and less harmful compounds, namely carbon dioxide (CO_2) and water (H_2O). The byproducts from degradation and the NOX that have not undergone reaction are released from the catalyst's surface. Subsequently, the goods are introduced into the solution, resulting in enhanced water quality characterised by reduced pollution levels.

The catalyst Co_3O_4 exhibits stability during the degrading process. It can be employed repeatedly for numerous cycles, rendering it a financially feasible and ecologically sustainable alternative for wastewater treatment.

Investigating the photocatalytic degradation of NOX employing Co_3O_4 as a catalyst yielded significant insights. The experiments involved different concentrations of Co_3O_4 and pH levels, with each reaction subjected to 90 min of visible light irradiation followed by 60 min of dark incubation to ensure environmental stabilization of the catalyst and drug. The degradation results indicate a clear correlation between the concentration of Co_3O_4 and the efficiency of NOX degradation. Specifically, at a Co_3O_4 concentration of 10 mg, the degradation percentage reached 65%, while increasing the catalyst concentration to 20 mg resulted in a noticeable improvement, with a degradation percentage of 70%, further increased to 84% at 30 mg, and notably reached 89% at 40 mg. A similar degradation efficiency of 90% was recorded at 50 mg. Given the similarity in results between 40 mg and 50 mg, subsequent pH studies were conducted using a 40 mg catalyst dosage. The influence of pH on NOX degradation was then examined with the 40 mg Co_3O_4 catalyst. The findings reveal a pH-dependent trend, wherein the degradation efficiency varies with pH levels. At pH 3, the drug degradation after 90 minutes of exposure to visible light was 67%. As we transitioned to a slightly alkaline environment with pH 5, the degradation efficiency notably increased to 79%. Further elevating the pH to 7 resulted in the highest observed degradation efficiency of 86%.

However, at higher pH levels of 9 and 11, the degradation efficiency slightly decreased to 81% and 80%, respectively. These results offer valuable insights into the photocatalytic degradation of NOX using Co_3O_4 as a catalyst, demonstrating the significant impact of both catalyst concentration and pH on the degradation process. The findings provide crucial information for developing effective and environmentally sustainable strategies for removing pharmaceutical contaminants from aqueous systems.

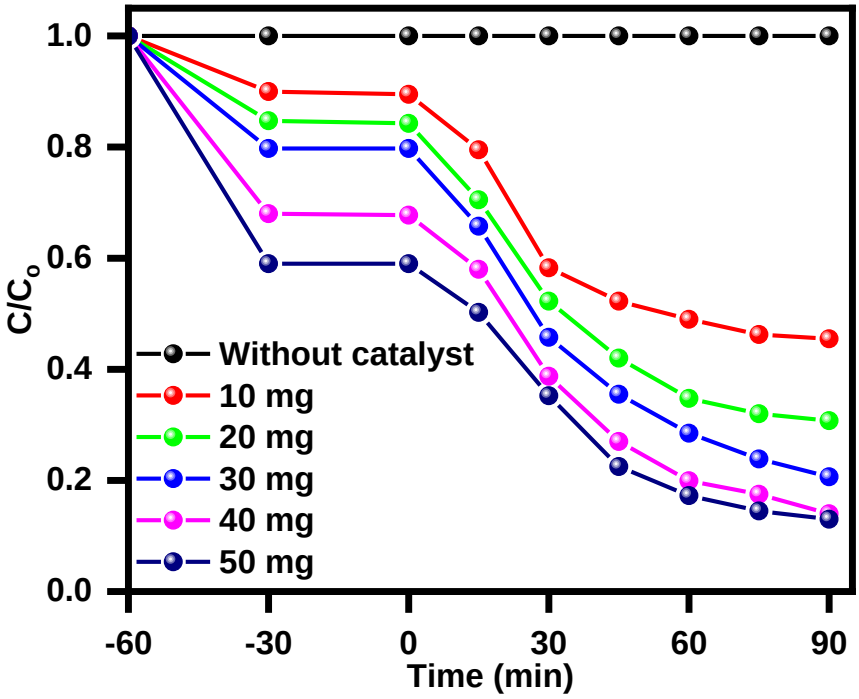

Fig. 4.10 Photocatalytic degradation activity of norfloxacin with Co_3O_4 nanoparticles *E. coli* (pBAD-YiaT-CF4) oxidised at 500 ˚C at different concentrations.

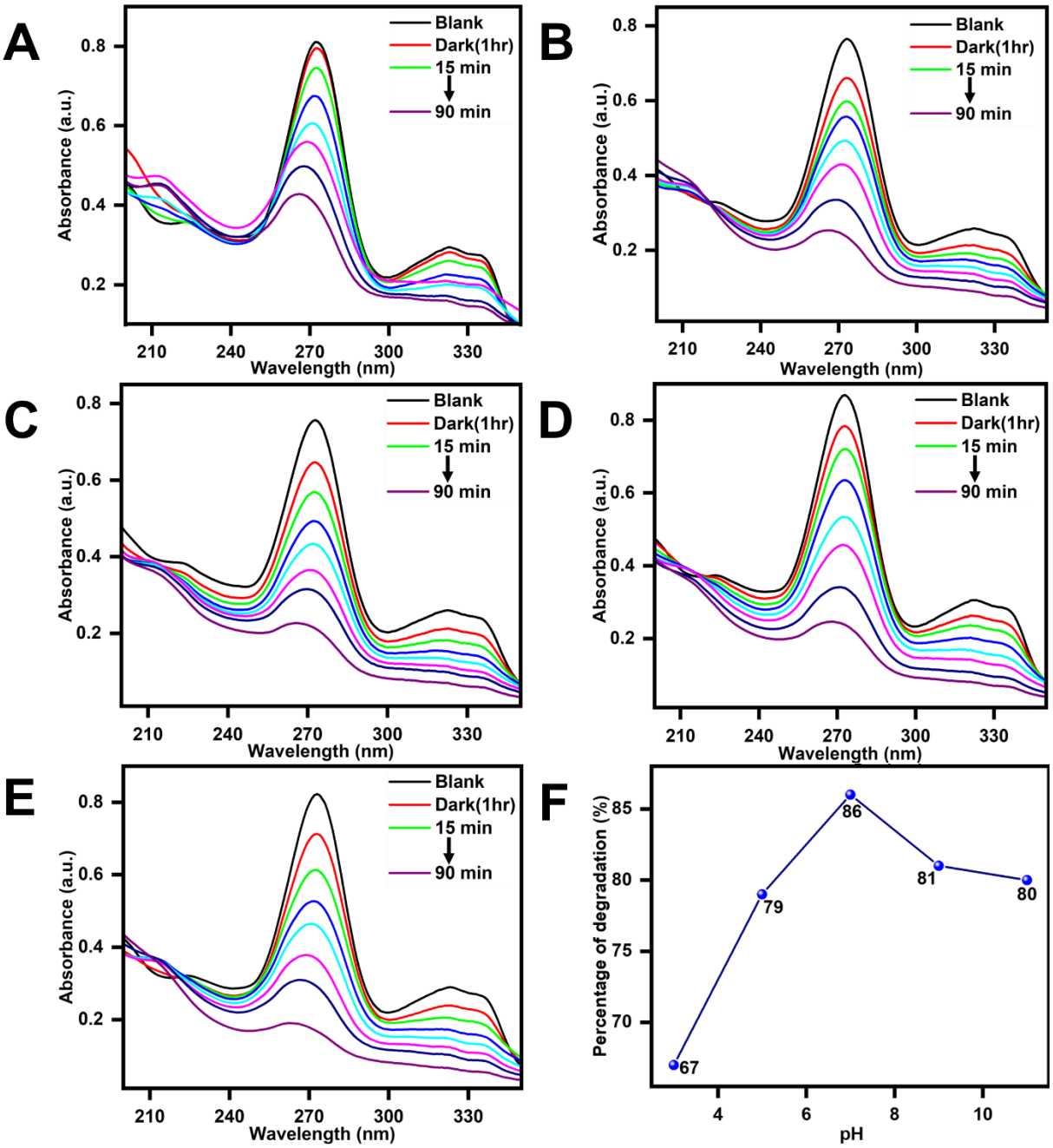

Fig. 4.11 Photocatalytic degradation activity of norfloxacin with Co_3O_4 nanoparticles *E. coli* (pBAD-YiaT-CF4) oxidized at 500 ˚C at different pH. A. pH3 B. pH5 C. pH7 D. pH9 E. pH 11 F. degradation percentage at different pH.

4.6 Conclusion

Our extensive examination of cobalt-binding peptides and their potential uses has provided significant findings and implications for biotechnology and environmental research. The recombinant strains, namely *E. coli* (YiaT-CF1), *E. coli* (YiaT-CF2), *E. coli* (YiaT-CF3), and *E. coli* (YiaT-CF4), indicate a significant preference for cobalt over nickel and manganese. *E. coli* (YiaT-CF4) had the most notable cobalt adsorption capacity of the options considered, suggesting its better efficacy in selectively binding cobalt ions. The results of this study indicate that *E. coli* (YiaT-CF4) have practical value in selectively absorbing or removing metals in various applications. In addition, recombinant *E. coli* (YiaT-CF4) was investigated after cobalt absorption using FE-SEM and EDS methodologies. The examination results demonstrated the presence of cobalt nanoparticles on the outer surface of the cells. The observation underscores the existence of several binding sites for cobalt ions, which facilitate chemical reactions that result in the binding of cobalt nanoparticles on the cellular membrane. This phenomenon presents opportunities for innovative methods in the adsorption of metals and the rehabilitation of the environment.

The potential uses of our research were further highlighted by creating cobalt oxide nanoparticles via calcination at a temperature of 500 °C. The effective synthesis of Co_3O_4 nanoparticles with high purity and well-defined crystalline structures was confirmed using characterization techniques such as FE-SEM, EDS, XRD, and UV-DRS. The potential of these nanoparticles for a range of technical applications, such as catalysis and environmental remediation, is considerable. Furthermore, our study on the photocatalytic degradation of norfloxacin (NOX) utilising Co_3O_4 as a catalyst has revealed a multifaceted mechanism encompassing generating electron-hole pairs and forming reactive oxygen species (ROS). The study's findings revealed a significant association between the concentration of Co_3O_4 and the

efficiency of NOX degradation, with the most effective degradation observed at a Co_3O_4 concentration of 50 mg. Furthermore, the pH-dependent degradation efficiency underscored the importance of pH levels, with a pH of 7 demonstrating the maximum degradation rate.

In conclusion, our study highlights the potential of peptides that bind to cobalt and their genetically engineered variants, the production of cobalt oxide nanoparticles and their use in photocatalytic applications across diverse scientific and technological fields. The discoveries enhance our comprehension of the interactions between metals and peptides, thereby establishing a basis for advancing pioneering biotechnological and environmental scientific solutions. Ultimately, these advancements hold the potential to benefit society by addressing concerns related to metal contamination and the presence of pharmaceutical pollutants in aqueous environments.

4.7 REFERENCES

1. Y. Yang, et al., Efficient with low-cost removal and adsorption mechanisms of norfloxacin, ciprofloxacin and ofloxacin on modified thermal kaolin: experimental and theoretical studies, J. Hazard. Mater. 430 (2022) 128500.

2. M.E. Zelaya Soulé, et al., Carbon/montmorillonite hybrids with different activation methods: adsorption of norfloxacin, Adsorption 25 (7) (2019) 1361–1373.

3. Y. Feng, et al., Norfloxacin removal from aqueous solution using biochar derived from luffa sponge, J. Water Supply: Res. Technol.-AQUA 67 (8) (2018) 703–714.

4. J. Huang, J. Cao, Y. Ding, Y. Hu, Y. Cen, H. Tang, Chemosphere 205 (2018) 531, Doi: http://dx.doi.org/10.1016/j.chemosphere.2018.04.138.

5. S. Babi _c, M. Periša, I. Škori _c, Chemosphere 91 (2013) 1635, Doi: HTTP://dx.doi. org/10.1016/j.chemosphere.2012.12.072.

6. G. Zhang, Y. Xue, Q. Wang, P. Wang, H. Yao, W. Zhang, J. Zhao, Y. Li, Chemosphere (2019), doi: http://dx.doi.org/10.1016/j.chemosphere.2019.05.015.

7. Y. Wang, et al., Effects of dissolved organic matter on the adsorption of norfloxacin on a sandy soil (fraction) from the Yellow River of Northern China, Sci. Total Environ. 848 (2022) 157495

8. T. Chahm, et al., Use of chemically activated termite feces a low-cost adsorbent for the adsorption of norfloxacin from aqueous solution, Water Sci. Technol. 79 (2) (2019) 291–301.

9. A. Nayak, B. Bhushan, S. Kotnala, Fabrication of chitosan-hydroxyapatite nano-adsorbent for removal of norfloxacin from water: isotherm and kinetic studies, Mater. Today: Proc. 61 (2022) 143–149.

10. M. Sun, et al., Adsorption behaviours and mechanisms of antibiotic norfloxacin on degradable and nondegradable microplastics, Sci. Total Environ. 807 (2022) 151042.

11. X. Cao, et al., Co-adsorption capabilities and mechanisms of bentonite enhanced sludge biochar for de-risking norfloxacin and Cu2 + contaminated water, Chemosphere 299 (2022) 134414.

12. X. Fang, et al., High-efficiency adsorption of norfloxacin using octahedral UIO-66-NH2 nanomaterials: dynamics, thermodynamics, and mechanisms, Appl. Surf. Sci. 518 (2020) 146226.

13. Y. Li, et al., Removal of Norfloxacin from aqueous solution by clay-biochar composite prepared from potato stem and natural attapulgite, Colloids Surf. A 514 (2017) 126–136.

14. Zhang, Y., et al., Mechanistic insight into different adsorption of norfloxacin on microplastics in simulated natural and actual surface water. Environ. Pollut., 2021. 284: p. 117537.

15. M.R. Azhar, et al., Adsorptive removal of antibiotic sulfonamide by UiO-66 and ZIF-67 for wastewater treatment, J. Colloid Interface Sci. 500 (2017) 88–95.

16. D.I. de Souza, et al., Nanofiltration for the removal of norfloxacin from pharmaceutical effluent, J. Environ. Chem. Eng. 6 (5) (2018) 6147–6153.

17. W. Liu, et al., Synergistic adsorption-photocatalytic degradation effect and norfloxacin mechanism of ZnO/ZnS@ BC under UV-light irradiation, Sci. Rep. 10 (1) (2020) 1–12.

18. J. He, et al., Understanding and characteristics of coagulation removal of microplastic and norfloxacin composite pollution during water treatment, Sci. Total Environ. 831 (2022) 154826.

19. D. Balarak, et al., Survey electrocoagulation process in the removal of norfloxacin antibiotic from aqueous solutions, J. Pharmaceutical Res. Int. 32 (3) (2020) 53–60.

20. W. Baran, et al., Removal of veterinary antibiotics from wastewater by electrocoagulation, Chemosphere 194 (2018) 381–389.

21. M. Bajpai, et al., A review on electrocoagulation process for removing emerging contaminants: theory, fundamentals, and applications, Environ. Sci. Pollut. Res. Int. 29 (2022) 1–30.

22. Y. Tian, et al., 0D/3D coupling of g-C3N4 QDs/hierarchical macro-mesoporous CuO-SiO2 for high-efficiency norfloxacin removal in photo-Fenton-like processes, J. Hazard. Mater. 419 (2021) 126359.

23. D. Yu, et al., Mineralization of norfloxacin in a CoFe–LDH/CF cathode-based heterogeneous electro-fenton system: preparation parameter optimization of the cathode and conversion mechanisms of H2O2 to· OH, Chem. Eng. J. 417 (2021) 129240.

24. S.L. Prabavathi, et al., Construction of heterostructure CoWO4/g-C3N4 nanocomposite as an efficient visible-light photocatalyst for norfloxacin degradation, J. Ind. Eng. Chem. 80 (2019) 558–567.

25. H. Zhang, et al., Preparation of Ce4 + -doped BaZrO3 by hydrothermal method and application in dual-frequent sonocatalytic degradation of norfloxacin in aqueous solution, Ultrason. Sonochem. 42 (2018) 356–367.

26. S. Ye, G. Zeng, H. Wu, C. Zhang, J. Dai, J. Liang, J. Yu, X. Ren, H. Yi, M. Cheng, C. Zhang, Crit. Rev. Biotechnol. 37 (2017) 1062, doi: http://dx.doi.org/10.1080/ 07388551.2017.1304357.

27. S. Ye, G. Zeng, H. Wu, C. Zhang, J. Liang, J. Dai, Z. Liu, W. Xiong, J. Wan, P. Xu, M. Cheng, Crit. Rev. Environ. Sci. Technol. 47 (2017) 1528, doi: http://dx.doi.org/ 10.1080/10643389.2017.1386951.

28. S. Ye, M. Yan, X. Tan, J. Liang, G. Zeng, H. Wu, B. Song, C. Zhou, Y. Yang, H. Wang, Appl. Catal. B Environ. 250 (2019) 78, doi: http://dx.doi.org/10.1016/j. apcatb.2019.03.004.

29. S. Ye, G. Zeng, H. Wu, J. Liang, C. Zhang, J. Dai, W. Xiong, B. Song, S. Wu, J. Yu, Resour. Conserv. Recycl. 140 (2019) 278, doi: http://dx.doi.org/10.1016/j. resconrec.2018.10.004.

30. L. Hao, L. Kang, H. Huang, L. Ye, K. Han, S. Yang, H. Yu, M. Batmunkh, Y. Zhang, T. Ma, Adv. Mater. 31 (2019) 1, doi: http://dx.doi.org/10.1002/adma.201900546.

31. Y. Wang, R.M. de Kruijff, M. Lovrak, X. Guo, R. Eelkema, J.H. van Esch, Angew. Chem. Int. Ed. 58 (2019) 3800, doi: http://dx.doi.org/10.1002/anie.201812412.

32. F. Chen, H. Huang, L. Ye, T. Zhang, Y. Zhang, X. Han, T. Ma, Adv. Funct. Mater. 28 (2018) 1, doi: http://dx.doi.org/10.1002/adfm.201804284.

33. H. Huang, X. Han, X. Li, S. Wang, P.K. Chu, Y. Zhang, ACS Appl. Mater. Interfaces. 7 (2015) 482, doi: http://dx.doi.org/10.1021/am5065409.

34. M. Mousavi, A. Habibi-Yangjeh, S.R. Pouran, J. Mater. Sci. Mater. Electron. 29 (2018) 1719, doi: http://dx.doi.org/10.1007/s10854-017-8166-x.

35. M. Pirhashemi, A. Habibi-Yangjeh, S. Rahim Pouran, J. Ind. Eng. Chem. 62 (2018) 1, doi: http://dx.doi.org/10.1016/j.jiec.2018.01.012.

36. M. Shekofteh-Gohari, A. Habibi-Yangjeh, M. Abitorabi, A. Rouhi, Crit. Rev. Environ. Sci. Technol. 48 (2018) 806, doi: http://dx.doi.org/10.1080/ 10643389.2018.1487227.

37. D. Cao, Y. Wang, M. Qiao, X. Zhao, J. Catal. 360 (2018) 240, doi: http://dx.doi.org/ 10.1016/j.jcat.2018.01.017.

38. J. Wen, J. Xie, X. Chen, X. Li, Appl. Surf. Sci. 391 (2017) 72, doi: http://dx.doi.org/ 10.1016/j.apsusc.2016.07.030.

39. P. Durán, J. Tartaj, C. Moure, Fully Dense, Fine-Grained, Doped Zinc Oxide Varistors with Improved Nonlinear Properties by Thermal Processing Optimization, Journal of the American Ceramic Society, 86 (2003) 1326-1329.

40. J. Wang, L. Gao, Photoluminescence Properties of Nanocrystalline ZnO Ceramics Prepared by Pressureless Sintering and Spark Plasma Sintering, Journal of the American Ceramic Society, 88 (2005) 1637-1639.

41. M. Mazaheri, A.M. Zahedi, M.M. Hejazi, Processing of nanocrystalline 8mol% yttria-stabilized zirconia by conventional, microwave-assisted and two-step sintering, Materials Science and Engineering: A, 492 (2008) 261-267.

42. M.I. Shliomis, A.F. Pshenichnikov, K.I. Morozov, I.Y. Shurubor, Magnetic properties of ferrocolloids, Journal of Magnetism and Magnetic Materials, 85 (1990) 40-46.

43. C. Bergemann, D. Müller-Schulte, J. Oster, L. à Brassard, A.S. Lübbe, Magnetic ion-exchange nano- and microparticles for medical, biochemical and molecular biological applications, Journal of Magnetism and Magnetic Materials, 194 (1999) 45-52.

44. C.-B. Wang, C.-W. Tang, S.-J. Gau, S.-H. Chien, Effect of the surface area of cobaltic oxide on carbon monoxide oxidation, Catalysis Letters, 101 (2005) 59-63.

45. C.-B. Wang, H.-K. Lin, C.-W. Tang, Thermal Characterization and Microstructure Change of Cobalt Oxides, Catalysis Letters, 94 (2004) 69-74.

46. F. Grillo, M.M. Natile, A. Glisenti, Low-temperature oxidation of carbon monoxide: the influence of water and oxygen on the reactivity of a Co3O4 powder surface, Applied Catalysis B: Environmental, 48 (2004) 267-274.

47. S.A. Needham, G.X. Wang, H.K. Liu, Synthesis of NiO nanotubes for use as negative electrodes in lithium-ion batteries, Journal of Power Sources, 159 (2006) 254-257.

48. X. Wang, W. Tian, T. Zhai, C. Zhi, Y. Bando, D. Golberg, Cobalt(ii,iii) oxide hollow structures: fabrication, properties and applications, Journal of Materials Chemistry, 22 (2012) 23310-23326.

49. N.M. Basith, J.J. Vijaya, L.J. Kennedy, M. Bououdina, S. Jenefar, V. Kaviyarasan, Co-Doped ZnO Nanoparticles: Structural, Morphological, Optical, Magnetic and Antibacterial Studies, Journal of Materials Science & Technology, 30 (2014) 1108-1117.

50. L.F. Liotta, H. Wu, G. Pantaleo, A.M. Venezia, Co3O4 nanocrystals and Co3O4–MOx binary oxides for CO, CH4 and VOC oxidation at low temperatures: a review, Catalysis Science & Technology, 3 (2013) 3085-3102.

51. H. Singh, A.K. Sinha, M.N. Singh, P. Tiwari, D.M. Phase, S.K. Deb, Spectroscopic and structural studies of isochronally annealed cobalt oxide nanoparticles, Journal of Physics and Chemistry of Solids, 75 (2014) 397-402.

52. C.S. Jincy, P. Meena, Synthesis, characterization, and NH3 gas sensing application of Zn doped cobalt oxide nanoparticles, Inorganic Chemistry Communications, 120 (2020) 108145.

53. A.S. Vijayanandan, R.M. Balakrishnan, Biosynthesis of cobalt oxide nanoparticles using endophytic fungus *Aspergillus nidulans*, Journal of Environmental Management, 218 (2018) 442-450.

54. S. Sundararaju, M. Arumugam, P. Bhuyar, Microbacterium sp. MRS-1, a potential bacterium for cobalt reduction and synthesis of less/non-toxic cobalt oxide nanoparticles (Co3O4), Beni-Suef University Journal of Basic and Applied Sciences, 9 (2020) 44.

55. N. Mubraiz, A. Bano, T. Mahmood, N. Khan, Microbial and Plant Assisted Synthesis of Cobalt Oxide Nanoparticles and Their Antimicrobial Activities, in: Agronomy, 2021.

56. E. Jang, H.-W. Shim, B.H. Ryu, D.R. An, W.K. Yoo, K.K. Kim, D.-W. Kim, T.D. Kim, Preparation of cobalt nanoparticles from polymorphic bacterial templates: A novel platform for biocatalysis, International Journal of Biological Macromolecules, 81 (2015) 747-753.

57. S. Iravani, R.S. Varma, Sustainable synthesis of cobalt and cobalt oxide nanoparticles and their catalytic and biomedical applications, Green Chemistry, 22 (2020) 2643-2661.

58. S. Marimuthu, A.A. Rahuman, A.V. Kirthi, T. Santhoshkumar, C. Jayaseelan, G. Rajakumar, Eco-friendly microbial route to synthesize cobalt nanoparticles using *Bacillus thuringi*ensis against malaria and dengue vectors, Parasitology Research, 112 (2013) 4105-4112.

59. Lamiable, A.; Thévenet, P.; Rey, J.; Vavrusa, M.; Derreumaux, P.; Tufféry, P. PEP-FOLD3: Faster de Novo Structure Prediction for Linear Peptides in Solution and in Complex. Nucleic Acids Res. 2016, 44 (W1), W449–W454.

60. Shen, Y.; Maupetit, J.; Derreumaux, P.; Tufféry, P. Improved PEP-FOLD Approach for Peptide and Miniprotein Structure Prediction. J. Chem. Theory Comput. 2014, 10 (10), 4745–4758.

61. Thevenet, P.; Shen, Y.; Maupetit, J.; Guyon, F.; Derreumaux, P.; Tuffery, P. PEP-FOLD: An Updated de Novo Structure Prediction Server for Both Linear and Disulfide Bonded Cyclic Peptides. Nucleic Acids Res. 2012, 40 (W1), W288–W293.

62. Zhang, J.; Dolg, M. ABCluster: The Artificial Bee Colony Algorithm for Cluster Global Optimization. Phys. Chem. Chem. Phys. 2015, 17 (37), 24173–24181.

63. Zhang, J.; Dolg, M. Global Optimization of Clusters of Rigid Molecules Using the Artificial Bee Colony Algorithm. Phys. Chem. Chem. Phys. 2016, 18 (4), 3003–3010.

64. Zhang, J.; Glezakou, V.-A. Global Optimization of Chemical Cluster Structures: Methods, Applications, and Challenges. Int. J. Quantum Chem. 2021, 121 (7), e26553.

65. Frisch, M. J.; Trucks, G. W.; Schlegel, H. B.; Scuseria, G. E.; Robb, M. A.; Cheeseman, J. R.; Scalmani, G.; Barone, V.; Petersson, G. A.; Nakatsuji, H.; Li, X.; Caricato, M.; Marenich, A. V.; Bloino, J.; Janesko, B. G.; Gomperts, R.; Mennucci, B.; Hratchian, H. P.; Ortiz, J. V.; Izmaylov, A. F.; Sonnenberg, J. L.; Williams; Ding, F.; Lipparini, F.; Egidi, F.; Goings, J.; Peng, B.; Petrone, A.; Henderson, T.; Ranasinghe, D.; Zakrzewski, V. G.; Gao, J.; Rega, N.; Zheng, G.; Liang, W.; Hada, M.; Ehara, M.; Toyota, K.; Fukuda, R.; Hasegawa, J.; Ishida, M.;

Nakajima, T.; Honda, Y.; Kitao, O.; Nakai, H.; Vreven, T.; Throssell, K.; Montgomery Jr., J. A.; Peralta, J. E.; Ogliaro, F.; Bearpark, M. J.; Heyd, J. J.; Brothers, E. N.; Kudin, K. N.; Staroverov, V. N.; Keith, T. A.; Kobayashi, R.; Normand, J.; Raghavachari, K.; Rendell, A. P.; Burant, J. C.; Iyengar, S. S.; Tomasi, J.; Cossi, M.; Millam, J. M.; Klene, M.; Adamo, C.; Cammi, R.; Ochterski, J. W.; Martin, R. L.; Morokuma, K.; Farkas, O.; Foresman, J. B.; Fox, D. J. Gaussian 16 Rev. A.03, 2016.

66. Stewart, J. J. Optimization of Parameters for Semiempirical Methods V: Modification of NDDO Approximations and Application to 70 Elements. J. Mol. Model. 2007, 13, 1173–1213.

67. Marenich, A. V.; Cramer, C. J.; Truhlar, D. G. Universal Solvation Model Based on Solute Electron Density and a Continuum Model of the Solvent Defined by the Bulk Dielectric Constant and Atomic Surface Tensions. J. Phys. Chem. B 2009, 113 (18), 6378–6396.

68. Sun, X.; Yu, G.; Xu, Q.; Li, N.; Xiao, C.; Yin, X.; Cao, K.; Han, J.; He, Q.-Y. Putative Cobalt-and Nickel-Binding Proteins and Motifs in Streptococcus Pneumoniae. Metallomics 2013, 5 (7), 928–935.

69. I.A. Rodionova, Y. Gao, J. Monk, Y. Hefner, N. Wong, R. Szubin, H.G. Lim, D.A. Rodionov, Z. Zhang, M.H. Saier, B.O. Palsson, A systems approach discovers the role and characteristics of seven LysR type transcription factors in Escherichia coli, Scientific Reports, 12 (2022) 7274.

70. X.-m. Lin, M.-j. Yang, H. Li, C. Wang, X.-X. Peng, Decreased LamB and Odp1 complex expression is crucial for antibiotic resistance in Escherichia coli, Journal of Proteomics, 98 (2014) 244-253.

71. M. Vahed, F. Ramezani, V. Tafakori, V.S. Mirbagheri, A. Najafi, G. Ahmadian, Molecular dynamics simulation and experimental study of the surface-display of SPA protein via Lpp-OmpA system for screening of IgG, AMB Express, 10 (2020) 161.

72. Maharani, N.Y. Structural, morphological, optical properties of Zr-doped Co3O4 nanoparticles. Part. Sci. Technol. 2022, 40, 662–674.

73. Feng, Z.; Zhu, X.; Yang, J.; Zhong, K.; Jiang, Z.; Yu, Q.; Song, Y.; Hua, Y.; Li, H.; Xu, H. Inherent Facet-Dominant effect for cobalt oxide nanosheets to enhance photocatalytic CO2 reduction. Appl. Surf. Sci. 2022, 578, 151848.

Chapter – 5

Conclusion and Future Perspectives

Conclusion and Future Perspectives

Cobalt, a highly adaptable transition metal located in the d-block of the periodic table, plays a crucial role in various industrial sectors. The impact of this phenomenon is particularly evident in the acrylic and ceramic sectors, as well as in electrocatalysis for diverse chemical processes, metallurgy, batteries, coatings, and electronics. In recent years, there has been a significant increase in the demand for cobalt, driven mostly by the growing battery industry. As a result, mining activities have intensified to fulfil this rising need. Although there have been advancements in finding alternate ways to extract cobalt, such as using microbial systems to create stable cobalt nanoparticles, there is still a need to further investigate the potential for microbial production of cobalt oxide nanoparticles. This thesis explores the capacity of microbial cell surface display (CSD) using metal-binding peptides (MBP) to retrieve cobalt. By utilising *Escherichia col*i as a framework to display cobalt-binding peptides (CBPs) on its outer membrane, a new opportunity arises for the recovery of cobalt and the treatment of wastewater. This novel technique holds promise for a sustainable society that depends on renewable resources. Peptide-engineered sorbents, which can selectively bind to cobalt over other metals in solutions, show potential without the need for additional chemicals or energy input, even under mild conditions. Incorporating CSD into peptide constructions offers several advantages, including decreased manufacturing expenses, increased adsorption capability, and improved product worth. The production of cobalt nanoparticles utilising whole-cell biosorbents is particularly remarkable, achieved by adsorption and calcination methods. The process of designing peptides enables the fabrication of customised nanoparticles, regardless of their intended use in wastewater treatment. The thesis emphasises the necessity of conducting additional research on the characteristics of nanoparticles produced on cell surfaces to advance peptide sequences. In addition, it investigates the use of cobalt oxide nanoparticles for various purposes such as cancer research, dye breakdown, and medication disintegration,

demonstrating their effectiveness in environmental cleanup and as substances that may absorb cobalt from contaminated water. The focus of this study is to create a genetically altered strain of *Escherichia coli* that has a strong attraction to cobalt. This strain can produce cobalt oxide nanoparticles, potentially used in cancer treatments. These discoveries are significant not just in the field of medicine, but also in the areas of wastewater treatment and environmental cleanup. They provide vital knowledge about the interactions between peptides and metals, showing potential uses in both industrial and environmental domains. This discovery represents a major advancement towards a sustainable and ecologically sensitive future by effectively utilising cobalt through the application of biotechnology and nanotechnology.